

**DOT/FAA/TC-17/46**

Federal Aviation Administration  
William J. Hughes Technical Center  
Aviation Research Division  
Atlantic City International Airport  
New Jersey 08405

# **A Test Protocol to Define Flammability and Toxic Hazard of Ceiling Impact Protective Material**

March 2018

Final Report

This document is available to the U.S. public through the National Technical Information Services (NTIS), Springfield, Virginia 22161.

This document is also available from the Federal Aviation Administration William J. Hughes Technical Center at [actlibrary.tc.faa.gov](http://actlibrary.tc.faa.gov).



U.S. Department of Transportation  
**Federal Aviation Administration**

## **NOTICE**

This document is disseminated under the sponsorship of the U.S. Department of Transportation in the interest of information exchange. The U.S. Government assumes no liability for the contents or use thereof. The U.S. Government does not endorse products or manufacturers. Trade or manufacturers' names appear herein solely because they are considered essential to the objective of this report. The findings and conclusions in this report are those of the author(s) and do not necessarily represent the views of the funding agency. This document does not constitute FAA policy. Consult the FAA sponsoring organization listed on the Technical Documentation page as to its use.

This report is available at the Federal Aviation Administration William J. Hughes Technical Center's Full-Text Technical Reports page: [actlibrary.tc.faa.gov](http://actlibrary.tc.faa.gov) in Adobe Acrobat portable document format (PDF).

**Technical Report Documentation Page**

1. Report No. <b>DOT/FAA/TC-17/46</b>		2. Government Accession No.		3. Recipient's Catalog No.	
4. Title and Subtitle <b>A TEST PROTOCOL TO DEFINE FLAMMABILITY AND TOXIC HAZARD OF CEILING IMPACT PROTECTIVE MATERIAL</b>				5. Report Date <b>March 2018</b>	
				6. Performing Organization Code	
7. Author(s) <b>James G. Quinteire<sup>1</sup>, Louise C. Speitel<sup>2</sup>; Haiqing Guo<sup>3</sup>; Sean B. Crowley<sup>2</sup>; Carleen Y. Houston<sup>2</sup></b>				8. Performing Organization Report No.	
9. Performing Organization Name and Address  <b><sup>1</sup>Department of Fire Protection Engineering University of Maryland College Park, MD 20742</b>  <b><sup>2</sup>Federal Aviation Administration William J. Hughes Technical Center Aviation Research Division Fire Safety Branch Atlantic City International Airport, NJ 08405</b>  <b><sup>3</sup>C-FAR Services, LLC 303 Quail Drive Marmora, NJ 08223</b>				10. Work Unit No. (TRAIS)	
				11. Contract or Grant No. <b>ANG-RM-ACT-15-T056</b>	
				13. Type of Report and Period Covered <b>Final Report</b>	
12. Sponsoring Agency Name and Address  <b>United States Army Tank Automotive Research Development and Engineering Center (TARDEC) Ground System Survivability (GSS) 6500 East 11 Mile Road Warren, Michigan 48397-5000</b>				14. Sponsoring Agency Code <b>US Army TARDEC-GSS</b>	
				15. Supplementary Notes <b>The FAA William J. Hughes Technical Center Aviation Research Division COR was Carleen Houston.</b>	
16. Abstract  <b>A test protocol is developed for assessing the fire hazard of a ceiling material in a combat ground vehicle. The hazards to the occupants include the thermal and toxic hazards from asphyxiant and irritant gases. An analysis is developed to determine the critical material fire properties that meet a safe level. The safe level is defined to consist of the prevention of flame spread over the ceiling and no incapacitation of the occupants for up to 5 minutes. Performance decrements due to eye and respiratory irritation from irritant gases were also considered. Experiments and analyses were conducted to develop the relationships for the critical fire properties in terms of physics and human tolerance to fire gases. A recommended level is based on that analysis and the incorporation of safety factors. The analysis consists of an engineering design that should clearly show the rationale for the protocol and a foundation for modifying it in the future based on new knowledge and information.</b>					
17. Key Words <b>Fire, Threat, Headliner, Flame spread, Toxicity, Available energy, Incapacitation, Asphyxiant, Thermal response Parameter, Safety factor, Effective concentration, Ceiling fire</b>			18. Distribution Statement <b>This document is available to the U.S. public through the National Technical Information Service (NTIS), Springfield, Virginia 22161. This document is also available from the Federal Aviation Administration William J. Hughes Technical Center at <a href="http://actlibrary.tc.faa.gov">actlibrary.tc.faa.gov</a>.</b>		
19. Security Classif. (of this report) <b>Unclassified</b>		20. Security Classif. (of this page) <b>Unclassified</b>		21. No. of Pages <b>123</b>	22. Price

## ACKNOWLEDGEMENTS

The authors thank Julie Klima and her TARDEC colleagues for providing us the opportunity to perform this work; Dhaval Dadia for providing the test vehicle and allowing its significant modifications; and Rick Whedbee for analyzing the combustion gases in the mock-up vehicle.

## TABLE OF CONTENTS

	Page
EXECUTIVE SUMMARY	xiii
1. OBJECTIVE	1
2. REPORT SUMMARY	1
2.1 Threat Scenarios	2
2.2 Occupant Fire Hazards	2
2.3 Characteristics of Ceiling Fires	2
2.4 Material Fire Properties	3
2.5 Pass-Fail Criteria	4
3. INTRODUCTION	6
4. FIRE THREAT SCENARIOS	7
5. FIRE HAZARDS FOR OCCUPANTS	10
6. EXPERIMENTAL RESULTS IN A SIMILATED VEHICLE FIRE	11
6.1 Experimental Mock-up of Vehicle Cabin	11
6.2 Design Fire Results	14
6.2.1 Temperature Results	15
6.2.2 Gas Results	16
6.2.3 Toxicity Results	17
6.2.4 Heat-Flux Results	19
7. ANALYSIS OF DESIGN HEAT FLUX	20
7.1 Case 1: Fire Below	21
7.2 Case 2: Ceiling Fire Alone	24
8. MODELS FOR IGNITION AND FLAME SPREAD	26
8.1 Will the Material Ignite?	26
8.1.1 Determination of CHF in flaming ignition	26
8.2 Time for Ignition	27
8.3 Flame Spread	28
9. PASS/FAIL CRITERIA FOR FIRE GROWTH	31

9.1	Case 1: Fire Below at 65 KW	31
9.2	Case 2: Ceiling Fire Alone	33
9.3	Summary	35
10.	METHODS TO DETERMINE MATERIAL PROPERTIES	35
11.	TOXICITY ASSESSMENT	38
11.1	FED <sub>f</sub> and FEC Methodologies	39
	11.1.1 FED <sub>f</sub> Equations	39
	11.1.2 FEC equations	40
11.2	Computation of Species Concentration for Flaming Period and 5 Minutes for Test Material	41
11.3	Validity Assessment of Formula Used for Concentration in Mock-up Compartment	42
	11.3.1 Temperature	42
	11.3.2 Species: CO and CO <sub>2</sub>	44
	11.3.3 Computation of the Species Concentrations for the Performance Criterion in the Engineering Analysis	46
12.	EXAMPLES OF MATERIAL DATA USING THE CONE CALORIMETER AND MOCK-UP COMPARTMENT	47
12.1	Material Results in the Mock-up Tests and Toxicity Assessments	48
12.2	Results and Processing of Cone Calorimeter Tests	55
	12.2.1 Determining HRP	55
	12.2.2 Determining TRP	56
	12.2.3 Determining CHF	57
	12.2.4 Determining the AEP	60
	12.2.5 Compilation	61
	12.2.6 Refinement of Results for Gray Foam	61
12.3	Critical Conditions Based on Scenario Heat Flux and Modeling Fire Growth	63
12.4	Toxicity Assessment from Cone Tests	64
	12.4.1 Methods of Gas Sampling and Analysis for Cone Tests	64
	12.4.2 Gas Yields for Cone Tests	65
	12.4.3 Predicted Mock-Up Vehicle Concentrations Obtained from Cone Tests	67
	12.4.4 Comparison of Gas Concentrations Predicted from Cone Tests Using Equation 61 and Concentrations Measured in the Mock-Up Vehicle and Cone Yields Scaled to the Vehicle Volume	69
	12.4.5 Toxicity Assessment in Test Vehicle Based on Cone Concentration Data	71

12.5	Performance in Other Flammability Tests	74
12.5.1	FAA/OSU Aircraft Cabin Lining Fire Test	74
12.5.2	ISO 9705 Room Corner Test	74
12.5.3	Estimation of Performance in the Steiner Tunnel Test, ASTM E 84	75
13.	CONCLUSIONS	76
14.	REFERENCES	80

## APPENDICES

A—TRANSPORTATION SECTORS FLAMMABILITY, SMOKE, AND TOXICITY PERFORMANCE CRITERION

B—FDS MODELING OF MOCK-UP TESTS BY HAI-QING GUO

## LIST OF FIGURES

Figure		Page
1	Typical combat vehicle wartime fire threats	7
2	Fire scenarios for the vehicle headliner	8
3	Energy release rate of 500 ml of heptane soaked in 30 cm diameter ceramic board	9
4	Sketch of mock-up cabin	12
5	Location of instrumentation	12
6	Mounted heat flux sensors: raw configuration installation and final thermal ceiling panel installation	13
7	Photographs of mock-up: Access door is closed during test	13
8	TARDEC “wood buck” model for fire testing	14
9	Ceiling flames: fire below and ceiling alone	14
10	Case 1 fire below, vertical temperatures: centered fire, near wall	15
11	Case 2 ceiling fire alone, vertical temperatures: centered fire, near wall	15
12	Case 1 fire below, vertical gas concentrations: centered fire, near wall	16
13	Case 2 ceiling fire alone, vertical gas concentrations: centered fire, near wall	17
14	Case 1 fire below, vertical FED <sub>1s</sub> : centered fire, near wall	18
15	Case 2 ceiling fire alone, vertical FED <sub>1s</sub> : centered fire, near wall	19
16	Heat-flux measurements for case 1: below fire	20
17	Heat-flux measurements for case 2: ceiling fire alone	20
18	Incident heat flux to ceiling from an axisymmetric fire plume	21
19	Experimental mock-up case 1 heat flux compared to theory	23
20	Correlations for flame radius in a ceiling fire	25
21	Correlation for heat flux for a ceiling fire in terms of flame radius, $L_f$	25
22	Comparison of measured heat flux and correlation for case 2	26
23	Relationship between the CHF for radiant and flame-heating at ignition	27
24	Example showing criteria for flame spread correlates flashover in ISO 9705 [10]	30
25	Approximation for the radial flame length of a fire plume impinging on a ceiling	32
26	Approximation for the radial flame extension for a ceiling fire	34
27	Critical flame spread HRP values for cases 1 and 2	35
28	Derivation of TRP and CHF from ignition data	37
29	Derivation of HRP from calorimeter data for polyurethane [9]	37



30	Variation of AEP with heat flux	38
31	Predicted gas temperature for centered fire below case 1 compared with data	44
32	Predicted concentration of carbon monoxide for centered fire below case 1 compared with mock-up test data	45
33	Predicted concentration of carbon dioxide for centered fire below case 1 compared with mock-up test data	46
34	Materials tested: headliner, white material, and gray foam	47
35	Temperature response with the 300 mL heptane fire igniting the material sections	49
36	Gas histories with the 300 mL heptane fire igniting the gray foam	49
37	Gas histories with the 300 mL heptane fire igniting the auto headliner	50
38	Gas histories with the 300 mL heptane fire igniting the white material	50
39	FED <sub>1S</sub> and V <sub>CO2S</sub> with the 300 mL heptane fire igniting the gray foam	51
40	FED <sub>1S</sub> and V <sub>CO2S</sub> with the 300 mL heptane fire igniting the auto headliner	51
41	FED <sub>1S</sub> and V <sub>CO2S</sub> with the 300 mL heptane fire igniting the white material	52
42	After-test photographs of burned materials	53
43	The damage area is shown for the gray foam: diameter of damaged area = 21" = 53.3 cm, radius = 26.7 cm	53
44	The damage area is shown for the DOT headliner: diameter of damaged area = 16" = 40.6 cm, radius = 20.3 cm	54
45	The damage area is shown for the white material: diameter of damaged area = 19" = 48.26 cm, radius = 24.1 cm	54
46	HRP from peakenergy release data from cone	56
47	TRP from ignition data	57
48	TRP and CHF for gray foam material	58
49	TRP and CHF for auto headliner	58
50	TRP and CHF for white material	59
51	HIPS flammability diagram	59
52	AEP for tested materials	60
53	Refined HRP determination for gray foam	61
54	Additional ignition data for gray foam	62
55	Refined CHF and TRP for gray foam	62
56	Refined AEP for gray foam	63
57	Ion chromatogram for gray foam sample: sample collected from the cone at 65kW/m <sup>2</sup>	65

58	Gas yields for gray foam run on the cone	66
59	Gas yields for auto headliner run on the cone	66
60	Gas yields for white material run on the cone	66
61	Comparison of cone gas yields for pure plastics: predicted assuming conservation of mass for N, Cl, F, and S versus 5-minute average for 35, 50, and 65kW/m <sup>2</sup>	67
62	Predicted mock-up vehicle concentrations for gray foam based on cone yields and equation 53 and 61 mass fractions	68
63	Predicted mock-up vehicle concentrations for auto headliner based on cone yields and equation 53 and 61 mass fractions	68
64	Predicted mock-up vehicle concentrations for white material based on cone yields and equation 53 and 61 mass fractions	68
65	Gray foam: comparison of CO and CO <sub>2</sub> concentrations in the mock-up vehicle with concentration obtained by applying equation 61 to the cone data at the assumed burn radius of 32 cm and the observed burn radius of 26.7 cm	69
66	Auto headliner: comparison of CO and CO <sub>2</sub> concentrations in the mock-up vehicle with concentration obtained by applying equation 61 to the cone data at the assumed burn radius of 32 cm and the observed burn radius of 20.3 cm	70
67	White material: comparison of CO and CO <sub>2</sub> concentrations in the mock-up vehicle concentration obtained by applying equation 61 to the cone data at the assumed burn radius of 32 cm and the observed burn radius of 24.1 cm	71
68	Comparison of toxicity models for asphyxiant gases using simulated vehicle gas concentrations obtained from 35, 50, and 65 kW/m <sup>2</sup> cone test average yields and equation 61	73
69	Comparison of toxicity models for irritant gases using simulated vehicle gas concentrations obtained from 35, 50, and 65 kW/m <sup>2</sup> cone test average yields and equation 61	73
70	Flowchart for test protocol to determine fire safety of a candidate head-impact material	79

## LIST OF TABLES

Table		Page
1	Canonical set of flammability parameters	36
2	Other materials tested	48
3	Cone data needed to develop properties	55
4	Material properties	61
5	Material pass-fail outcome	64
6	Comparison of toxicity results for various toxicity models for cone tests averaged for 35, 50, and 65kW/m <sup>2</sup> based on applying equation 61 to asphyxiant gas cone yields	72
7	Comparison of toxicity results for various toxicity models for cone tests averaged for 35, 50 and 65kW/m <sup>2</sup> based on applying equation 61 to irritant gas cone yields	72
8	Estimate of FAA/OSU performance, $\dot{q}'' = 65 \text{ kW/m}^2$ and $\dot{Q}'' \leq 65 \text{ kW/m}^2$	74
9	Estimation of performance in ISO 9705, $\dot{q}'' = 60 \text{ kW/m}^2$ and $\dot{Q}_{crit}'' = 50 \text{ kW/m}^2$	75
10	Estimation of performance in 25 ft (7.6 m) tunnel test $\dot{q}'' = 35 \text{ kW/m}^2$ and $\dot{Q}_{crit}'' = 100 \text{ kW/m}^2$	75
11	Estimation of performance in UL 94, $\dot{q}'' = 60 \text{ kW/m}^2$ and $\dot{Q}_{crit}'' = 300 \text{ kW/m}^2$ for V-0	76
12	Recommend Headliner Protocol	78

## LIST OF SYMBOLS AND ACRONYMS

$A$	Area
$c$	Specific heat
$D$	Diameter
$F_i$	Concentration of each irritant gas, $i$ expected to seriously compromise occupants' tenability
$g$	Gravitational acceleration
$k$	Thermal conductivity
$k\rho c$	Thermal inertia
$h_c$	Convective heat transfer coefficient
$H$	Height to ceiling
$\Delta h_c$	Heat of combustion
$\Delta h_{ox}$	Heat of combustion per unit mass of oxygen
$L$	Heat of gasification
$L_H$	Radial flame extension
$m$	Mass
$\dot{m}''$	Mass flux
$\phi_i$	Average concentration of an irritant gas species
$ppm$	parts per million (volume/volume)
$\dot{q}''$	Heat flux
$\dot{Q}''$	Energy release rate per unit area
$r$	Radius
$t$	Time
$T$	Temperature
$T_\infty$	Initial or ambient temperature
$v$	Velocity
$w$	axisymmetric fire plume impact
$X$	Mole fraction
$Y_i$	Species $i$ mass fraction
$Y_{ox,\infty}$	Oxygen mass fraction in the ambient
$z'$	<i>Virtual origin.</i>
$\rho$	Density
AEP	Available energy parameter
CFD	Computational fluid dynamics
CHF	Critical heat flux for piloted ignition
FDS	Fire Dynamics Simulator
FEC	Fractional effective concentration
$FEC_{crit}$	Fractional effective concentration, critical
$FED_I$	Fractional effective dose for incapacitation
$FED_{I,crit}$	Fractional effective dose for incapacitation, critical
$FED_{Ii}$	Fractional effective dose for incapacitation for a gas species
$FED_{I,Heat}$	Fractional effective dose for incapacitation due to convective heat
HRP	Heat release parameter
HRR	Heat release rate

OD	Outer Diameter
PFA	Perfluoroalkoxy fluoropolymer
SFPE	Society of Fire Protection Engineers
TARDEC	US Army Tank Automotive Research Development and Engineering Center
TRP	Thermal response parameter
$V_{CO_2}$	Multiplication factor for the enhanced uptake of other gases

### Subscripts

<i>a</i>	Ambient
<i>b</i>	Burning
<i>crit</i>	Critical
<i>f</i>	Flame
<i>I</i>	Incapacitation
<i>ign</i>	Ignition
$\infty$	Initial or ambient
<i>p</i>	Pyrolysis
<i>s</i>	Spread, surface
<i>v</i>	Vaporization

### Superscripts

$\dot{X}$	per unit time
$X''$	per unit area
$X'''$	per unit volume
$\bar{X}$	average value

## EXECUTIVE SUMMARY

This study was conducted for the United States Army Tank Automotive Research Development and Engineering Center by the FAA with the goal of developing fire safety performance requirements for ceiling materials designed to cushion head impact in combat vehicles. The approach was to identify combat fire threats to military-vehicle ceiling-liner materials, quantify hazards to the occupants associated with the fire threat; characterize the fire-threat model, measure fire growth of ceiling-lining materials for a representative vehicle and fire threat; determine which material properties govern fire growth; and use these properties in fire-performance criteria that will ensure the safety of combat vehicle occupants for at least 5 minutes. The performance criteria include recommended safety factors to favor an increased degree of safety. A survey of fire-safety requirements for public transportation and military vehicles was also conducted.

Engineering analysis, bench-scale fire tests, and full-scale tests of ceiling materials in a representative military vehicle compartment were conducted at the FAA William J. Hughes Technical Center, Atlantic City Airport, NJ. As a result of these studies, the following material fire performance safety criteria are recommended for head-impact mitigating materials used in military combat vehicles.

The test protocol is as follows: The ceiling lining material should be tested in a bench scale fire calorimeter operating on the oxygen consumption principle according to a standard method (ASTM E 1354-15) at several external heat fluxes in the range of 5–75 kW/m<sup>2</sup> and the time-to-ignition,  $t_{\text{ign}}$ , (seconds) and heat release rate (HRR) (kW/m<sup>2</sup>) history recorded for the duration of flaming combustion to determine ignitability and flame-spread characteristics of the material. The combustion gases should be collected for only the period of flaming combustion at an external heat flux of 50kW/m<sup>2</sup> to determine the yields of toxic gases. The driving force for flame spread on the burning material at the ceiling will be the difference between the heat flux from its flame ( $\approx 30$  kW/m<sup>2</sup>) and the minimum heat flux for it to ignite (i.e., critical heat flux for piloted ignition [CHF]). The following sequence will comprise the selection process for vehicle headliners exposed to a combat fire threat to ensure that ignition does not occur, or flames do not spread over the vehicle compartment ceiling causing hazardous conditions. Meeting the ignitability criterion or the flame spread and the toxicity criteria qualifies the material for use as a headliner in military combat vehicles.

### IGNITABILITY

1. The material will not ignite if the measured CHF is greater than the heat flux from the fire threat, which is assumed to be  $\text{CHF}_{\text{crit}} = 30 \text{ kW/m}^2$ . The CHF is determined by a bracketing procedure described in ASTM E 1354-15. If CHF is less than  $\text{CHF}_{\text{crit}}$ , the material will ignite, and the thermal response parameter (TRP) will determine the ignition delay.
2. If TRP is greater than  $\text{TRP}_{\text{crit}} = 350 \text{ kW-s}^{1/2}/\text{m}^2$ , the material will take more than 2 minutes to ignite, after which flame spread and toxicity will determine the fire hazard. The TRP is obtained as the slope of a line fitted to the square root of the measured time-to-ignition ( $\sqrt{t_{\text{ign}}}$ , s<sup>1/2</sup>) on the ordinate versus the reciprocal of the external heat flux on the abscissa ( $1/q_{\text{ext}}$ , m<sup>2</sup>/kW).

IGNITABILITY CRITERION:  $\text{CHF} > \text{CHF}_{\text{crit}}$  or  $\text{TRP} > \text{TRP}_{\text{crit}}$

## FLAME SPREAD

1. The heat release parameter (HRP) is the slope of a line fitted to the maximum/peak heat release rate during the test (i.e., peak heat release rate, kW/m<sup>2</sup>) on the ordinate versus the external heat flux ( $q_{ext}$ , kW/m<sup>2</sup>) on the abscissa. Based on a determination that HRR = 70 kW/m<sup>2</sup> is needed for ceiling flame spread, the critical HRP for flame spread is  $HRP_{crit} = 70 \text{ kW/m}^2 / (30\text{-CHF})$ .
2. The material has the potential to spread flames along the ceiling if the fuel load, also called the available energy parameter (AEP) (kJ/m<sup>2</sup>) is greater than  $AEP_{crit} = (HRP)(TRP)2(30\text{-CHF})/900 \text{ kW}^2/\text{m}^4$ , where HRP is the dimensionless HRP. The AEP is the area under the HRR versus time curve after flaming has ceased and represents the maximum heat that can be generated by burning.

FLAME SPREAD CRITERION:  $HRP < HRP_{crit}$  or  $AEP < AEP_{crit}$

## TOXIC POTENCY OF SMOKE

The toxic potency of the smoke is computed from the yields of the asphyxiant gases (e.g., carbon monoxide, carbon dioxide, and hydrogen cyanide) and the irritant gases (e.g., hydrogen chloride, hydrogen bromide and hydrogen fluoride, nitrogen dioxide, and sulfur dioxide) obtained by sampling the gases during flaming combustion of the sample at  $q_{ext} = 50 \text{ kW/m}^2$  in the cone calorimeter, run in accordance with ASTM E 1354-15.

1. Fractional effective is obtained by applying the FAA survival model to the concentration for each gas. CO<sub>2</sub> multiplication factor for the enhanced uptake due to the presence of CO<sub>2</sub> is applied to the concentration term of each gas in this model
2. Incapacitation is predicted to occur when the sum of the fractional effective doses of asphyxiant combustion gases  $FED_I$  is equal to the critical fractional effective dose for incapacitation  
 $FED_{I,crit} = 0.3$  after 5 minutes in the vehicle.

ASPHYXIAN GAS CRITERION:  $FED_I < FED_{I,crit} = 0.3$

3. The fractional effective concentration (FEC) of the irritant gases is computed from the sum of the average concentration of each gas divided by its tenability endpoint  $F_i$ .
4. Irritant effects are predicted when the sum of the FEC of irritant combustion gases. FEC is equal to the FEC critical ( $FEC_{crit}$ ) = 0.3 after 5 minutes in the vehicle.

IRRITANT GAS CRITERION:  $FEC < FEC_{crit} = 0.3$

The time when either  $FED_I$  or  $FED_{crit}$  reach a specified critical threshold  $FED_{I,crit}$  or  $FEC_{crit}$ , respectively, determines the time to compromised tenability relative to the chosen safety criteria.

## 1. OBJECTIVE

A test protocol was requested to measure the fire thermal and toxicity hazard of ceiling-cushioning materials in the occupant compartment of an armored military vehicle, subject to accidental or wartime fire-ignition incidents. The ignition threat should not be a significant hazard to the occupants, and material acceptance criteria must be rational.

## 2. REPORT SUMMARY

This report summary is included for the reader to gain an overview and summary of the details in this comprehensive report. It contains the main features of the study, allowing the reader to appreciate the process of developing a fire-test protocol by engineering design. There are considerable details in the report involving tests, data, mathematical analyses, and decisions to skew the results toward a more conservative endpoint. In addition, the appendices contain the application of computational fluid dynamics (CFD) modeling to scenario fire tests, and a compilation of common tests and regulations currently used in various transportation sectors.

The US Army Tank Automotive Research Development and Engineering Center (TARDEC) supported this study. The overall objective is to develop a fire test protocol and acceptance criterion to assess the fire thermal and toxicological threats to vehicle occupants under combat and accident conditions. The specific project objective is directed at ceiling materials designed to cushion head impact. Visibility due to smoke and automatic fire suppression were not considered in this study.

A concern of the Army was to address the rationale of the test protocol. In previous considerations, many fire tests were identified, but none demonstrated a clear, if any, connection to the scenario of a ceiling fire and its hazard to vehicle occupants.

Consequently, the approach taken here was to establish a protocol based on the scenario of a vehicle ceiling fire. An engineering design approach was used. Although many fire tests exist, it is believed this is the first time a test has been developed to fit the fire scenario threat by analysis. In the past, test methods have been developed distinct from the scenario, and rating systems for determining a material's acceptance were empirically established based on judgment, past tradition, or alignment with full-scale scenario experiments.

In the past, with little science to ground the foundation of a fire test, it was acceptable to endorse its standing in fire regulations. However, the existence of many different tests and regulations among agencies in the US and countries worldwide makes it cumbersome for commerce and society. The current approach is a step to change this state of fire testing.

Over the past 50 years, a scientific foundation has been established for fire. Its scope and depth is manifested in the Society of Fire Protection Engineers (SFPE) Handbook of Fire Protection Engineering [1,2] and other literature and publications. This study relies on the SFPE body of work along with specific experiments conducted. The body of this report elaborates on the details of the process. A summary is presented focusing on the following key points:

1. Identification of the threat scenarios
2. Specific fire hazards to the occupants
3. Characteristics of the threat fires



4. Scenario modeling using material properties
5. Pass-fail criteria

## 2.1 THREAT SCENARIOS

In a combat vehicle, the fire-threat scenarios to a ceiling material can be accidental or combat related. Only survivable crew thermal attacks will be considered viable and relevant to a material test. Non-survivable weapon attacks do not apply. The design attack fire for the test should be a substantial ignition source for the ceiling. Two fires were defined:

- Case 1: Fire below the ceiling with no harm to the crew
- Case 2: Developing ceiling fire alone

The fire threat from below must be of no harm to the crew, must impinge with a flame on the ceiling, and should represent a worst-case fuel.

Case 1 Design fire: 65 kW from a 30 cm diameter pool, 76 cm below the ceiling (representative of heptane).

Analyses and experimental data demonstrated occupant tolerance to this fire.

## 2.2 OCCUPANT FIRE HAZARDS

Two fire hazards were considered with respect to the crew. First was the thermal hazard due to fire growth. It was decided that flame spread over the ceiling would not be allowed. The second hazard was the toxicity level of the combustion gases to the crew. The asphyxiant gases (e.g., CO, CO<sub>2</sub>, and HCN) would be considered along with the effects of acid gases. It was decided that the crew should be fully functional in a typical vehicle for up to 5 minutes. In the course of discussions with the sponsor when conducting vehicle simulation fires, it was decided that the test mock-up vehicle was a worst-case cabin because of its small size and limited vents. The cabin selected for evaluating the 5-minute toxicity criteria is specified as a steel chamber: 2.2 x 3.2 x 2 m high with 61 x 15.3 cm high-top wall vents.

## 2.3 CHARACTERISTICS OF CEILING FIRES

Mock-up test fires and studies in the literature on ceiling fires established the characteristics of the ceiling fire in a compartment. In the developing stage of a compartment fire (as applicable here), fire growth on a material is governed by the heat flux received from its own flame. Cases 1 and 2 portray two distinct types of flames. Case 1 gives a buoyant plume flame in combination with the burning ceiling. This is a radial-driven boundary-layer flame with sharply decreasing velocity and, therefore, decreasing heat flux. Case 2 has an entirely different flame. It is made up of cellular flames of boundary layer depth indicative of the Rayleigh instability of a cold gas (fuel) above a hot gas (flame). The flame extension and heat flux distributions for cases 1 and 2 are very different. Fortunately, they have been studied by Hasemi and coworkers [1–4].

Based on the literature, and consistent with the mock-up tests, the average heat flux over the design fire of case 1 can be represented as:

$$\bar{q}_{65kw}'' = 25 \text{ kW/m}^2. \quad (1)$$

In general, the heat flux for a pool fire 76 cm below the ceiling is:

$$\bar{q}'' = \frac{0.211 \dot{Q}^{0.1}}{(r + 0.76)^{3.3}} \text{ in kW, m} \quad (2)$$

and  $L_H$  shows its sharp decrease with radius. The flame radial extension is:

$$L_H = 0.269 \dot{Q}^{1/3} - 0.76 \approx 0.06 \dot{Q}^{1/2} \text{ kW, m} \quad (3)$$

with  $\dot{Q}$  as the total energy release rate of the design fire and the ceiling fire.

For case 2, the average heat flux is:

$$\bar{q}'' = 5.4 \dot{Q}^{0.36} \text{ in kW, m} \quad (4)$$

and its radial flame extension is:

$$L_H \approx 0.126 \dot{Q}^{1/2} \text{ kW, m} . \quad (5)$$

These results developed from the literature were generally corroborated in the mock-up experiments.

## 2.4 MATERIAL FIRE PROPERTIES

The test protocol is based on a measurable set of properties that:

1. Do not allow flame spread over the ceiling, and in the event of ignition of the ceiling there is no flame spread.
2. Do not allow incapacitation or a substantial performance decrement within 5 minutes.

The relationships among the properties are based on the principles of fire physics and toxicity benchmarks for humans.

First, the relevant fire properties will be enumerated. These properties have all been demonstrated to be reasonably constant and signatures of a particular material or end-use product. The literature [1–2, 5–13] contains many examples and demonstrations of their development and tabulation for both simple and complex products. It is emphasized that these properties should be measured during the flaming phase and established from data over peak burning conditions. The properties must also be established by a sufficient set of data over a range of incident radiant heat fluxes as measured in apparatus, such as ASTM E 1354 or E 2058.

The properties and their descriptions are below:

- The critical heat flux (CHF) for piloted ignition controls whether ignition does occur. It can be found by identifying the minimum incident radiant heat flux to cause piloted ignition with a sustained flame by testing at different radiant heat fluxes. It is directly related to the ignition temperature of the material.
- The thermal response parameter (TRP) controls the time-to-ignition under a given heat flux. It is directly related to the ignition temperature of the material along with its thermal properties: conductivity, density, and specific heat.
- The heat release parameter (HRP) controls the rate of energy released in fire per unit area. On average, it is the heat of combustion divided by the heat of gasification, or energy of combustion per energy required.
- The available energy parameter (AEP) controls the burning time. It is commonly recorded in ASTM E 1354 as the total energy in MJ/m<sup>2</sup> of material. It relates to the heat of combustion and material thickness.
- Yield of species,  $y_i$ , in a fire is given in terms of mass of species produced per mass of fuel lost. Here the well-ventilated values for flaming combustion are specified as the developing fire is considered. For under-ventilated flaming fires, each yield of an incomplete product increases as less air is available.

These properties can vary for a material depending on the process used to derive the property. However, in general, for a given material, they can be regarded as fixed within an acceptable range of experimental variation, depending on accuracy and the reduction process.

In recent years, fire scientists have moved beyond these simple properties to include more chemical properties for the decomposition of materials in fire. A test protocol based on such advanced properties is not practical or feasible. The simple properties listed here are robust and sufficient to categorize a material in fire.

## 2.5 PASS-FAIL CRITERIA

These properties govern the outcome of fire hazard conditions in a particular fire or even test method. Relationships between the properties and certain common fire tests are discussed in this report. The main objective is how they relate to the combat vehicle ceiling material and what values they should comprise to be safe within the specifications. It was found that case 1 presents a more severe condition over case 2 and, therefore, case 1 forms the basis of the final results. Modeling with respect to the specified hazard conditions is expressed in terms of the following relationships:

The material should not ignite:  $\text{CHF} > \text{CHF}_{crit} = 25 \text{ kW/m}^2$ , and material passes;

or:

The material will ignite after 2 minutes subject to the design fire:  $\text{TRP} > \text{TRP}_{crit} = 274 \text{ kW-s}^{1/2}/\text{m}^2$ , and passes;

or:

The region ignited does not cause incapacitation of the occupants during 5-minute exposure:  $FED_I < FED_{I,crit} = 0.3$ . The species mass fractions are computed from their yields for a prescribed ignited radius of 0.32 m (based on the flame extension for the ignition heat flux) by:

$$\begin{aligned}
 Y_i &= 0.0193 AEP (y_i / \Delta h_c) \\
 &\text{or in molar concentration (\%), } X_i \\
 X_i &= 28 Y_i / (MW_i) \times 100\%.
 \end{aligned}
 \tag{6}$$

and:

The region ignited does not cause significant eye irritation or upper-respiratory tract irritation for the occupants during a 5-minute exposure that can impede escape or adversely affect the warfighters from performing their mission: fractional effective concentration (FEC) < fractional effective concentration, critical ( $FEC_{crit}$ ) = 0.3

and:

The region ignited does not lead to rapid flame spread over the ceiling:

$$HRP < HRP_{crit} = 140 / (30 \text{ kW/m}^2 - CHF) \tag{7}$$

or

$$AEP < AEP_{crit} = TRP^2 (30 - CHF) HRP / 900 \text{ kJ/m}^2, \text{ and material passes.} \tag{8}$$

Judgment on acceptable values of the critical parameters must be considered in a regulation. This analysis has included approximations, and no safety factors have been introduced. A suggestive modification of the critical values based on their accuracy and safety factors commensurate with scientific uncertainties are put forth as follows:

$$CHF_{crit} = 30 \text{ kW/m}^2 (+ 20 \%) \tag{9}$$

$$TRP > TRP_{crit} = 350 \text{ kW-s}^{1/2}/\text{m}^2 (+20 \%) \tag{10}$$

$$HRP_{crit} = 70 / (30 \text{ kW/m}^2 - CHF) (-50 \%) \tag{11}$$

$$AEP_{crit} = TRP^2 (30 - CHF) HRP / 900 \text{ kJ/m}^2 \text{ (no change)} \tag{12}$$

$$FED_{I,crit} = 0.3 \tag{13}$$

$$FEC_{crit} = 0.3 \tag{14}$$

### 3. INTRODUCTION

The U.S. Army is considering requirements to mitigate head-impact injury in a military vehicle interior space for vehicle occupants (mounted crew/warfighter). The intent of the requirements is to generate interior head-impact protective-vehicle-component designs and material selection, which are capable of withstanding high-velocity, multidirectional forces associated with blast, crash, and rollover events. The headliner material used for impact protection must also ensure fire safety for the occupants and not present a fire hazard by itself. Although the rate of occurrence of military-vehicle fires may be low, the severity of potential injury or even death to mounted crews, once a fire does occur, is high. The addition of large overhead roof materials poses new potential fire-related hazards, such as crew skin burns and internal lung damage, smoke and toxic fume incapacitation, and egress hindrance.

The purpose of this study is to design a testing protocol to ensure a reasonable degree of fire safety to the occupants. Both the flammability and fire-toxicity aspects of head-protection materials are considered.

Although many flammability tests and some toxicity protocols exist, they are not justifiably connected to a particular fire-hazard scenario. The measure of safety is expressed in the test-rating index and is not relatable to a direct level of safety for the threat scenario. A summary of tests in the civilian and military transportation sectors for the measurement and regulation of interior-use materials is listed in appendix A. These tests are founded on historical development, and few, if any, of their regulatory requirements can be translated into fire-hazard performance for the material's end use.

In this study, perhaps for the first time, an engineering-design approach will be used to link the test-performance measures with specific levels of fire safety in the scenario. Judgments will be made to arrive at design standards, but such judgments will not diminish from the engineering validity of the results. Their transparency will enable substitute judgments to be imposed because safety criteria might need adjusting.

The design approach taken here is based on the premise that materials have properties that relate to their fire growth and the production of species in smoke. This has been well established by Tewarson [1] and others. Indeed, fire modeling uses these properties to predict the fire growth and toxic nature of smoke. The measurement of the fire properties will use standard test devices, such as ASTM E 1354, the cone calorimeter [14], or ASTM E 2058, the FM Fire Propagation Apparatus [15]. Fire modeling will use specific formulas from the literature [2, 5, 16].

The design process used here will consist of specific elements:

- Fire threat scenarios are considered for the interior of combat vehicles.
- Fire hazards for the occupants are established.
- Heat flux levels are determined for the threat scenarios.
- Specific properties are identified for measurement, and their method of determination is established.
- Based on the safety criteria, an acceptable set of material properties levels are established.

#### 4. FIRE THREAT SCENARIOS

The focus is on the means in which a fire can occur within the cabin space of the vehicle. Survivable wartime attacks are considered, and interior artillery shell blasts are excluded. In the scenarios, no vehicle extinguishing system was considered to be activated. The fire threat for the ceiling impact material is considered with the vehicle standing upright. The material is evaluated as a ceiling fire.

McCormick [17] presented a variety of fire threats to combat vehicles. Some of his photographs are listed in figure 1. These included interior fireballs from weapons and external fires from weapons. For this study, the hazard from the ceiling material is the exclusive threat, although it is likely to occur from a weapon attack.



**Figure 1. Typical combat vehicle wartime fire threats**

The ignition sources for the ceiling material are considered to be accidental in nature or the result of wartime involvement. Ignition sources will not include:

- A fireball from a weapon or fuel breach.
- A large sudden fire that threatens occupants.

Accidental ignition sources will include:

- Electrical high-resistant fault in contact with the headliner material.
- Spill of flammable liquid resulting in a flame touching the ceiling.
- Occupant ignition of seat or other combustibles that can result in flame touching ceiling.

Incendiary weapon ignition sources will include:

- External fire from tires, fuel spill, Molotov cocktail, or improvised explosive device.
- Fire that can enter cabin from below due to breach.
- Resulting cabin fire with a flame impinging on the ceiling.

The headliner-igniting fire shall not be a threat to the occupants. However, it should be sufficient in size to have the capability of igniting a headliner material. It can start exactly at the ceiling and be promoted as a sole ceiling fire, or it can start from a fire below the ceiling that initially can promote the ceiling fire-spread with impingement on the ceiling. The two fire-growth scenarios are shown in figure 2.

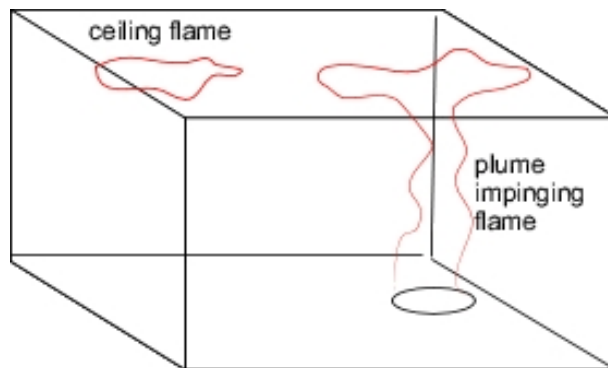


**Figure 2. Fire scenarios for the vehicle headliner**

The “fire-below” scenario considers a real fuel fire with its flame impinging on the ceiling. Without that impingement, there would not be a pilot flame to enable ignition, and the heat flux would not be sufficient to cause auto-ignition of a ceiling material. The selection of this design threat fire is somewhat arbitrary. It must impinge and be realistic. A worst-case fuel is selected as heptane because anything less would not have flame impingement. This is judged by the fact that for a given diameter pool fire, the energy release rate from combustion controls the flame height, and that energy is directly related to the fuel’s heat of combustion divided by the heat of gasification. This ratio is the HRP and is 85 for heptane. Most other liquid fuels have smaller values, and plastics range from approximately 1–35. By experiment, a 30-cm-diameter heptane pool fire gave flame

impingement radius of at least 25 cm along the ceiling when at a distance below the ceiling of 76 cm (30 inches).

The design fire below was chosen as a 30-cm heptane-soaked 1.2 cm low-density ceramic board burning 76 cm below the ceiling. Figure 3 shows the experimental results for 300 and 500 ml of heptane. The burning rate and energy release rates decrease exponentially over time, as shown. A heat of combustion for heptane was taken as 41.2 kJ/g. A 65 kW fire is maximum for the heptane and will be taken in design. The extent of flame impingement and its heat flux on the ceiling will determine the potential for ignition and spread. The heat flux will be measured and theoretically incorporated into design. In summary, the fire threat below is designed as:

65 kW at 76 cm below the headliner material.

Although the experimental heptane fire decreased over time, the design fire for the protocol is taken as constant over time, in the analyses to follow, for determining the critical material property relationships.

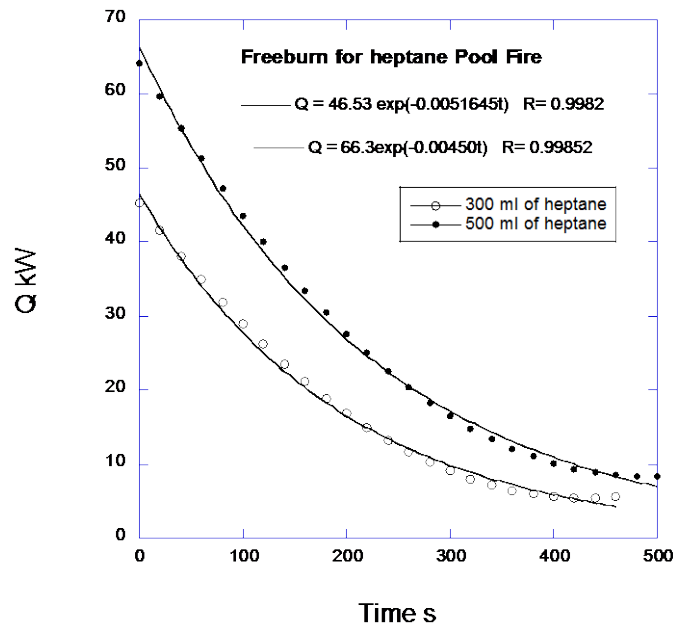


**Figure 3. Energy release rate of 500 ml of heptane soaked in 30 cm diameter ceramic board**

For experimental purposes, the fire at the ceiling will also be represented as a 30-cm diameter heptane-soaked disc. However, studies on ceiling fires will show that the heat flux for such fires is primarily determined by flame radius. The heat flux is similar to the flame radius. The flame radius is determined by the energy release rate of the burning ceiling. The heat-flux levels found in the literature will be confirmed by experiments in this study.



## 5. FIRE HAZARDS FOR OCCUPANTS

For the fire-below scenario, the design igniting fire is not to be a threat to the occupants. The threshold radiant heat flux to bare skin for a first-degree burn is  $1.7 \text{ kW/m}^2$  [3]. A 65 kW heptane fire (radiant fraction of 0.40) will give an exposure radiant heat flux of  $1.7 \text{ kW/m}^2$  at 1.22 m radially away from this design fire. Occupants positioned more than 1.22 m away from this internal design vehicle fire would not be considered at risk of getting burned. The piloted ignition threshold for common materials is generally considered approximately  $10 \text{ kW/m}^2$  for thin materials and higher for thick materials. Therefore, clothing and other materials should not be at risk for ignition with this design fire. In section 6.1, a mock-up of a small combat vehicle interior shows there is no heat threat from the design fire to occupants sitting in the vehicle. This heptane fire also does not place the occupants at risk for toxicity.

The hazard to the occupants considered here is to be comprised solely of the combustion of the headliner material. The hazard is twofold: thermal and toxic. The thermal threat would be radiant heat and hot gases from ignition of the ceiling and its continued spread. Sustained flame spread cannot be allowed.

A material would not be a thermal threat if flame spread is not possible under the “fire-below” or the “ceiling-alone” scenario.

Under the “fire-below” scenario, flame spread would not occur if ignition did not occur in 2 minutes. It is reasoned that the occupants would reduce or extinguish the attacking fire in that time.

The threat from toxicity would be more complex for a given material. It was decided that the occupants would need up to 5 minutes before they could exit the vehicle after the fire event.

Two toxicity models are used to assess survivability:

1. An incapacitation model is used to obtain a fractional dose for incapacitation ( $FED_I$ ). Asphyxiant gases and convective heat contribute to this dose. The effect of carbon dioxide on respiratory uptake of asphyxiant gases is included in this model.
2. An irritant model is used to obtain an FEC. The effects of eye and upper-respiratory-tract irritation can affect the performance of the warfighter and escape efficiency.

When  $FED_I = 1$  or  $FEC = 1$ , incapacitation or performance decrement respectively is predicted for 50% of the population.

A critical threshold of 0.3 for each endpoint accounts for sensitive individuals. The threshold can be set lower for the additional level of safety that may be needed for effective combat in war.

The time when either  $FED_I$  or  $FEC$  reaches a specified critical threshold  $FED_{I,crit}$  or  $FEC_{crit}$ , respectively, determines the time to compromised tenability relative to chosen safety criteria.

The hazard to the occupants was computed from the  $FED_I$  and  $FEC$  formulas based on convective-heat and gas-concentration histories in a small compartment with typical natural ventilation.

The toxicity models are discussed in greater depth in Section 11.1.

## 6. EXPERIMENTAL RESULTS IN A SIMILATED VEHICLE FIRE

The driving force for fire growth and the production of smoke and toxic gases is the heat flux the fuel material receives. The heat flux controls whether ignition will occur and whether the fire will continue and spread. The material being assessed for its potential fire hazard needs to be evaluated in the context of its use. The headliner is evaluated as a ceiling material. The two scenarios considered are a “fire-below” and a “ceiling alone” fire. The heat flux relevant in these scenarios must be established. These heat fluxes can be determined by experiment and by using available formulas in the literature. Both will be used. The SFPE Handbook [2] contains a chapter on heat flux in fire, authored by Lattimer, in which many formulas were developed by Hasemi and coworkers. These formulas will be used. In addition, an experimental mock-up of a small combat vehicle cabin was conducted to confirm the heat fluxes and their behavior, as found in the literature. Once confirmed, the literature formulations were used to more fully express the heat flux as a function of position under the flame radius.

### 6.1 EXPERIMENTAL MOCK-UP OF VEHICLE CABIN

The two fire scenarios were examined in a small representation of a typical crew cabin of a military vehicle. The objective was to establish the environment to the crew under the two scenarios. The baseline design fires selected need to be no serious threat to the crew. This was confirmed in the tests to be discussed with respect to temperatures and gas-concentration exposures to low crew locations in the mock-up. The small size of the mock-up would present these tests as a worst case in the array of combat test vehicles.

A steel compartment that had been used as a hardened aircraft cargo container was modified for use. A suspended flat ceiling of 2 x 3 feet, ceramic low-density, ½-inch-thick board was constructed to hang on a steel grid. The suspension allowed for two water-cooled heat-flux sensors to be mounted flush with the ceiling to measure the incident flame heat flux in the two scenarios. Figure 4 shows a sketch of the mock-up. Figure 5 shows a two-dimensional view with the locations of measuring instruments. A vertical array of 12 thermocouples traversed from near 1 inch of the suspended ceiling to within 1 inch of the compartment’s floor with interspersed spacing of approximately 6 inches (15 cm). Gas products were sampled at three vertical locations to measure the concentrations of oxygen, carbon dioxide, and carbon monoxide. The heat-flux sensors were mounted (see figure 6) at the center of the baseline fire for each scenario and 25 cm off-center. Figure 7 shows two photographs of the steel mock-up. It is common that a combat vehicle would have hatches or doors for egress, but all would have two fully open vents on the forward wall at ceiling level. These were incorporated into the mock-up to provide natural ventilation during the fire tests. These are shown in figure 4.

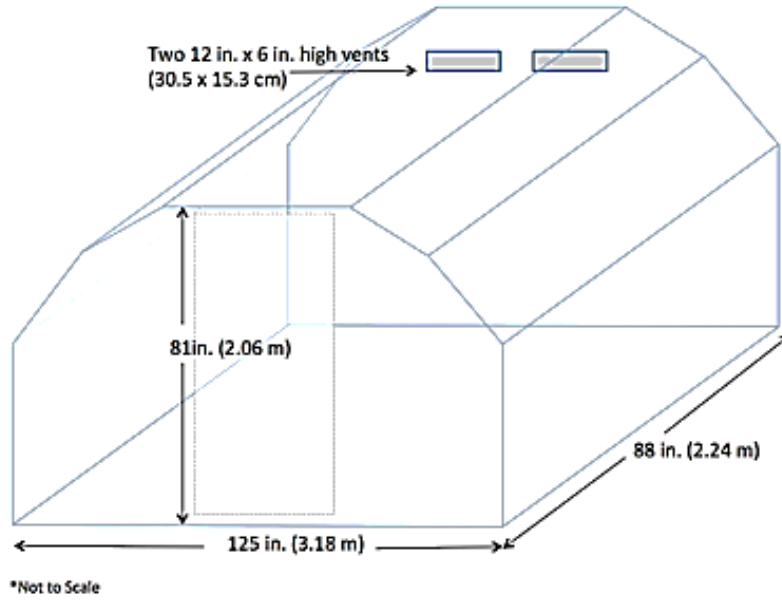


Figure 4. Sketch of mock-up cabin

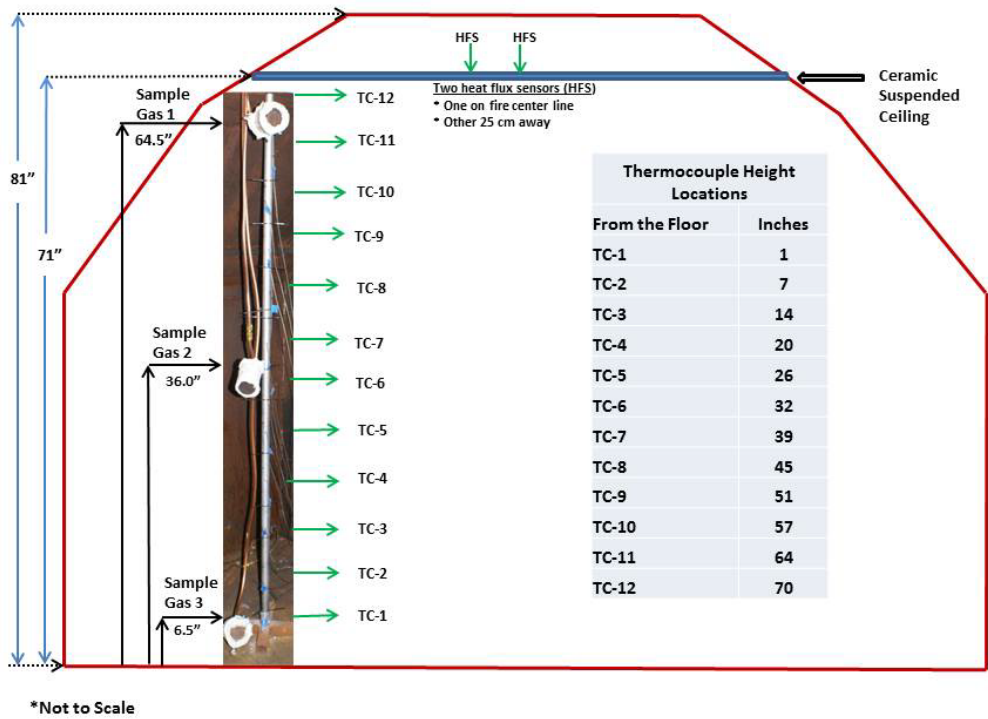
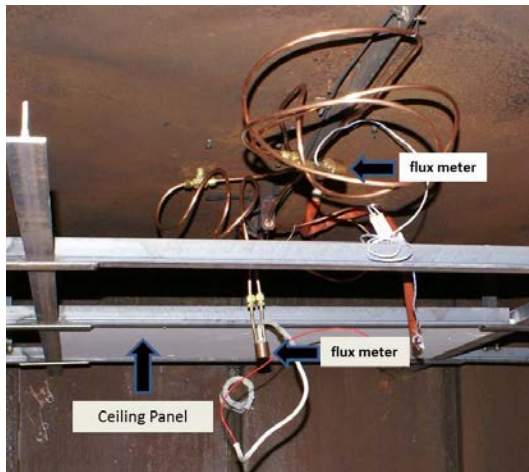
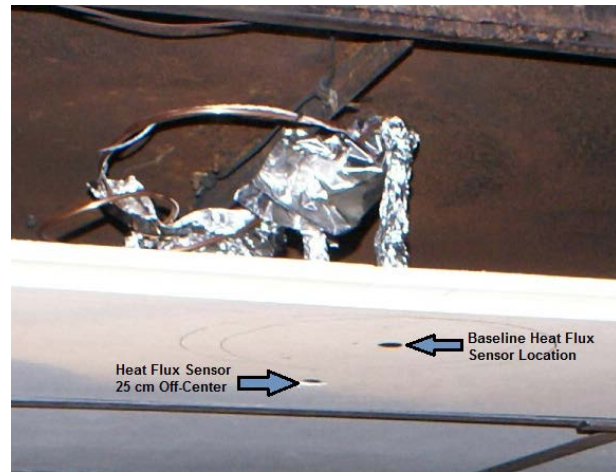


Figure 5. Location of instrumentation



(a)

Raw configuration installation



(b)

Final thermal ceiling panel installation

**Figure 6. Mounted heat flux sensors: (a) raw configuration installation and (b) final thermal ceiling panel installation**



**Figure 7. Photographs of mock-up: Access door is closed during test**

Nominally the mock-up had a floor-to-ceiling distance of approximately 1.8 m and a floor area of roughly 2.2 x 3.2 m. The approximate volume is 12 m<sup>3</sup>. A TARDEC “wood buck” container for simulating vehicle fires (see figure 8) has exterior dimensions of: width: 125 inches (3.2); length: 288 inches (7.3 m); and height: 94 inches (2.4 m). The interior height and width dimensions of the current test mock-up are similar to the TARDEC model.



**Figure 8. TARDEC “wood buck” model for fire testing**

## 6.2 DESIGN FIRE RESULTS

Two design fires are considered: 1) fire below, and 2) ceiling alone. In the first case, the ceiling fire is driven by a 30 cm diameter, 500 ml heptane-soaked, 1.2 cm low-density ceramic board burning 76 cm below the ceiling. In the second case, the heptane-soaked 30 cm diameter board is mounted flush with the ceiling. The heptane is covered with thin plastic wrap before ignition to prevent evaporation. The two cases are shown in the photographs of the ceiling flames taken through a front vent (see figure 9). For case 2, one heat-flux sensor is mounted at the center of the 30 cm disc. For both cases, the flame extended beyond the heat-flux sensor located 25 cm off-center. In this arrangement, the heat flux sensors would measure the flame incident heat flux at the center and at a radius of 25 cm. For case 1, the heat flux would correspond to the fire below. In a real event, that igniting fire would attack the headliner material and potentially cause it to ignite and possibly spread. For case 2, the ceiling would have been ignited by intentional or accidental means, and the heat fluxes measured would determine if continued flame spread would occur. Based on properties of a headliner material, the appropriate heat-flux distribution would determine if it could be ignited and could spread.



**Figure 9. Ceiling flames: (a) fire below and (b) ceiling alone**

For each design fire, two configurations were examined. The first is a fire just adjacent to the wall opposite the vents. The second is a centered fire. For each, the array of thermocouples and the gas sampling station (see figure 5) were away from the fire.

### 6.2.1 Temperature Results

Figure 10 shows the results for case 1 (below fire) with the fire centered and adjacent to the rear wall. Figure 11 shows the results for case 2 (the ceiling fire alone).

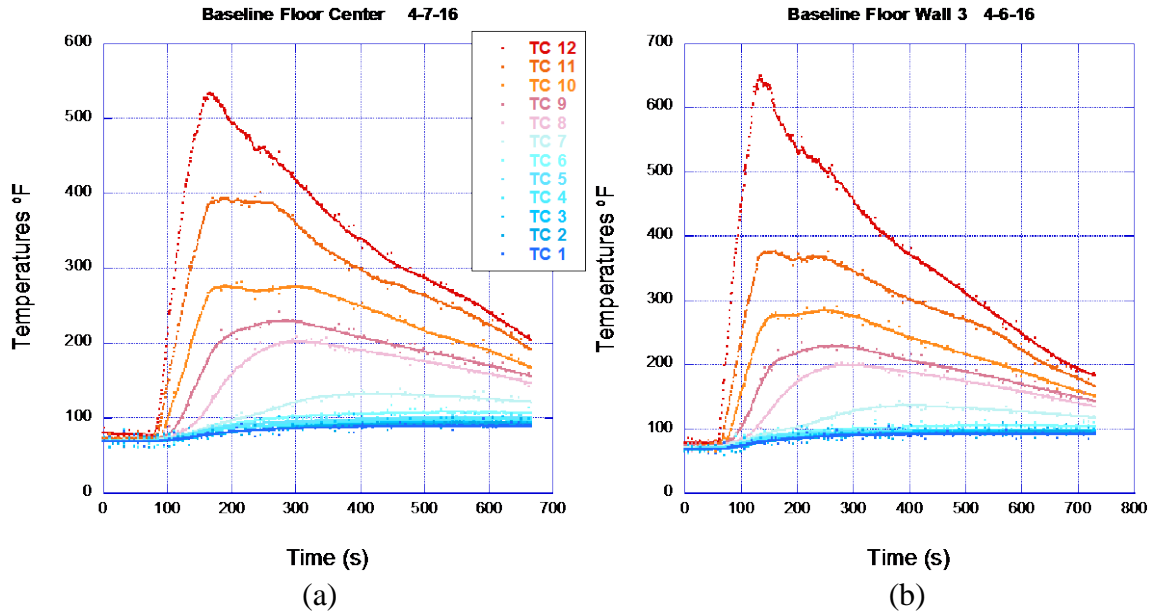


Figure 10. Case 1 fire below, vertical temperatures: (a) centered fire, (b) near wall

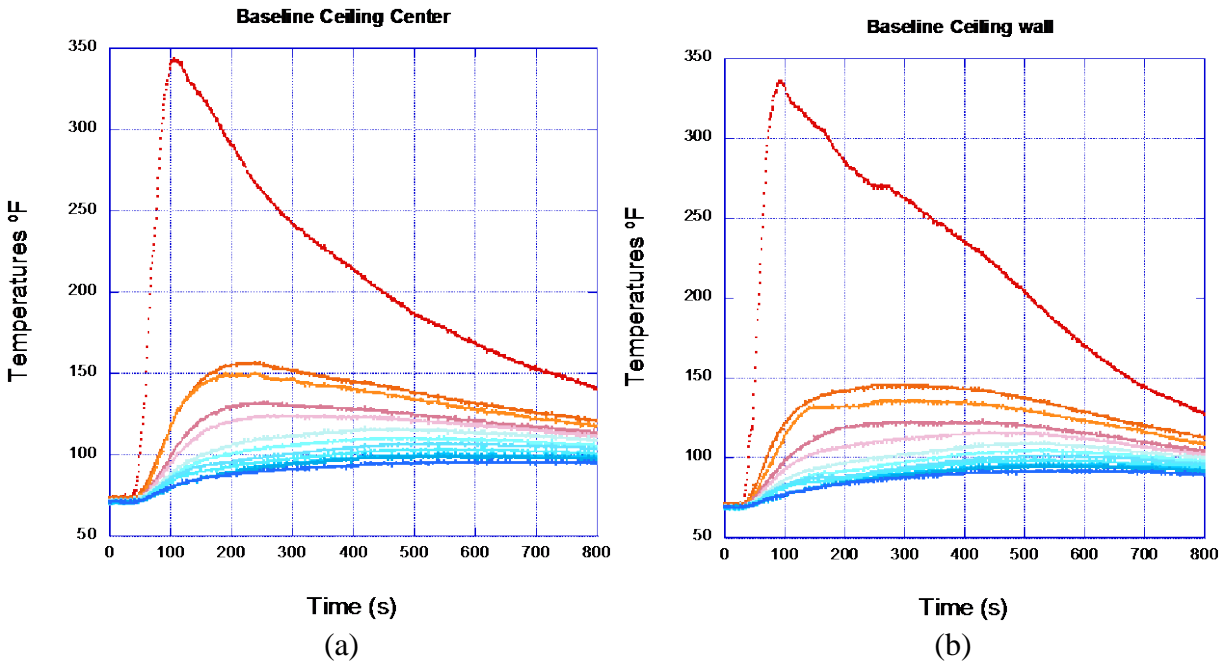


Figure 11. Case 2 ceiling fire alone, vertical temperatures: (a) centered fire, (b) near wall

In all cases, the temperatures below 32 inches (0.81 m) from the floor (TC 6) are below 120 °F (49 °C). It can be judged that the baseline design fires are not significantly harmful to occupants, especially for 5 minutes (300 s) duration.

### 6.2.2 Gas Results

The corresponding gas concentration histories are shown in figures 12 and 13. All plots were corrected for sample line delays only. Ignition occurred at approximately 2 minutes into the test.

The gases in the baseline floor fires were well stratified for the duration of the test.

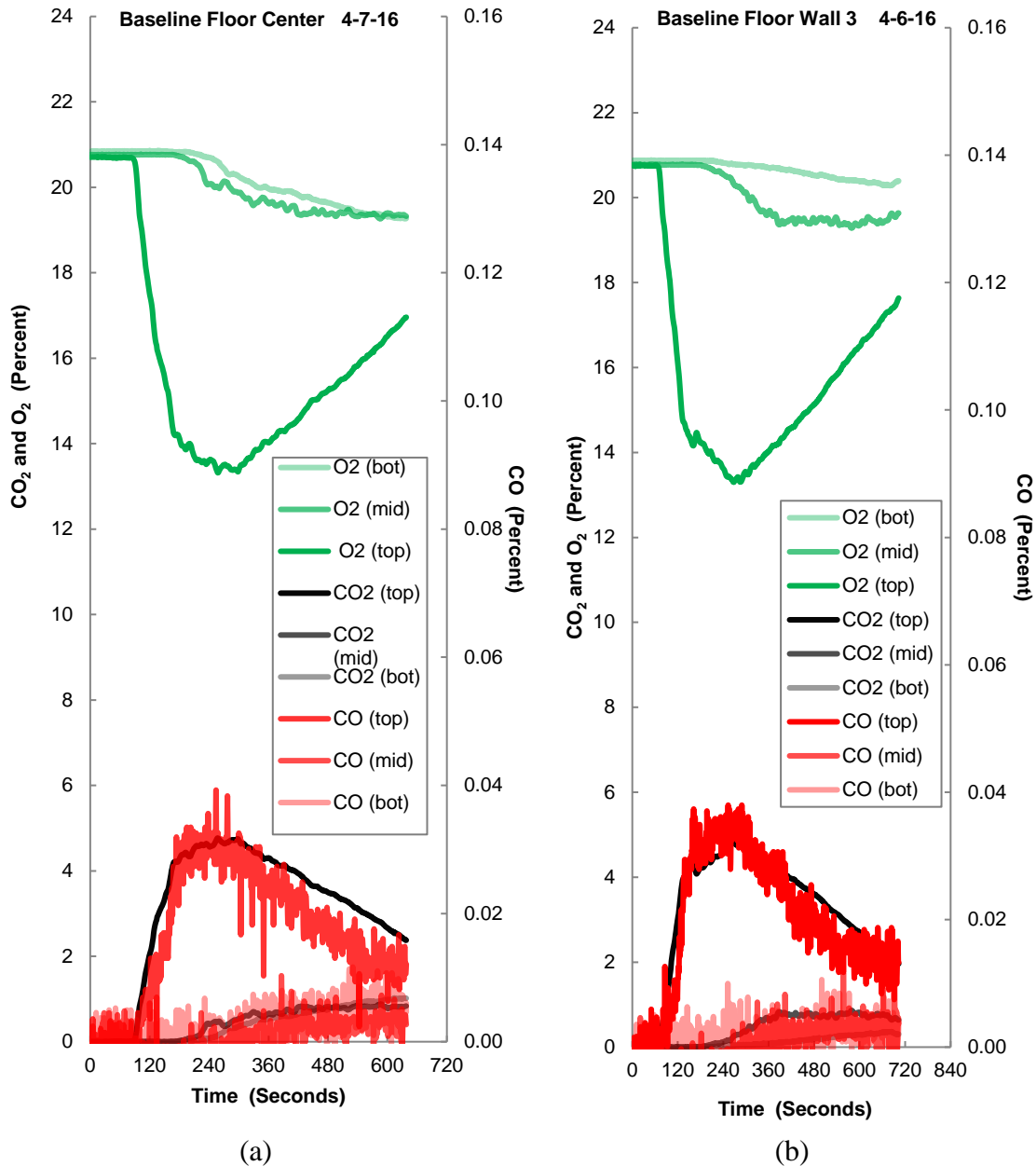
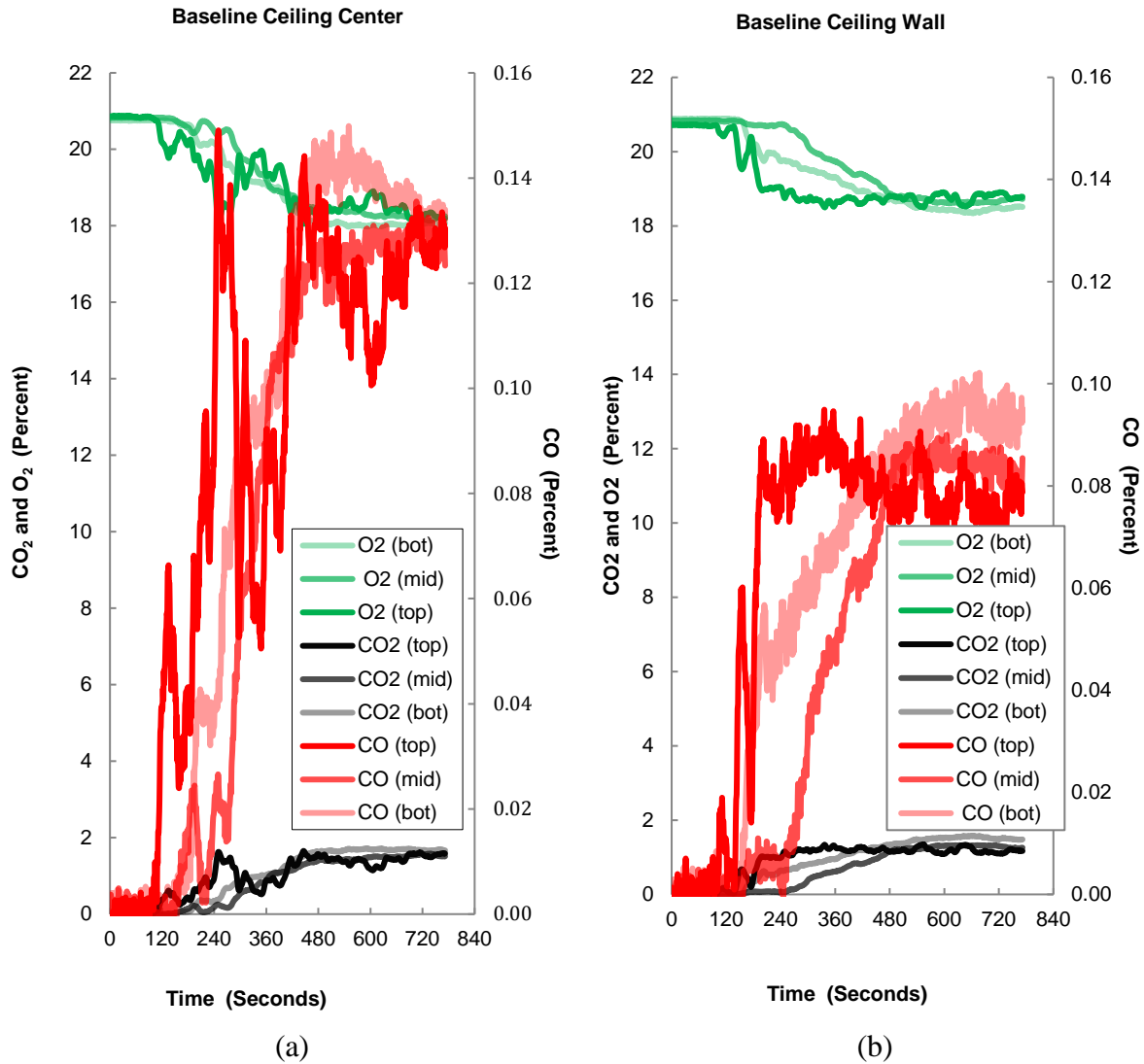


Figure 12. Case 1 fire below, vertical gas concentrations: (a) centered fire, (b) near wall

The gases for both ceiling fire tests were initially stratified but were well mixed at 3–5 minutes after ignition.



**Figure 13. Case 2 ceiling fire alone, vertical gas concentrations: (a) centered fire, (b) near wall**

### 6.2.3 Toxicity Results

The corresponding  $FED_I$  results are shown in figures 14 and 15. Note  $FED_{I\ crit}$  (0.3) is exceeded for the top position in the baseline floor fires with convective heat being the predominant hazard (see figure 14). There is a significant gas hazard at the upper position. Hazards from convective heat and asphyxiant gases are minimal at these lower positions, so the asphyxiant gas and convective heat hazards are acceptable if the occupants stay low in the cabin.



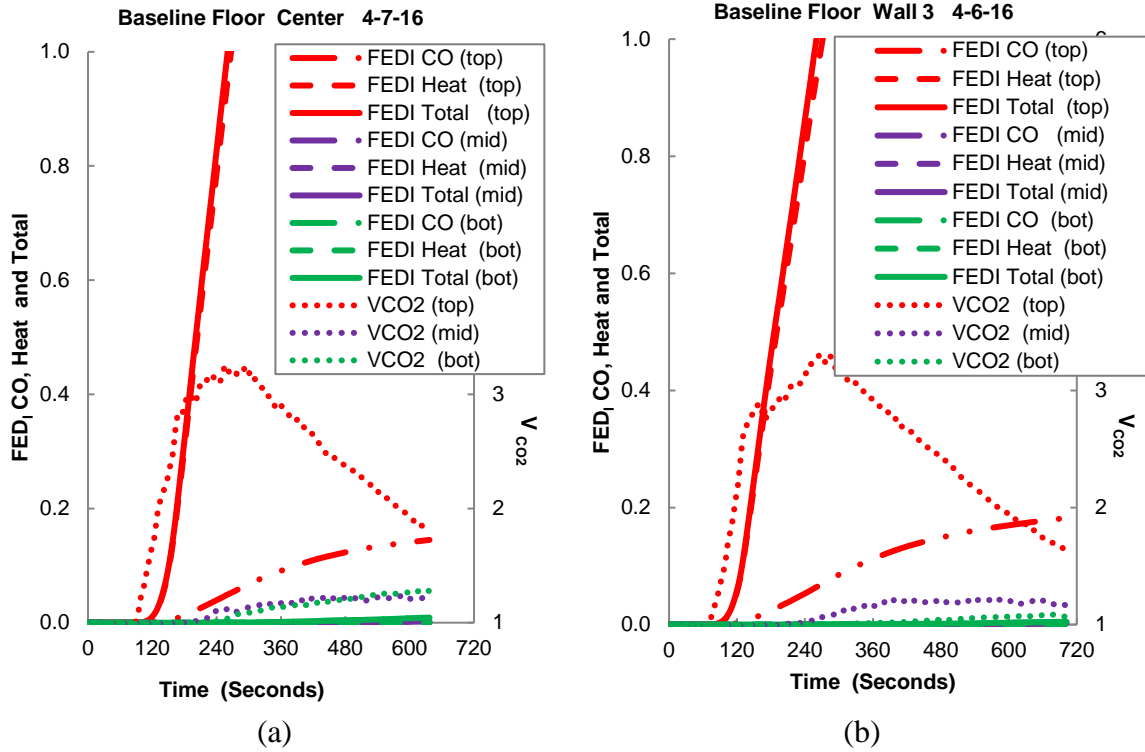


**Figure 14. Case 1 fire below, vertical FEDIs: (a) centered fire, (b) near wall**

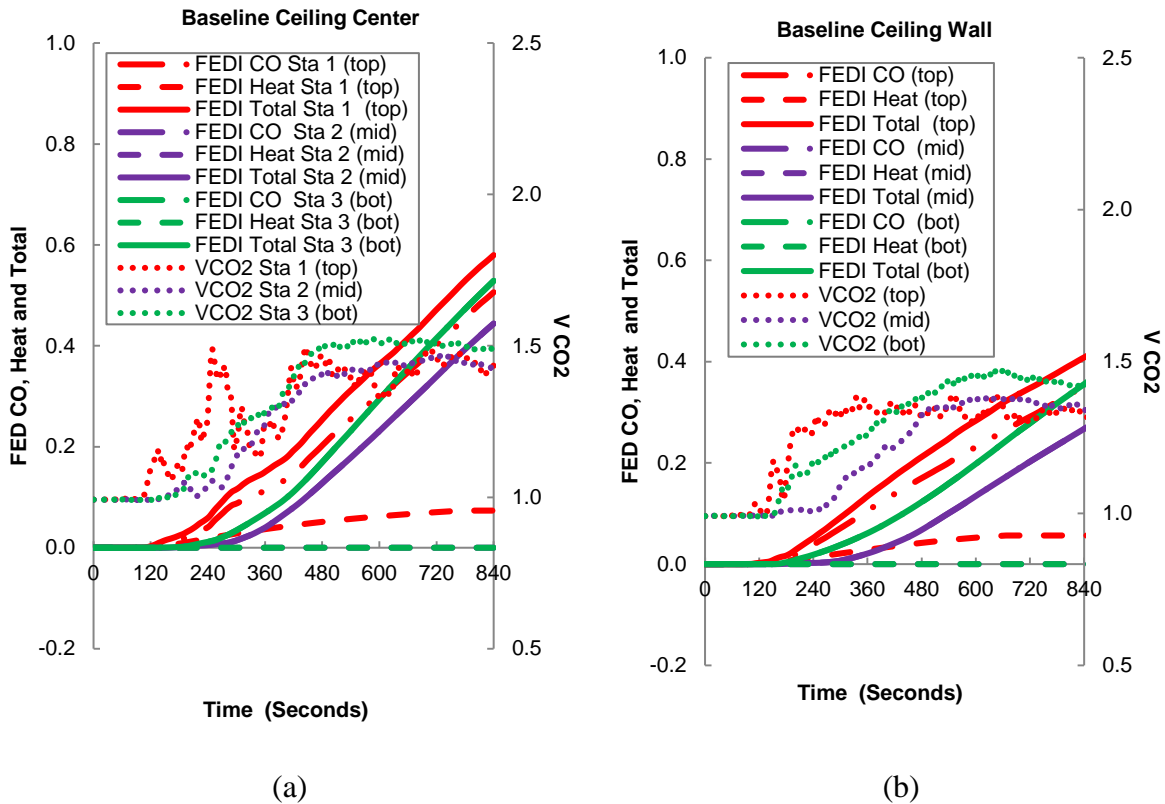


**Figure 15. Case 2 ceiling fire alone, vertical FED<sub>I</sub>s: (a) centered fire, (b) near wall**

In the case of the baseline ceiling fires, the primary hazard at all sampling heights is the asphyxiant gases, not convective heat (see figure 15). Heat contributed to the hazard only for the upper sampling position. There is no convective-heat threat for passenger occupants seated in the vehicle. The FED<sub>I Heat</sub> is close to 0 for the first 5 minutes of the test at the lower positions.

The FED<sub>I Total</sub> did not reach 0.3 at any of the three positions for the first 5 minutes after ignition. The lower positions had significant contributions to the FED from the apparently well-mixed gases. In the case of the baseline-ceiling center fire, the FED total 5 minutes after ignition was 0.192, 0.109, and 0.110 at the top, mid, and bottom locations, respectively. In the case of the baseline-ceiling wall fire, the FED<sub>I Total</sub> 5 minutes after ignition was 0.173, 0.041, and 0.089 at the top, mid, and bottom locations, respectively.

#### 6.2.4 Heat-Flux Results

The heat-flux measurements are important from these mock-up experiments. They give the levels of heat flux that are designed to represent the fire threat to a headliner material. They control the fire growth and toxic gas production for a material. Figure 16 shows the results of case 1, and figure 17 shows the results of case 2. As the burning rate decreases over time (see figure 3), the heat fluxes accordingly decrease. The 80% peak average values are indicated in the figures (these

are determined by identifying the peak value and then averaging over time all of the surrounding values above 80 % of the peak).

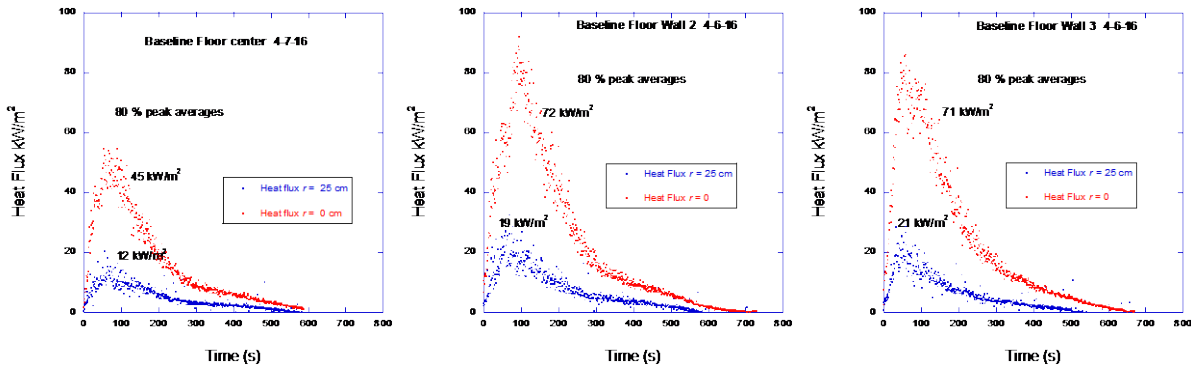


**Figure 16. Heat-flux measurements for case 1: below fire**

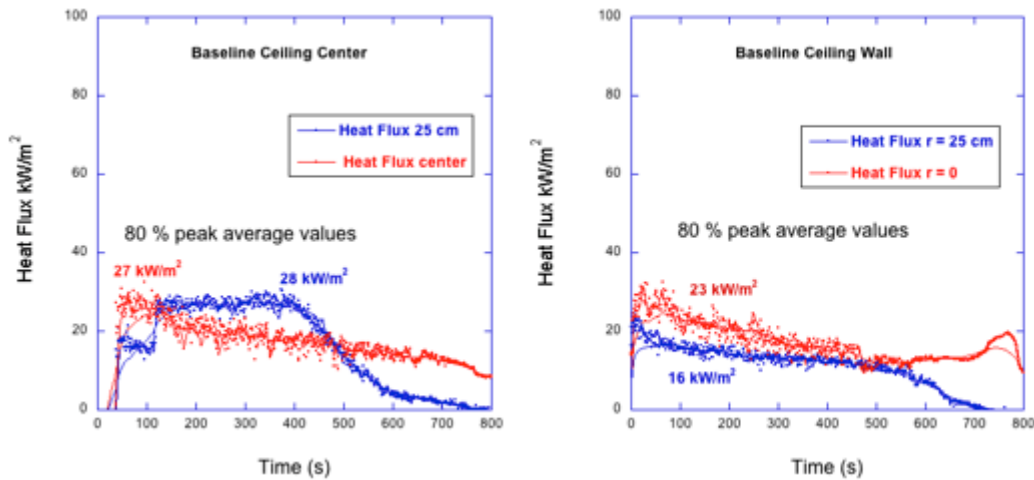


**Figure 17. Heat-flux measurements for case 2: ceiling fire alone**

For the fire below (case 1), the flames impinge on the ceiling and cover both heat-flux sensors. A very sharp decrease is observed for the heat flux as the radius increases. This decrease is important to resolve because the ignition and flame spread on a material experiencing this heat will correspond to the distribution. Furthermore, it is observed that the configuration adjacent to the wall produced heat fluxes higher than the center configuration.

For the ceiling fire alone (case 2), the overall heat flux is lower than case 1. It decreases with radius but not as fast.

## 7. ANALYSIS OF DESIGN HEAT FLUX

The design heat fluxes need to be predicted as a function of radius and in relationship to the flame radius over the ceiling. This is necessary because the heat flux under the ceiling flame is responsible for ignition and flame spread. For case 1, the impinging flame, that heat flux varies significantly with radius. The maximum value at the centerline cannot be solely responsible for ignition. Moreover, the flame extension beyond the ignited region is particularly responsible for

spread with its associated heat-flux distribution. The experimental data are not sufficient to arrive at relationships needed to predict the flame radius and its associated heat-flux distribution. The data must be supplemented with theory developed by generalized studies. However, the data from the mock-up experiments must be consistent with the theoretical formulations. This consistency level is a measure of the validation of this approach for using the scenario heat-flux signatures to evaluate material flammability from fire properties.

The work of Hasemi and coworkers [4, 18] provides the formulas for predicting the flame radius and heat-flux distributions in cases 1 and 2. They are presented here and will be incorporated subsequently into modeling fire growth.

### 7.1 CASE 1: FIRE BELOW

Figure 18 gives the heat-flux distribution for case 1 an axisymmetric fire plume impacting the ceiling in terms of the dimensionless variable,  $w$ . That parameter is composed of the radial position ( $r$ ), the distance to the ceiling ( $H$ ), the flame radius ( $L_H$ ), and the virtual origin of the fire below ( $z'$ ).

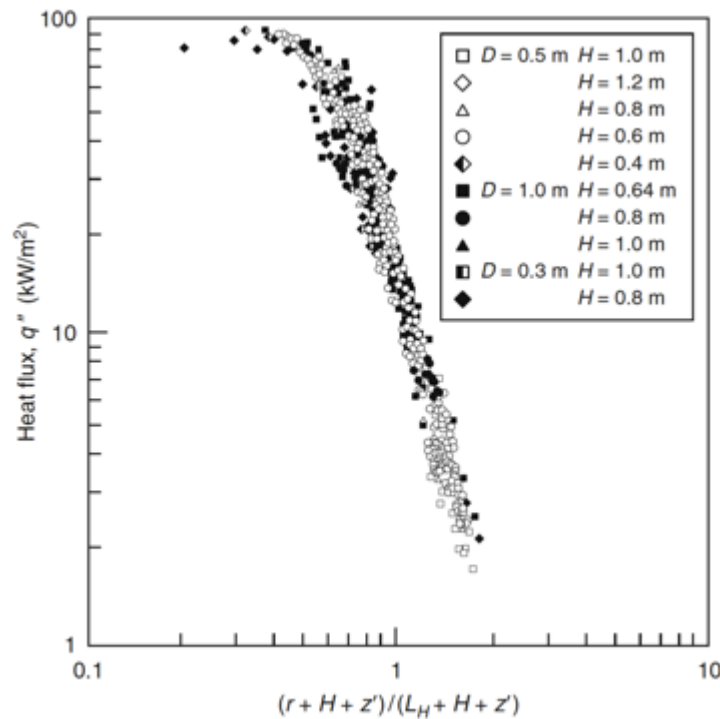


**Figure 18. Incident heat flux to ceiling from an axisymmetric fire plume [2, 4]**

Although the data in figure 18 are based on propane as a fuel, the heat flux for these relatively thin boundary-layer ceiling flames is not expected to be a strong function of flame radiation. Therefore, these data should apply generally, especially over the height and diameter ranges indicated, and should be consistent with the scenario adopted for the combat vehicle.

The data in figure 13 can be represented analytically as:

$$\begin{aligned}\dot{q}'' &= 88 \text{ kW/m}^2, w \leq 0.6 \\ \dot{q}'' &= 16.22w^{-3.31}, w \geq 0.6\end{aligned}\tag{15}$$

The needed parameters are given as follows:

$$w \equiv \frac{r + H + z'}{L_H + H + z'}$$

where the virtual origin,  $z'$ , is based on the plume

energy release rate  $\dot{Q}$  and its diameter,  $D$

$$z' = 2.4D(Q_D^{*2/5} - Q_D^{*2/3}), Q_D^* \leq 1$$

$$z' = 2.4D(1 - Q_D^{*2/5}), Q_D^* \geq 1$$

the flame radius  $L_H$  is based on the plume

energy release rate  $\dot{Q}$  and its distance,  $H$ ,

to the ceiling

$$\frac{L_H + H}{H} = 2.89Q_H^{*1/3}$$

and dimensionless energy is defined as

$$Q_x^* \equiv \frac{\dot{Q}}{\rho_\infty c_p T_\infty \sqrt{g} x^{5/2}}$$

For case 1, the maximum energy release of the heptane fire is selected (65 kW). The diameter of the fire is 30 cm, and the distance to the ceiling is 76 cm. The computed flame radius  $L_H$  is found from the formula as 32 cm. This result is consistent with the observations during the tests that the flame extended just beyond the heat flux sensor at 25 cm radius (see figure 8). This is the design condition (65 kW from a 30 cm diameter pool, 76 cm below ceiling with a ceiling flame impingement of 32 cm radius).

The heat-flux distribution can be computed for the case 1 design condition. In general, the heat flux can be expressed from the previously stated formulation (ignoring the small effect of the virtual origin ( $z'$ )) as:

$$\dot{q}'' = 0.25H^{0.55}\dot{Q}^{1.1} / (r + H)^{3.3} \text{ in m, kW},\tag{16}$$

and the flame radius as:

$$L_H = H(0.28\dot{Q}^{1/3} - 1) \text{ in m, kW}.\tag{17}$$

For  $H = 0.76$  m,

$$\dot{q}'' = 0.211\dot{Q}^{1.1} / (r + 0.76)^{3.3} \text{ in m, kW}, \text{ and}\tag{18}$$

$$L_H = 0.269\dot{Q}^{1/3} - 0.76 \text{ in m, kW} . \quad (19)$$

The flame incident heat flux as a function of radius is shown in figure 19 for the design case along with the 80% peak average values measured for the two configurations in the case 1 mock-up. The data were taken for the heptane fire decreasing from 65 kW, but this maximum is used in the theory. The theory with its dependencies on energy-release rate and other variables will be used in further analyses.

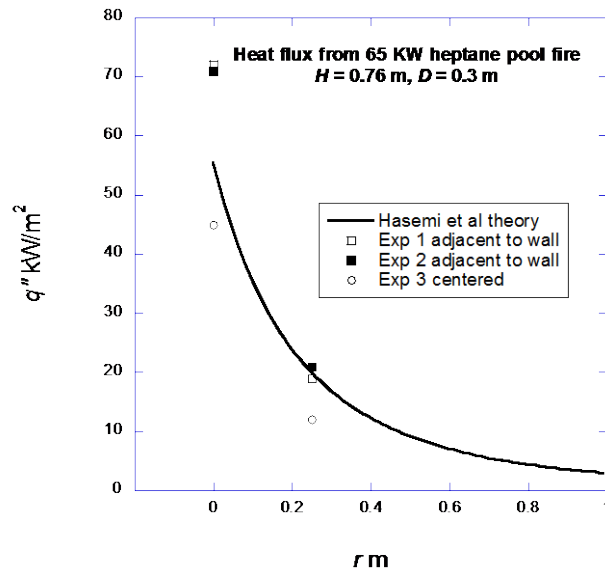


**Figure 19. Experimental mock-up case 1 heat flux compared to theory**

The theory is in good agreement with the experimental results, and—except for the centerline of the plume—agrees with the more severe fire adjacent to the wall. The theory will be used as a design heat flux, as it is generally higher than the data, except at  $r = 0$ , for the more severe configuration.

In summary, the measured (time-averaged peak) heat fluxes for case 1 are at  $r = 0$ : 45 and 71–72 kW/m<sup>2</sup>; and  $r = 25$  cm: 12 and 19–21 kW/m<sup>2</sup>, respectively, for the centered fire and wall adjacent fire. The theoretical predictions are  $r = 0$ , 52 kW/m<sup>2</sup> and  $r = 25$  cm, and 20 kW/m<sup>2</sup>. The computed flame radius for the 65 kW design fire threat is 32 cm.

For the lesser experimental fire of 46 kW maximum, shown in figure 3, the theoretical results are 35 and 13 kW/m<sup>2</sup> with a flame of radius 20 cm (see equation 19).

As the heat flux decreases rapidly with radius, the heat flux under the flame is most significant. This heat flux controls the burning rate and the flame spread. The heat flux beyond the flame tip will decrease much faster as the temperature drops. The average heat flux over the flame will be adopted as controlling for burning and spread (for this case,  $w \sim r + 0.69$ ). From the formula, the average heat flux can be computed as a function of radius for the design heat flux of case 1.

The average heat flux is computed over the flame radius from:

$$\bar{q}'' = \frac{1}{\pi L_H^2} \int_0^{L_H} \dot{q}'' 2\pi r dr . \quad (20)$$

Substituting the design case formula for heat flux and flame radius gives:

$$\bar{q}'' = 5.4 \dot{Q}^{0.36} \text{ in kW, kW/m}^2 \quad (21)$$

after a best fit is made for 30–300 kW. The average flame heat flux for the design fire of 65 kW is 24.3 kW/m<sup>2</sup>. Later in this report, material segments were burned in the mock-up, but at a maximum heptane output of 46 kW. The average flame heat flux at 46 kW would be 21.2 kW/m<sup>2</sup>.

## 7.2 CASE 2: CEILING FIRE ALONE

Hasemi and coworkers [2, 18] studied the heat-flux distribution and flame radius from an axisymmetric fire at the ceiling. They used a gas burner of two diameters ( $\phi$ ,  $D$ ), 9 and 16 cm, and energy release rates up to 46 kW. The burning rate was not measured for the ceiling fire in the mock-up tests because that would have proved very difficult in the ceiling configuration. The burning rate was expected to be less than 65 kW for case 1 in the pool-burning configuration. The fire diameter in the mock-up was 30 cm. It is believed that the data of Hasemi et al. are applicable to the scenario of case 2.

Figure 20 shows his results for flame radius, and figure 21 shows his general results for the heat flux distribution. Considering the formula for the larger diameter (16 cm), the flame radius is computed at 89 cm for 65 kW. Again, the burning rate is less in this configuration, and the flame radius is over-estimated. The heat-flux measurements interpreted from figure 21 indicate that the heat flux can range from approximately 20–25 kW/m<sup>2</sup> near  $r = 0$ . As the radius increases, the heat flux falls. The measured results give peak average values of 23–27 kW/m<sup>2</sup> at  $r = 0$ . A fit of the data in figure 22 is shown as a line-curve in figure 17 along with the data at 65 kW. The correlation theory shows reasonably similar values with the measurements. Because the correlation is based on much more ceiling-fire data, it will be used to predict the fire performance of materials for case 2.

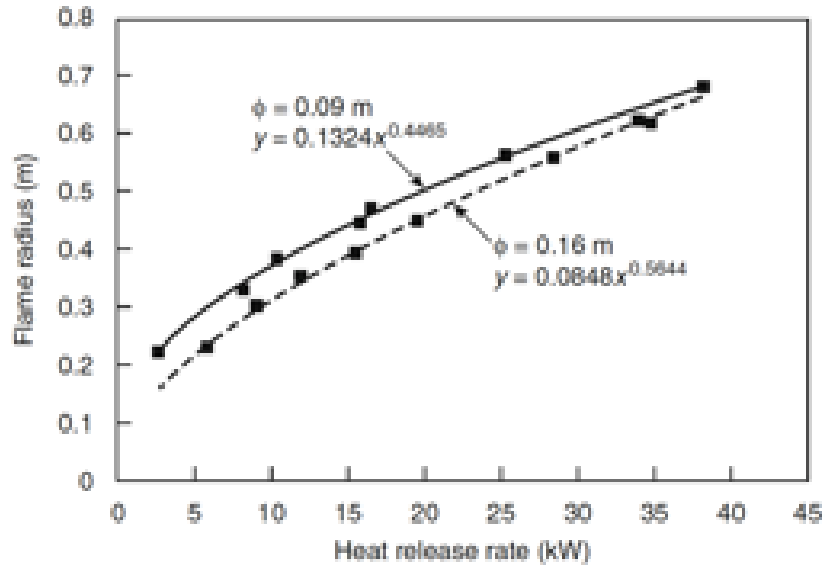


Figure 20. Correlations for flame radius in a ceiling fire [2]

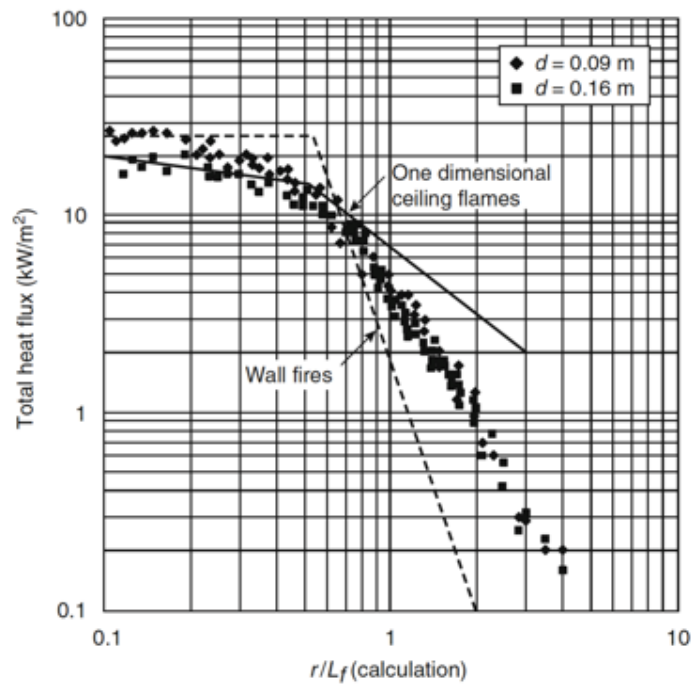
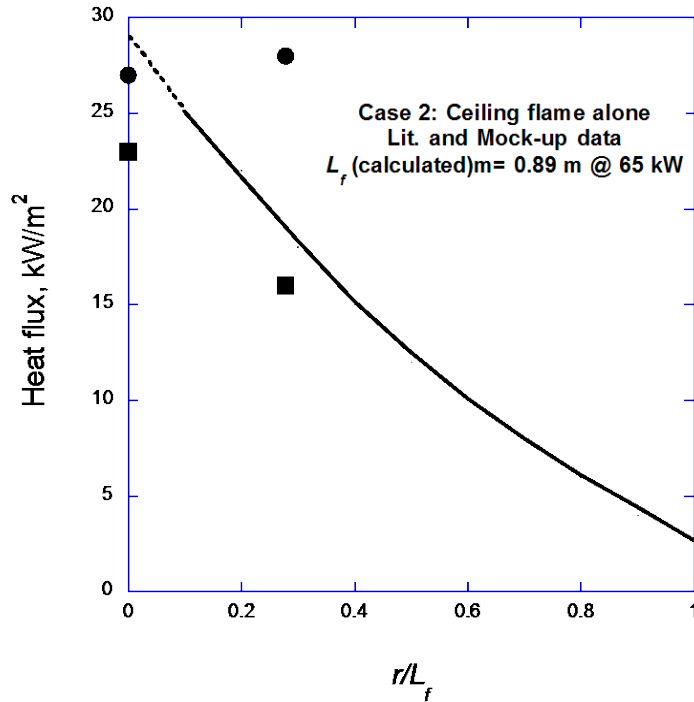


Figure 21. Correlation for heat flux for a ceiling fire in terms of flame radius,  $L_f$  [2]





**Figure 22. Comparison of measured heat flux and correlation for case 2**

## 8. MODELS FOR IGNITION AND FLAME SPREAD

The thermal threat for the material is evaluated under the following criteria:

1. Will the material ignite?
2. Will the material ignite in 2 minutes?
3. Will the material spread?

Models for ignition and flame spread are needed to evaluate the materials in terms of the scenario heat flux and the material properties.

### 8.1 WILL THE MATERIAL IGNITE?

The parameter governing the condition for ignition is called the critical heat flux (CHF). This applies to case 1 with the flaming fire below. In case 2, the ceiling is assumed to have ignited by accidental or intentional means. The CHF for flaming ignition is required.

#### 8.1.1 Determination of CHF in flaming ignition

CHF is normally determined under radiant heating conditions in such a device as ASTM E 1354 (Cone Calorimeter). In that device, the CHF (radiant) is the minimum radiant heat flux to allow piloted ignition. It is related to the ignition temperature of the material for piloted ignition,  $T_{ig}$ . Under radiant heating, the material experiences a convective heat loss. Under flaming ignition, there is only a re-radiation heat loss. Thus, the CHFs for flaming and radiant heating are related through the ignition temperature and the convective heat-transfer coefficient. The convective heat-

transfer coefficient for the Cone has been found by Xin as 5 W/m<sup>2</sup>-K [6]. For this value, the two CHF's can be related over a range of ignition temperatures to 700 °C (see figure 23). It is seen that they are nearly the same. Consequently, the CHF as found under radiant heating will be taken as that applicable to case 1.

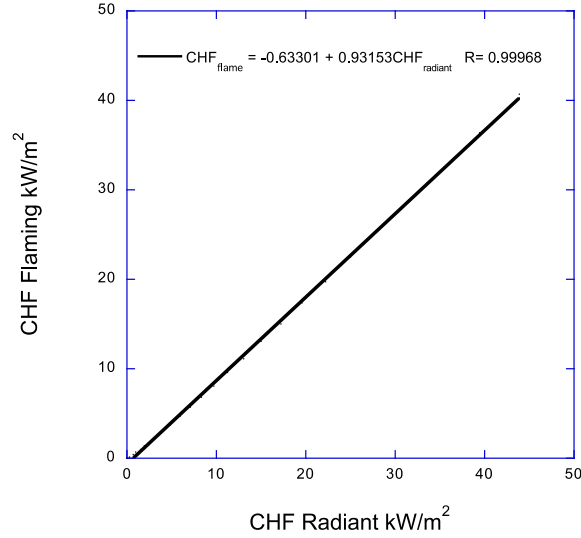


**Figure 23. Relationship between the CHF for radiant and flame-heating at ignition**

The CHF under radiant heat is commonly found by reducing the heat flux until piloted ignition does not occur. This is a tedious process. Alternatively, the CHF can be found from a proper extrapolation of time-to-ignition data versus heat flux [19]. Both of these approaches require sufficient data at both high and low flux values near the CHF.

## 8.2 TIME FOR IGNITION

Under a constant and high heat flux, the time for a material to ignite can be determined from the equation:

$$t_{ig} = \left( \frac{TRP}{\dot{q}_{incident}''} \right)^2. \quad (22)$$

Sometimes in the literature, the net heat flux is used instead of the incident flux. Equation 22 holds exactly at high heat flux, and the use of the net heat flux is not correct at low flux values. The thermal response parameter (TRP), coined by Tewarson, is a material property combining the ignition temperature with the material properties conductivity, density, and specific heat as:

$$TRP = \left( \frac{\pi}{4} k \rho c_p \right)^{\frac{1}{2}} (T_{ig} - T_{\infty}), \quad (23)$$

This result can be derived from the heat conduction in a semi-infinite solid with linearized surface heat loss in the limit of small time or high external heat flux. A plot of the square root of the time-

to-ignite against the reciprocal of the incident heat flux gives TRP as the slope for a linear fit of the data.

At lower values of heat flux, as the CHF is approached, a more general approximate equation applies. This unified theory for predicting the time-to-ignite addresses both high and low heat flux conditions with respect to the CHF. The following equation is proposed, which can be a suitable correlating function of ignition delay times over the entire heat flux range [20]:

$$\frac{CHF}{\dot{q}_{ext}''} = 1 - \exp\left(-\frac{CHF}{TRP} \sqrt{t_{ig}}\right). \quad (24)$$

The CHF may be derived from this equation for low values of incident external heat flux, but it is much more accurate to determine the CHF by probing the level of heat flux needed.

### 8.3 FLAME SPREAD

The simplest model for flame spread represents the rate of growth of the pyrolysis front ( $r_p(t)$ ) as approximately the flame extension ( $L_H - r_p$ ) beyond the front divided by the time ( $t_f$ ) for the flame extension to ignite the next region. The heat flux over the flame extension is assumed uniform and constant in time, and is considered negligible beyond the flame extension. The equation for the scenarios considered here for axisymmetric flame spread is given as follows:

$$\frac{dr_p}{dt} = \frac{L_H - r_p}{t_f}. \quad (25)$$

Here  $t_f$  is the time for ignition computed under the flame heat flux. Before burnout, the radial flame length is a function of the igniting fire and the material burning over radius,  $r_p$ . The contribution of energy release rate by the material in radial spread is presented as:

$$\begin{aligned} \dot{Q}_{material} &= \pi r_p^2 \dot{Q}'' \\ &\text{in quasi-steady burning} \\ \dot{Q}'' &= \dot{q}_{net}'' HRP \\ &\text{where} \\ \dot{q}_{net}'' &\approx \dot{q}_{incident}'' - CHF \\ &\text{and HRP is a material property} \end{aligned} \quad (26)$$

The property HRP is the ratio of the heat of combustion to heat of gasification. It is found from a device, such as ASTM 1354, from plotting the peak energy release rate as a function of incident heat flux. It represents the condition under peak burning. The net heat flux here is overestimated because CHF is less than the re-radiated surface heat flux.

### 8.3.1 Condition for flame spread

The flame cannot spread unless  $L_H > r_p$ . An analytical result can be found if  $L_H = C\dot{Q}^{1/2}$ .

The scenarios of cases 1 and 2 can be represented in this form in which the criterion for flame spread is:

$$C\left(\pi(\dot{q}_{incident}'' - CHF)HRP\right)^{1/2} > 1$$

or *no spread* will occur if

$$HRP \leq \frac{1}{C^2 \pi (\dot{q}_{incident}'' - CHF)} \quad (27)$$

Another way to interpret this relationship is to note that there is a critical energy release rate per unit area that needs to be exceeded by the material for flame spread to occur. This critical value will be shown as:

$$\dot{Q}_{crit}'' = \frac{1}{\pi C^2} \text{ for axisymmetric radial spread} \quad (28)$$

and  $\dot{Q}_{crit}'' = \frac{1}{C}$  for linear spread with  $L_H = C\dot{Q}'$ .

For upward flame spread, the critical material energy release rate needed for spread is 100 kW/m<sup>2</sup> [21]; for the ISO 9705 room corner test, it is 50–100 kW/m<sup>2</sup> [7–10]; for the ASTM E 84 tunnel test, it is also 100 kW/m<sup>2</sup> [22]; and for the UL 94 small-scale laminar flame test, it is approximately 300 kW/m<sup>2</sup> [11]. All these cases occur under different heating conditions. The imposed flame heat flux, CHF, and HRP will determine the critical energy release of the material. The pass/fail point for the FAA flammability test for aircraft interior lining material as measured in the OSU apparatus at a radiant heat flux of 35 kW/m<sup>2</sup> is an energy release rate of 65 kW/m<sup>2</sup>. The turbulent boundary-layer flame in that apparatus is approximately 30 kW/m<sup>2</sup> [12]. To pass that test, the HRP of the material must be such that:

$$(\dot{q}_{flame}'' + \dot{q}_{radiant}'' - CHF)HRP \leq 65 \text{ kW/m}^2 \quad (29)$$

The analyses for cases 1 and 2 will be more involved, particularly case 1, because the energy contributing to the flame radius is the design fire threat (65 kW) plus the energy from the burning material.

### 8.3.2 Failure to spread because of burnout

The criterion for spread given by HRP ignores the possibility of burnout. The burning time ( $t_b$ ) is controlled by how much mass or energy is available in gasifying the solid fuel. If the burning time is less than the time for the new material to ignite in spread, then spread cannot occur. The burning time is given in terms of the AEP or energy per unit surface area of material.

$$t_b = \frac{AEP}{(\dot{q}''_{incident} - CHF)HRP}, \quad (30)$$

and the time-to-ignite in flame spread is given by:

$$t_f = \left( \frac{TRP}{\dot{q}''_{incident}} \right)^2. \quad (31)$$

The criterion for no spread due to burnout is:

$$\frac{t_b}{t_f} = \frac{AEP \dot{q}''_{incident}}{TRP^2 (\dot{q}''_{incident} - CHF) HRP} \leq 1$$

or

$$AEP \leq \frac{TRP^2 (\dot{q}''_{incident} - CHF) HRP}{\dot{q}''_{incident}}. \quad (32)$$

Therefore, there will be no flame spread if HRP or AEP are below critical values for a scenario represented by the appropriate heat flux.

An example of using these two criteria for flame spread was shown in the work of Lian [10] in correlating flashover (or rapid flame spread over room wall and ceiling lining materials).

Figure 24 shows that most of the materials that led to flashover had a critical energy output above 50 kW/m<sup>2</sup> and an ignition time less than the burn time.

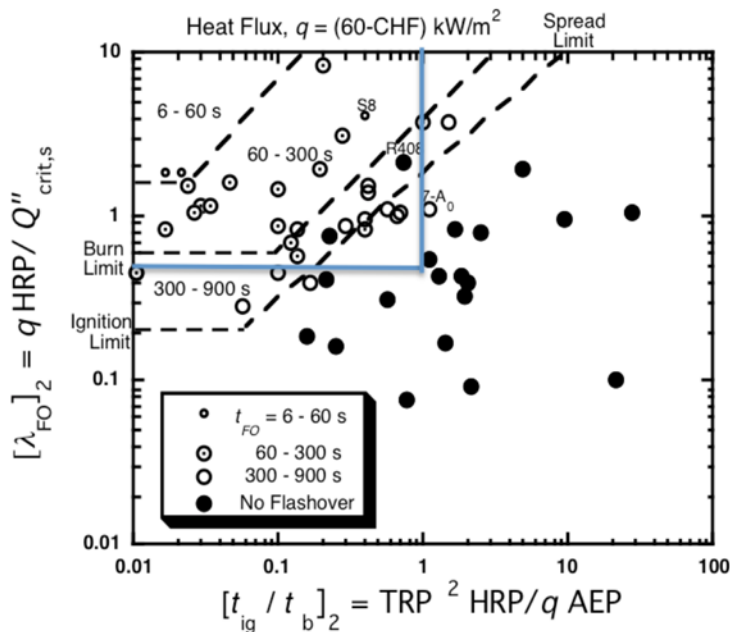


Figure 24. Example showing criteria for flame spread correlates flashover in ISO 9705 [10]

## 9. PASS/FAIL CRITERIA FOR FIRE GROWTH

A material would not be a thermal threat if flame spread is not possible under the fire-below or the ceiling-alone scenario.

Under the fire-below scenario, it is considered that flame spread will not occur if ignition does not occur in 2 minutes. It is reasoned that the occupants would have reduced or extinguished the design igniting fire by that time.

The following conditions are considered as passing for cases 1 and 2:

### 9.1 CASE 1: FIRE BELOW AT 65 KW

The imposed heat flux from the design flame is taken as the average heat flux under the 65 kW flame: Eq. (21)  $\bar{q}'' = 5.4\dot{Q}^{0.36}$  in kW, kW/m<sup>2</sup> or 24.2 kW/m<sup>2</sup>. This is rounded up to 25 kW/m<sup>2</sup>.

#### Pass

CHF > Design flame average heat flux: 25 kW/m<sup>2</sup>

If CHF > 25 kW/m<sup>2</sup>, the ceiling will not be ignited.

Pass: Time to ignite > 2 minutes (120 s)

Under a heat flux of 25 kW/m<sup>2</sup>, TRP > 274 kW-s<sup>1/2</sup>/m<sup>2</sup> will give an ignition time greater than 2 minutes.

Examine now the conditions for flame spread.

The equation for the flame-spread rate in terms of pyrolysis radius is:

$$\begin{aligned}\frac{dr_p}{dt} &= \frac{L_H - r_p}{t_f} \\ t = 0, r_p &= L_H \\ t < t_b & \text{ (burnout time)}\end{aligned}\tag{33}$$

Figure 25 shows an approximation for the flame radius in terms of the energy release rate. It is convenient for this analysis to use a flame radius formula that follows the half-power with energy release rate.

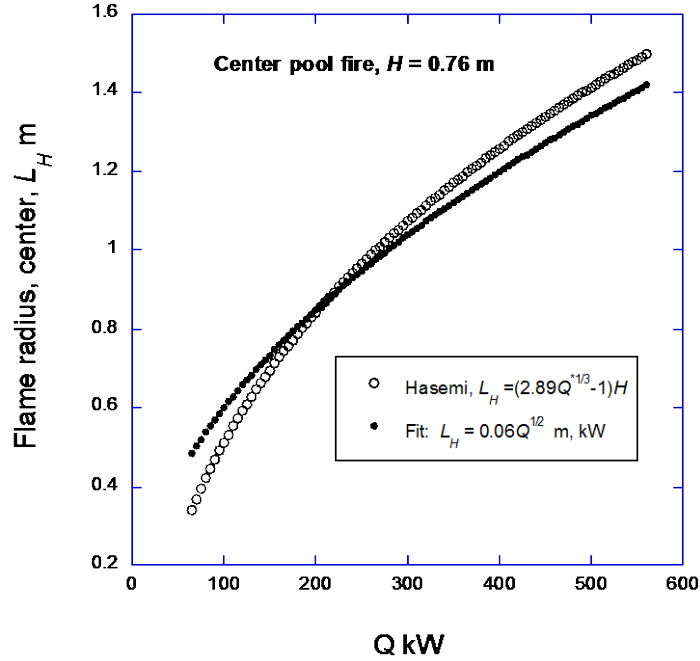


**Figure 25. Approximation for the radial flame length of a fire plume impinging on a ceiling**

$$L_H(m) \approx 0.06\dot{Q}(kW)^{1/2} \quad (34)$$

For the fire below (case 1), the flame length is based on the design fire plus the ignited ceiling.

$$L_H = C \left( \dot{Q}_o + \dot{Q}'' \pi r_p^2 \right)^{1/2}$$

where

$$\dot{Q}_o = 65kW$$

$$C = 0.06 \text{ m/kW}^{1/2} \quad (35)$$

This is the case in which the design flame ignites the ceiling material and stays burning. In the differential equation for  $r_p$ , the initial condition is  $r_p(0) = C\dot{Q}_o^{1/2} \approx 0.32 \text{ m}$ .

To solve the differential equation, it is linearized in  $r_p$  by expanding the half-power expression about  $r_p(0)$ :

$$L_H = C \left\{ \dot{Q}_o^{1/2} \left[ \left( 1 + \pi \dot{Q}'' C^2 \right)^{1/2} - \frac{\pi \dot{Q}'' C^2}{\left( 1 + \pi \dot{Q}'' C^2 \right)^{1/2}} \right] + \left[ \frac{\pi \dot{Q}'' C}{\left( 1 + \pi \dot{Q}'' C^2 \right)^{1/2}} \right] r_p \right\}. \quad (36)$$

On substituting into the differential equation, the parameter governing exponential growth is the coefficient of  $r_p$ . No flame spread will occur if:

$$\left[ \frac{\pi \dot{Q}'' C^2}{(1 + \pi \dot{Q}'' C^2)^{1/2}} \right] < 1. \quad (37)$$

The critical energy release rate per unit area for flame spread in case 1 with the design fire always on is:

$$\dot{Q}_{crit}'' = \frac{1.62}{\pi C^2} = 143 \text{ kW/m}^2 \rightarrow 140 \text{ kW/m}^2. \quad (38)$$

To examine the HRP and CHF needed for passing, the flame heat flux for the material needs to be determined. The expression used for the average heat flux over the flame radius for case 1 is Eq. (21):  $\bar{q}'' = 5.4 \dot{Q}''^{0.36}$  in kW, kW/m<sup>2</sup>.

The highest value is taken for the design fire on, and the heat flux just over the ignited radius:

$$\bar{q}'' = 5.4 \left[ 65 + \pi (0.32)^2 \dot{Q}_{crit}'' \right]^{0.36} = 27.7 \rightarrow 30 \text{ kW/m}^2 \quad (39)$$

Pass: No flame spread if  $HRP < 140 \text{ kW/m}^2 / (30 \text{ kW/m}^2 - CHF)$

If  $HRP > 140 \text{ kW/m}^2 / (30 \text{ kW/m}^2 - CHF)$ , then examine burnout time.

If burnout time is less than the ignition time for flame spread, then the flame will cease as well.

$$\frac{t_b}{t_f} = \frac{AEP \bar{q}''^2}{TRP^2 (\bar{q}'' - CHF) HRP} \leq 1$$

or

$$AEP \leq \frac{TRP^2 (30 - CHF) HRP}{30^2} \quad (40)$$

Pass:  $AEP < TRP^2 (30 \text{ kW/m}^2 - CHF) HRP / 900$ .

## 9.2 CASE 2: CEILING FIRE ALONE

In this case, the ceiling is ignited by some hot element at the ceiling itself. The region of early ignition is unknown, but a distinct ignited region is considered. The question is: Will it spread? The heat flux under this spread condition is governed by the mock-up experiments and the work of Hasemi et al. (see figures 18 and 21, respectively).

Experimental heat fluxes (Figure 22) in the mock-up at  $r = 0$  and  $r = 25$  cm are 27 and 28 kW/m<sup>2</sup>, respectively, for a centered axisymmetric fire. For an axisymmetric fire of 0.3 m diameter, 500 ml heptane adjacent to a wall are 23 and 16 kW/m<sup>2</sup>, respectively. These results are similar to Hasemi, decreasing from approximately 30 to 3 kW/m<sup>2</sup> as  $r$  increases along the flame. The integrated average heat flux over the flame is found to be 8.9 kW/m<sup>2</sup>.



To assess flame spread, the flame radius is needed as a function of the energy release rate. Here the correlation of Hasemi et al. [4] is approximated as a half-power dependence to obtain an analytical solution. Figure 26 shows an approximation for the flame length for case 2. The governing differential equation for case 2 is given as follows:

$$\begin{aligned}\frac{dr_p}{dt} &= \frac{L_H - r_p}{t_f} \\ L_H &= C[\dot{Q}''\pi r_p^2]^{1/2} \\ L_H &= C[(\bar{q}'' - CHF)HRP\pi]^{1/2} r_p\end{aligned}\quad (41)$$

Substituting:

$$\frac{dr_p}{dt} = \frac{L_H - r_p}{t_f} = \frac{(C[\dot{Q}''\pi]^{1/2} - 1)r_p}{t_f}, \text{ and} \quad (42)$$

$$\dot{Q}_{crit}'' = \frac{1}{\pi C^2} = \frac{1}{\pi(0.12)^2} = 22.1 \text{ kW/m}^2 \rightarrow 25 \text{ kW/m}^2 \quad (43)$$

The average heat flux under the flame is rounded up from 8.9 to 10 kW/m<sup>2</sup>. The condition for no flame spread is then:

$$(\bar{q}'' - CHF)HRP < 25 \text{ kW/m}^2 \text{ or } HRP < 25/(10 - CHF).$$

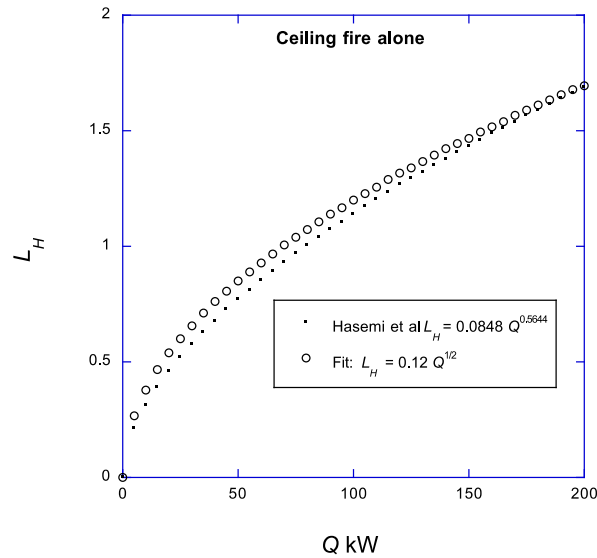


**Figure 26. Approximation for the radial flame extension for a ceiling fire**

Cases 1 and 2 have similar formulas for the flame spread condition. The more severe of the two will be adopted. Figure 27 shows the two critical HRP values against CHF. The HRP for case 1 is less than case 2, except for very low values of CHF. Consequently, the flame-spread criterion will be based solely on case 1.

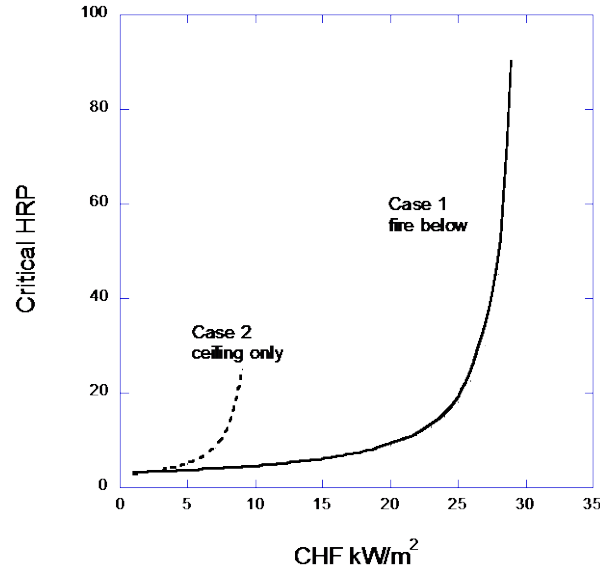


**Figure 27. Critical flame spread HRP values for cases 1 and 2**

### 9.3 SUMMARY

The delineation of the pass-fail point is based on case 1.

If  $\text{CHF} > 25 \text{ kW/m}^2$ , material passes (no ignition).

If  $\text{CHF} < 25 \text{ kW/m}^2$ , examine TRP.

If  $\text{TRP} > 274 \text{ kW-s}^{1/2}/\text{m}^2$ , material passes (no ignition in 2 minutes).

If  $\text{TRP} < 274 \text{ kW-s}^{1/2}/\text{m}^2$ , examine HRP.

If  $\text{HRP} < 140/(30 \text{ kW/m}^2 - \text{CHF})$ , material passes (no spread).

If  $\text{HRP} > 140/(30 \text{ kW/m}^2 - \text{CHF})$ , examine AEP.

If  $\text{AEP} < \text{TRP}^2(30 \text{ kW/m}^2 - \text{CHF})\text{HRP}/900 \text{ kJ/m}^2$  material passes (too thin to spread).

### 10. METHODS TO DETERMINE MATERIAL PROPERTIES

Data from material testing in ASTM E 1354 at several heat flux levels can be used to derive the needed properties. The data must apply only to the flaming period of burning. The properties are expressed in terms of four parameters. These parameters can be used to predict aspects of fire growth knowing their exposure heat flux. Table 1 lists the parameters. They have been measured and listed for many materials [1, 2, 5, 8–10, 23].

**Table 1. Canonical set of flammability parameters**

Parameter	Physical Meaning	Measurement Means
HRP Heat Release Parameter	$\Delta h_c / L$ <ul style="list-style-type: none"> <li>• Heat of combustion/heat of gasification</li> <li>• Combustion energy to energy needed to vaporize solid</li> </ul>	Slope of peak heat release rate and flux
TRP Thermal Response Parameter	$\sqrt{\frac{\pi}{4} k \rho c (T_{ig} - T_o)}$ <p>For a given heat flux, TRP<sup>2</sup> is directly proportional to the time to ignite</p>	Slope of (time-to-ignition) <sup>-1/2</sup> and applied (heat flux) <sup>-1</sup>
CHF Critical Heat Flux	Proportional to ignition temperature and is the minimum heat flux needed for ignition	Lowest flux for piloted ignition
AEP Available Energy Parameter	Total energy released in burning per unit area	<ul style="list-style-type: none"> <li>• Integral of cone energy release rate per unit area with time</li> <li>• Area under heat release rate and flux curve</li> </ul>

The HRP is the ratio of combustion energy released to the energy required to vaporize. Multiplying it by the absorbed material heat flux gives the heat release rate (HRR) per unit area that occurs in combustion. The TRP is a combination of the thermal inertia and the temperature rise needed for ignition of a thermally thick material. Dividing the TRP by the imposed heat flux and squaring the result will give the time for ignition to occur. The CHF is a surrogate for the (piloted) ignition temperature but depends on the convective heat transfer coefficient,  $h_c$ . The imposed heat flux must exceed CHF for a material to ignite. Finally, the AEP is the energy that can be released during burning, usually expressed as MJ/m<sup>2</sup>. AEP is related to the thickness of a material and its completeness of combustion. All these parameters are considered constants for a given material in natural fire conditions during a particular scenario. They are independent of the imposed heat flux. However, together with the scenario heat flux, they can predict whether a material will ignite or when it will ignite, the HRR, and the duration of burning.

Data giving the time to sustained ignition at a given radiant heat flux are used to derive the properties CHF and TRP. An example for a specific material is shown in figure 28. A plot of the square root of the ignition time against the reciprocal of radiant heat flux can be used to derive TRP. The data at high heat flux should be favored. The graph in figure 28(b) shows how the CHF might be derived by probing the non-ignition region. However, its determination should be done more directly by repeated ignition tests.

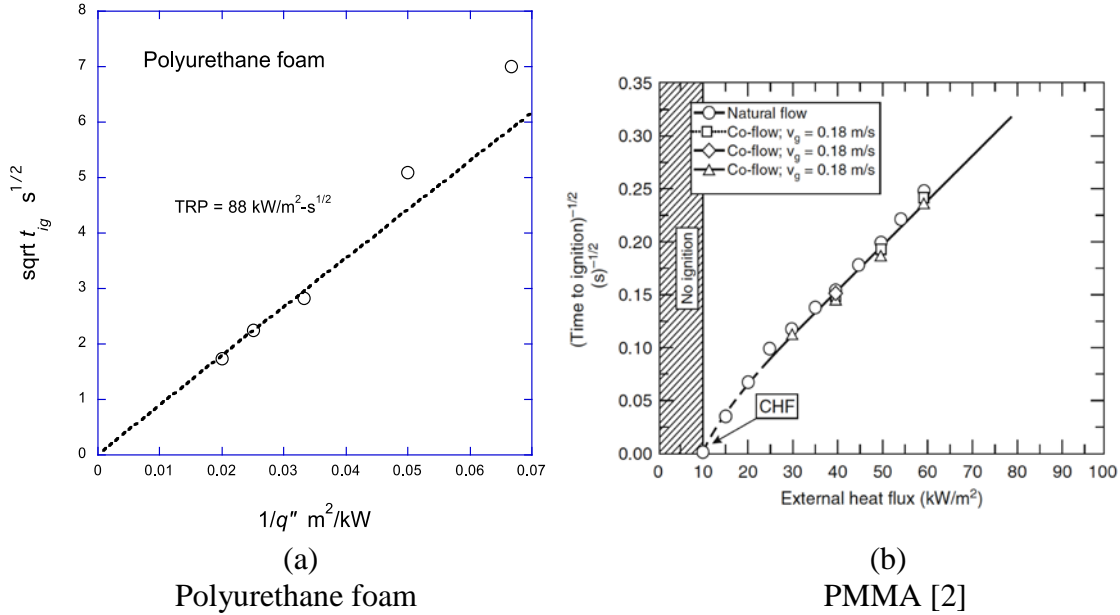


**Figure 28. Derivation of TRP and CHF from ignition data**

The HRP is found from the slope of the HRR with imposed heat flux. The HRR from Cone test was selected as the 80% peak average over time for each heat flux. An example is shown in figure 29 for polyurethane backed with paper. The best linear fit gives the HRP. For the peak average data, the HRP here for polyurethane is approximately 3.5.

**Figure 29. Derivation of HRP from calorimeter data for polyurethane [9]**

In ASTM 1354, the AEP is given as a standard part of the test. Figure 30 shows an example of its expected constancy over heat flux. The value is approximately 30.8 MJ/m<sup>2</sup>. At low heat fluxes, at which burning can be incomplete, the value of AEP can drop. The higher values at which burning

is more complete should be recorded. In general, it is recommended that 6–10 tests be conducted accordingly at heat flux levels.

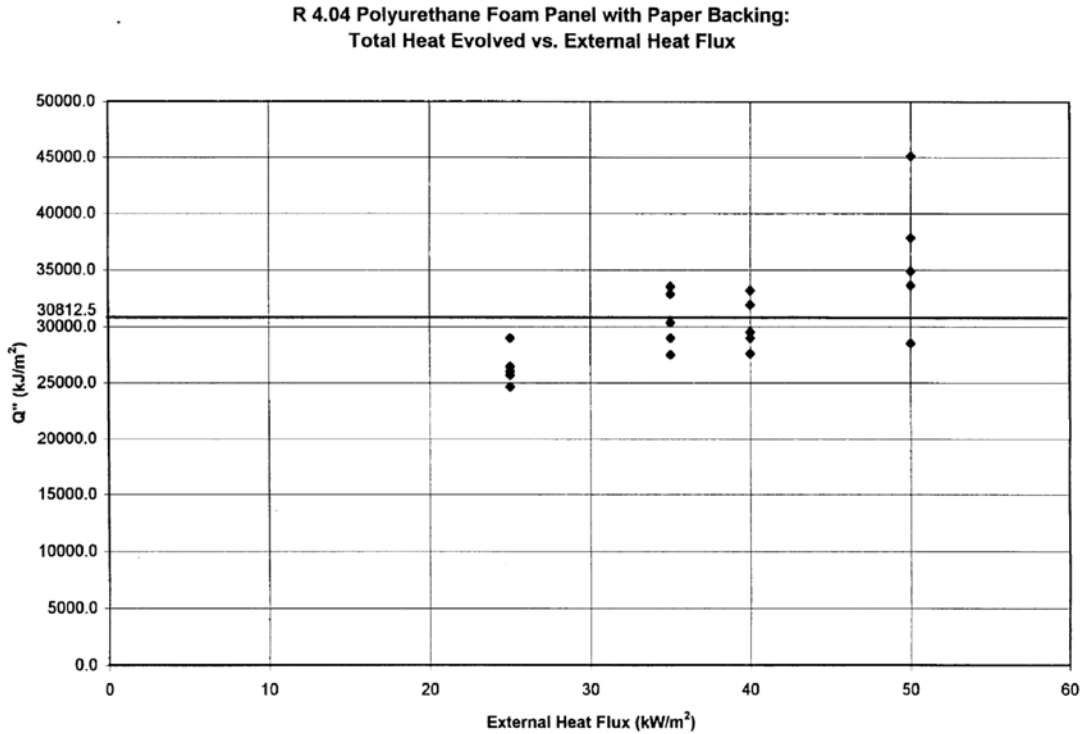


**Figure 30. Variation of AEP with heat flux [9]**

## 11. TOXICITY ASSESSMENT

The assessment of toxicity to the occupants will be based on the sole tested material contribution, not the igniting fire. An assessment for toxicity will be required if the material is considered to have ignited within 2 minutes for case 1, but will not spread. This means:

$$\text{TRP} < 274 \text{ kW}\cdot\text{s}^{1/2}/\text{m}^2 \text{ and } \text{HRP} < 140/(30 \text{ kW}/\text{m}^2 - \text{CHF})$$

This small-vented cabin will yield the worst conditions for toxic hazard compared with commonly larger vehicles and increased venting.

Under these conditions, the material must be evaluated for its toxic hazard. The test chamber is based on the mock-up size and the vents within. The design cabin is taken as:

2.2 x 3.2 x 2 m high with a top wall vent of 61 x 15.3 cm high.

The following assumptions are made with respect to modeling the properties of the enclosure during the burning of the tested material:

- The enclosure gases are quasi-steady.
- Well-mixed gas is uniform.

- Vent flow rate is steady.
- Toxic and energy inputs are from material only.
- The ignited region is considered to be a 0.32 m radius section of the headliner.
- The fractional effective dose for incapacitation ( $FED_I$ ) and the FEC are based on a 5-minute exposure.
- Ignition is taken at time zero.

### 11.1 $FED_I$ AND FEC METHODOLOGIES

The  $FED_I$  and FEC formulas are based on several factors:

- The toxic gas species measured for the material in terms of yield,  $y_i$ .
- Yield is defined here as mass of species produced per mass loss of material while flaming.
- Gas concentrations are obtained from the yield and combustion properties of the material using equation 53 (gases exiting vents) or equation 61 (fixed volume and perfect mixing) and the molecular weights of each gas species and air.
- The total  $FED_I$  and the total FEC may be based on a value less than 1 to account for more susceptible populations,  $FEC_{crit}$ .
- $FED_I$  and/or FEC of 1 statistically are designed to protect only one-half of the population.
- A critical threshold of 0.3 will protect sensitive populations. Critical thresholds of less than 0.3 can be set depending on the population to protect. For example, for the warfighter— for which mental acuity, alertness, clear visibility, and fast response times are important— consideration maybe given to lower  $FED_{I\ crit}$  and  $FEC_{crit}$  to a value below 0.3.  $FED_{I\ crit}$  and  $FEC_{crit}$  are set to 0.3 in this paper.
- The toxicity criteria are:  $FED_I < \text{fractional effective dose for incapacitation, critical}$  ( $FED_{I\ crit}$ ), and  $FEC < FEC_{crit}$ .

#### 11.1.1 $FED_I$ Equations

The equations for  $FED_I$  will be given here for illustration. They are based on an FAA Survival Model [11, 22].

$FED_{I\ crit}$  is selected, and the toxic species presented in the material is computed for the design compartment. The governing formula for assessing incapacitation is given as:

$$FED_{I\ crit} \leq FED_I = \sum_i^n FED_{I\ Gases} + FED_{I\ Heat} \quad (44)$$

The  $FED_I$  is the sum of the individual species fractional dose integrated over time. It includes incapacitation due to convective heat.

The multiplication factor for the enhanced uptake of other gases,  $V_{CO_2}$ , was factored into the concentration term in the regression equation for each asphyxiant gas.

Where:

$$V_{CO_2} = \frac{\exp(0.2496 \times C_{CO_2} + 1.9086)}{6.8} \text{ where } C_{CO_2} \% \text{ CO}_2 \quad (45)$$

Time is expressed in minutes and temperature in degrees Celsius for the following  $FED_I$  equation. Concentrations of CO and CO<sub>2</sub>, are in units of percent. The units for the concentrations of HCN are in ppm.

$$FED_I = FED_{I \text{ Gases}} + FED_{I \text{ Heat}} \quad (46)$$

$$= FED_{I \text{ CO}} + FED_{I \text{ HCN}} + FED_{I \text{ Heat}} \quad (47)$$

$$= \frac{1}{3.4250} \int (V_{CO_2} \times C_{CO}) dt \quad \text{when } V_{CO_2} \times C_{CO} > 0.01\%$$

$$+ \int \frac{(V_{CO_2} \times C_{HCN} - 63) dt}{564} \quad \text{when } V_{CO_2} \times C_{HCN} > 63 \text{ ppm} \quad (48)$$

$$+ \frac{1}{4.1 \times 10^{+8}} \int T^{3.61} dt \quad \text{when } T > 50^\circ\text{C}$$

### 11.1.2 FEC equations

The equations for FEC given here are based on the 2012 ISO Standard for irritant gas toxicity [12].

FECs are determined for each irritant at each discrete increment of time. The time at which their sum exceeds a specified threshold value represents the time to compromised tenability relative to chosen safety criteria. The irritant gases include hydrogen fluoride (HF), hydrogen chloride (HCl), hydrogen bromide (HBr), nitrogen dioxide (NO<sub>2</sub>), and sulfur dioxide (SO<sub>2</sub>). Formaldehyde and acrolein are not expected decomposition products of headliner materials.

The total FEC is the sum of the individual species fractional concentrations.

$$X_{FEC} = \frac{\varphi_{HCl}}{F_{HCl}} + \frac{\varphi_{HBr}}{F_{HBr}} + \frac{\varphi_{HF}}{F_{HF}} + \frac{\varphi_{SO_2}}{F_{SO_2}} + \frac{\varphi_{NO_2}}{F_{NO_2}} + \frac{\varphi_{acrolein}}{F_{acrolein}} + \frac{\varphi_{formaldehyde}}{F_{formaldehyde}} + \sum \frac{\varphi_{irritant}}{F_i} \quad (49)$$

Where:

$\varphi_i$  is the average concentration, expressed in ppm, of the irritant gas,  $i$ .

$F_i$  is the concentration, expressed in ppm, of each irritant gas that is expected to seriously compromise occupants' tenability.

$$F_{HCl} \quad 1000 \text{ ppm} \quad F_{NO_2} \quad 250 \text{ ppm}$$

$F_{HBr}$	1000 ppm	$F_{acrolein}$	30 ppm
$F_{HF}$	500 ppm	$F_{formaldehyde}$	250 ppm
$F_{SO_2}$	150 ppm		

FECs are determined for each irritant. FECs are concentration dependent.  $FEC_{crit}$  is a threshold level defined for each model that cannot be exceeded.

## 11.2 COMPUTATION OF SPECIES CONCENTRATION FOR FLAMING PERIOD AND 5 MINUTES FOR TEST MATERIAL

During the flaming period, the energy release rate is given as for the region ignited by the design fire:

$$\begin{aligned}\dot{Q} &= (30 - CHF)HRPA_{ignited} \\ A_{ignited} &= \pi L_H^2 \\ L_H &= 0.32 \text{ m, the radius of the the 65 kW design fire} \\ \text{or} \\ \dot{Q} &= 0.32(30 - CHF)HRP \text{ in m, kW}\end{aligned}\tag{50}$$

The mass fraction of species  $i$  ( $Y_i$ ) is given in terms of the yield (mass of species  $i$  per mass of fuel lost), vent flow rate, and mass loss rate.

$$Y_i = \frac{\dot{Q}}{\dot{m}} \frac{y_i}{\Delta h_c}\tag{51}$$

The vent mass flow rate is found to be [16]:

$$\dot{m} = \frac{2}{3} C \sqrt{2g\rho_a} A \sqrt{H} [DensityFactor]\tag{52}$$

The density factor is approximately 0.2 for compartment temperatures above 200°C, the flow coefficient is 0.68, the ventilation factor is found from the vent dimensions, and under these conditions the mass flow rate through the vent is computed as 17 g/s. This matches the maximum flow rate computed in appendix B. Accordingly, the mass fraction is found for the flaming period as:

$$\begin{aligned}Y_{i,b} &= (0.0189 \text{ kJ/g})(30 - CHF)HRPy_i / \Delta h_c \\ \Delta h_c &\text{ is the heat of combustion of the material, kJ/g}\end{aligned}\tag{53}$$

The mass fraction should be computed for the flaming period. The flaming time is given by:



$$t_b = \frac{AEP}{(\dot{q}_{incident}'' - CHF)HRP}, \quad (54)$$

and the dilution of the concentration is computed as:

$$Y_i = Y_{i,b} e^{-\frac{\dot{m}}{m}(t-t_b)}. \quad (55)$$

The response time for dilution is the mass of gas in the compartment divided by the vent mass flow rate. This is estimated as  $1.2 \text{ kg/m}^3 \times (298/473\text{K}) \times (2.2 \times 3.2 \times 2 \text{ m}) / 0.017 \text{ kg/s}$  or 626 s. Because the response time is very long relative to 5 minutes, the computed species mass fraction will be taken as a constant over the 5 minutes as  $Y_{i,b}$ .

$$(Y_{i,b} = (0.0189 \text{ kJ/g})(30 - CHF)HRP y_i / \Delta h_c.) \quad (56)$$

The toxicity assessment of a material must be in the context of the hazard it presents to a person in a given scenario. Here we consider the scenario to be the mock-up compartment because that is the worst environment for a combat vehicle because of its small size and limited ventilation. Anything bigger or with more open vents would be less of a hazard.

Also, using a maximum mass fraction without any decay for the prescribed 5-minute exposure period is an overestimate in an effort to improve safety. The recommendation is to use the computed concentration over the exposure period; then to compute the  $FED_I$  and  $FEC$  for the yields measured, and compare to the  $FED_{I,crit}$  and  $FEC_{crit}$ , respectively. This procedure is based on a simple well-mixed model. It is fair to question its use. The accuracy of this approach can be assessed by using the data from the mock-up tests.

### 11.3 VALIDITY ASSESSMENT OF FORMULA USED FOR CONCENTRATION IN MOCK-UP COMPARTMENT

In the mock-up tests of case 1, the concentrations and temperature of the compartment gases and the well-mixed system over time are computed. The mock-up fire energy release rate shown in figure 3 is taken as  $66.3 \exp(-0.0045t(\text{s})) \text{ kW}$  of heptane. This is the actual value in the mock-up testing, not the fixed design value for the performance assessment. This actual value must be used for any predictions.

#### 11.3.1 Temperature

The compartment surface area is  $30 \text{ m}^2$ . The heat loss to the compartment surfaces is considered linear in temperature, and a heat transfer coefficient of  $7.5 \text{ W/m}^2\text{-K}$  is estimated. Assuming a constant vent flow rate, the average temperature in the compartment is estimated as:

$$\begin{aligned}
mc_p \frac{dT}{dt} + \dot{m}c_p(T - T_a) &= \dot{Q} - hA_s(T - T_a) \\
t = 0, T &= T_a \\
\dot{Q} &= Ae^{-bt} \\
\text{Becomes} \\
\theta = T - T_a \\
K &= \frac{\dot{m}c_p + hA_s}{mc_p} \\
C &= \frac{A}{mc_p} \\
\frac{d\theta}{dt} + K\theta &= Ce^{-bt} \\
\theta &= \left( \frac{C}{K - b} \right) (e^{-bt} - e^{-Kt})
\end{aligned} \tag{57}$$

Properties:

$$\dot{m} = 17 \text{ g/s}$$

$$c = 1 \text{ J/g-K}$$

$$h = 7.5 \text{ W/m}^2\text{-K}$$

$$A_s = 30 \text{ m}^2$$

$$m(300^\circ\text{C}) = 8.79 \text{ kg}$$

$$b = 0.0045 \text{ s}^{-1}$$

$$A = 66.3 \text{ kW}$$

Becomes:

$$T - T_a = 328 \left( e^{-0.0045t} - e^{-0.0275t} \right) ^\circ\text{C} \tag{58}$$

This result is compared with the floor centered baseline vertical temperature array data in figure 31. It reasonably captures the ensemble of the vertical temperature array.

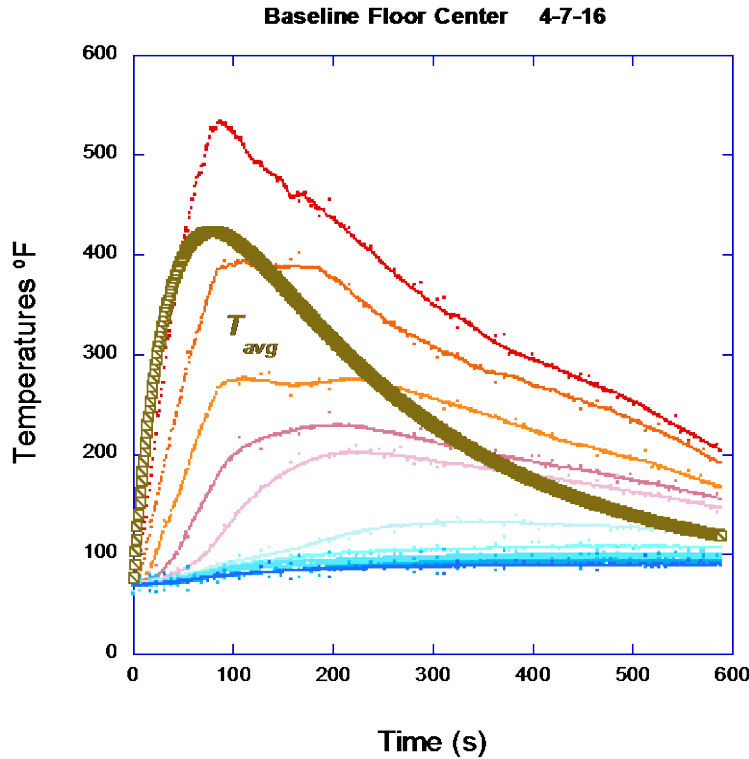


Figure 31. Predicted gas temperature for centered fire below case 1 compared with data

### 11.3.2 Species: CO and CO<sub>2</sub>

Let us now examine the accuracy of a uniform-system model to predict the gas concentrations measured in the mock-up. A conservation of species mass for the compartment gases with a constant vent flow exchange of 17 g/s gives:

$$m \frac{dY_i}{dt} + \dot{m} Y_i = y_i \dot{Q} / \Delta h_c$$

$Y_i$  is the mass fraction of the product species produced

$y_i$  is the mass yield of species  $i$  per fuel mass loss

$\dot{Q}$  is the energy release rate of the heptane fire

$\dot{m}$  is the mass flow rate exchange of smoke and air

$m$  is the mass of gas in the compartment

$\Delta h_c$  is the heat of combustion of the heptane, 41.2 kJ/g

$t$  is time

(59)

Following the analysis of temperature, the solution for a species can be shown as follows:

$$\begin{aligned} \frac{dY_i}{dt} + K_y Y_i &= C_y e^{-bt} \\ t = 0, Y_i &= 0 \\ K_y &= \frac{\dot{m}}{m} \\ C_y &= \frac{A y_i}{m \Delta h_c} \\ \dot{Q} &= A e^{-bt} \\ Y_i &= \left( \frac{C_y}{K_y - b} \right) \left( e^{-bt} - e^{-K_y t} \right) \end{aligned} \tag{60}$$

$$Y_i = 0.0700 y_i \left( e^{-0.00193t} - e^{-0.0045t} \right)$$

or for molar concentration in %

with molecular weight,  $M_i$

$$X_i(\%) = 100 Y_i \frac{29}{M_i}$$

Specifically, for the yields of CO and CO<sub>2</sub>, respectively as 0.01 and 2.86 for heptane [1], figures 32 and 33 show the comparison of the predicted concentrations from equation 60 with the mock-up test data for heptane. The predicted values are computed for a well-mixed exiting gas mixture. They are in reasonable agreement with the top measurements of the mock-up cabin.

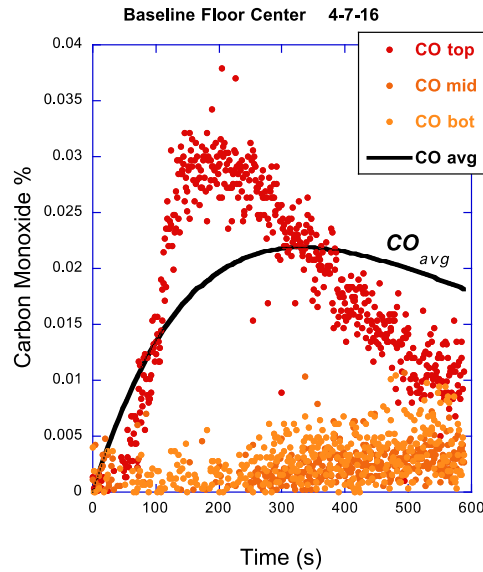


**Figure 32. Predicted concentration of carbon monoxide for centered fire below case 1 compared with mock-up test data**

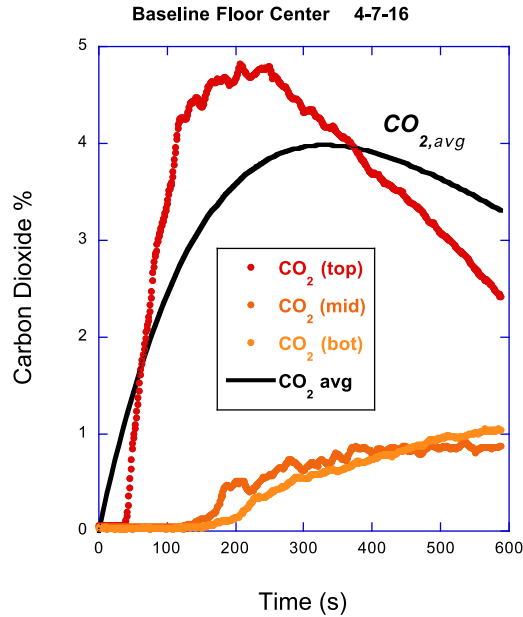


**Figure 33. Predicted concentration of carbon dioxide for centered fire below case 1 compared with mock-up test data**

For the purpose of assessing toxic hazard to occupants, it would appear that a well-mixed model is adequate. Alternatively, a more elaborate analysis could be used to compute the toxic gas concentration. Such an analysis based on CFD would attempt to accurately predict the stratification shown in figures 12 and 13. A CFD model was used with the actual fire input and heptane yields.

Appendix B contains an exercise using the CFD code, Fire Dynamics Simulator (FDS), to compute the results of the mock-up experiments. Its accuracy and comprehensive predictions in space and time can be contemplated for use in a hazard assessment. However, that exercise is beyond the scope of the current work.

### 11.3.3 Computation of the Species Concentrations for the Performance Criterion in the Engineering Analysis

Equation 53 would be the implied means to compute the species concentrations in the performance analysis:  $Y_{i,b} = (0.0189 \text{ kJ} / \text{g})(30 - CHF)HRPy_i / \Delta h_c$ .

However, when that approach is used to estimate the CO and CO<sub>2</sub> concentrations for the heptane mock-up experiments (see figures 32 and 33), the results far overestimate the top measured values. For example, using a fixed 65 kW fire with an exchange of 17 g/s would give a mass fraction for the heptane species of 0.093  $y_i$ , or 0.093 % for CO and 16.5 % for CO<sub>2</sub>. A more accurate, but simple, analysis was examined with favorable results.

The exchange rate of mass in the mock-up and design cabin is 17 g/s, giving an air exchange time of approximately 981 s for the 14.1 m<sup>3</sup>. During the 5-minute toxic hazard evaluation, the air exchange could be ignored as a first approximation and the cabin considered closed. For the 500 ml of heptane used in the mock-up tests, the mass of heptane consumed is 0.342 kg, and the

mass of gas in the cabin (based on an air density of 1.184 kg/m<sup>3</sup> at 25 °C) is 16.7 kg. The mass fraction of the species for this case becomes:  $Y_i = 0.0205 y_i$ , or 0.02 % for CO and 3.75 % for CO<sub>2</sub>. These values are much more in line with the top data in figures 32 and 33. Additional testing of this approach provided good estimates for actual species data in mock-up testing with materials. The formula for the computation of species in the performance criterion analysis is now specified to be:

$$Y_i = 0.0193 AEP(y_i / \Delta h_c)$$

or in molar concentration (%),  $X_i$

$$X_i = 28Y_i / (MW_i) \times 100\%.$$
(61)

## 12. EXAMPLES OF MATERIAL DATA USING THE CONE CALORIMETER AND MOCK-UP COMPARTMENT

Three materials were tested in the cone calorimeter to develop the data needed to compute the properties. These materials represented candidate headliner materials. The sponsor supplied two, and one was obtained as a typical automobile headliner. The two supplied will be designated as white material and gray foam. They are described as follows:

- Headliner – This is a used headliner for a pickup truck assumed to pass FMVSS302. It consists of a foam fabric thin outer shell on a cardboard-like base.
- White material – This is white encapsulated foam used as a fire-resistant building-insulation material. It is poly-organo-siloxane in composition. Its MSDS describes it as non-combustible.
- Gray foam – This is a homogeneous foam polymer consisting of polyvinylchloride, chloroprene, and acrylonitrile butadiene rubber. Its MSDS describes it as having the following flammability ratings: PMVSS302: 0 burn rate; UL 94: HF-1 @ 1/16 inch, V-0 @ 1/2 inch.

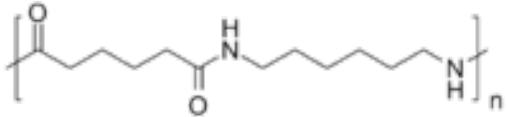
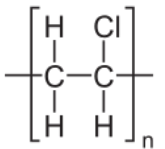
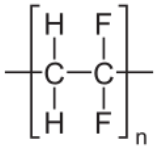
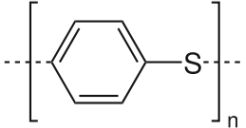
Figure 34 shows photographs of the materials in their as-used-state.



**Figure 34. Materials tested: (a) headliner, (b) white material, and (c) gray foam**

- Other materials – Additional materials were tested that are expected to produce HF, HCl, HCN, and SO<sub>2</sub> thermal decomposition products to check the chemical method of analysis. These materials are nylon 66 (PA66), polyvinylchloride (PVC), polyvinylidene chloride (PVDF), and polyphenylene sulfide (PPS). Their structures, formulas, and formula weights are shown in table 2.

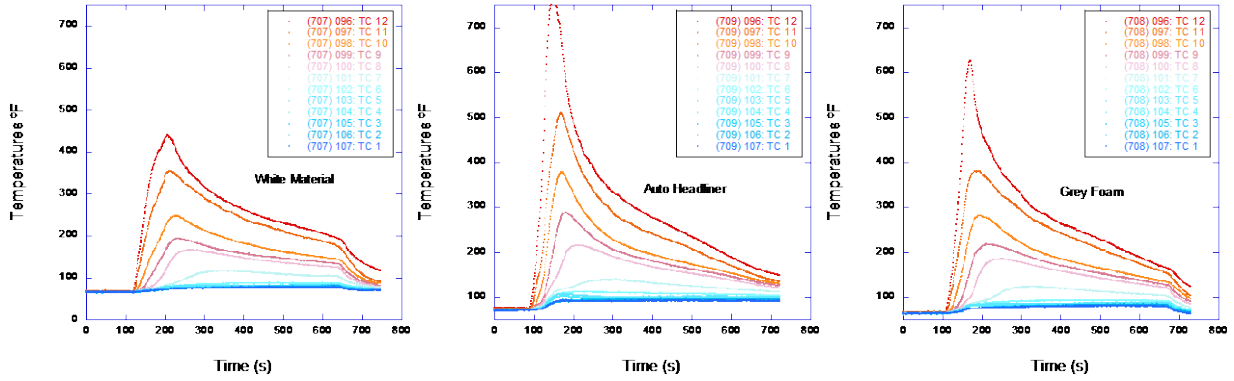
**Table 2. Other materials tested**

Material	Structure	Formula	Formula Weight (g/mole)
PA66		$-(C_{12}H_{22}N_2O)_n-$	227.15
PVC		$-(C_2H_3Cl)_n-$	62.448
PVDF		$-(C_2H_2F_2)_n-$	64.034
PPS		$-(C_6H_4S)_n-$	108.161

### 12.1 MATERIAL RESULTS IN THE MOCK-UP TESTS AND TOXICITY ASSESSMENTS

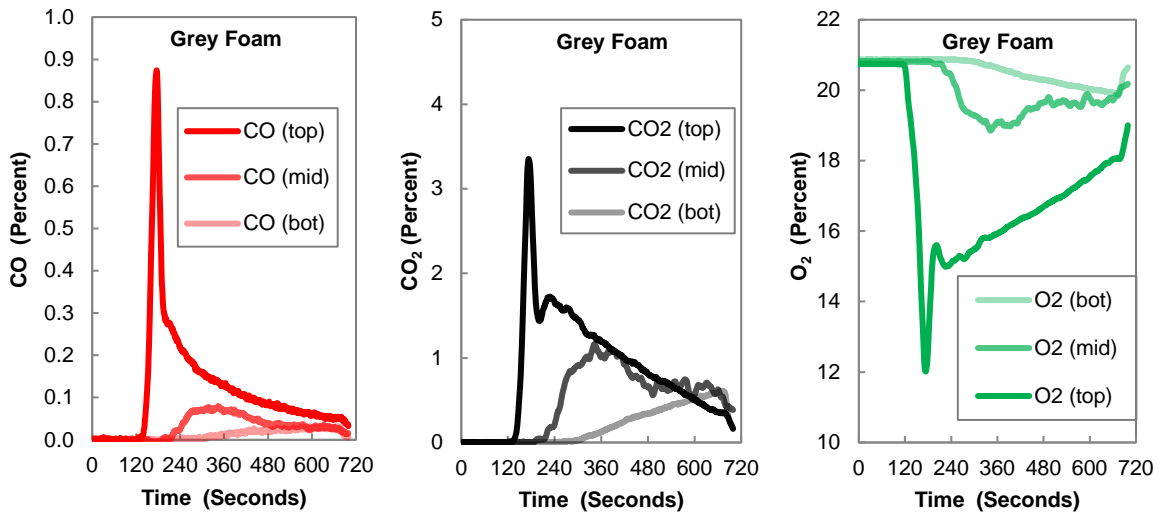
The headliner, white material, and gray foam were subject to a heptane fire in the mock-up vehicle. Sections of material were mounted on the ceiling with a heptane fire 0.76 m centered below. Each section was approximately 60 x 120 cm. For these tests, the amount of heptane used to saturate the 0.3 m disc was cut back to 300 mL in an attempt to reduce its burning time. As shown in figure 3, the maximum energy release dropped to approximately 46 kW, and the fire decayed over time as  $46.5 \exp(-0.00516t(s))$  kW. This means that the maximum flame radius attack was  $L_H = 0.269 (45 \text{ kW})^{1/3} - 0.76 \text{ m} = 0.197 \text{ m}$ , and its heat flux is lower than the design protocol.

Figure 35 shows the temperature response of the vertical thermocouple array for the burning materials. The white material has the lowest peak, and it occurs later than the others. This means it has the lowest energy release rate, and it ignited later. These results are consistent with the HRP and TRP values for the white material relative to the others. Ignoring the effect of CHF, because this may not be accurate for the materials, the temperature response is in accordance with the HRP values of the materials: highest for the headliner (HRP = 3.7), next for the gray foam (HRP = 3.1), and lowest for the white material (HRP = 2.2). It should also be realized that in this exponentially decaying attack fire, the later ignition of the white material would also have produced a lower flame heat flux and energy release, accordingly.



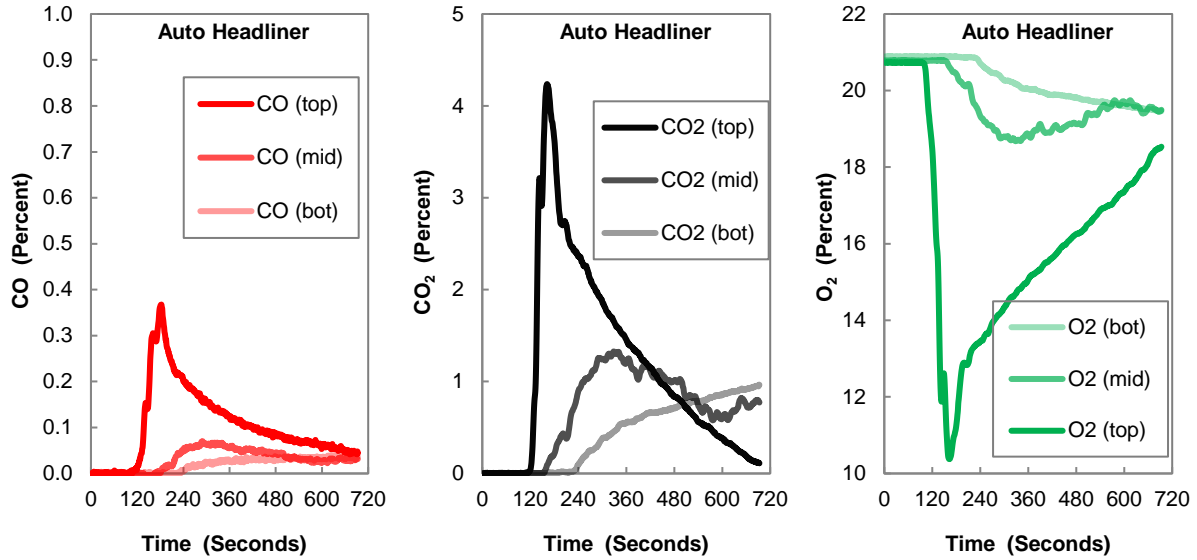
**Figure 35. Temperature response with the 300 mL heptane fire igniting the material sections**

Figures 36–38 show the gas histories at the three sample heights for the burning materials. The white material has the latest peak concentrations, and it occurs later than the others.

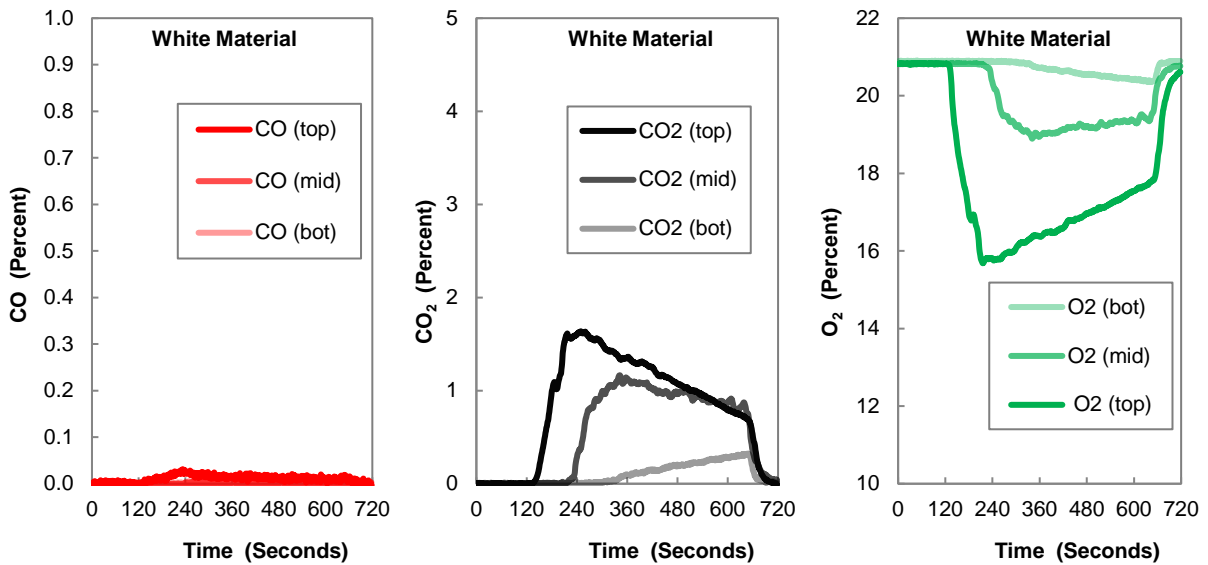


**Figure 36. Gas histories with the 300 mL heptane fire igniting the gray foam**



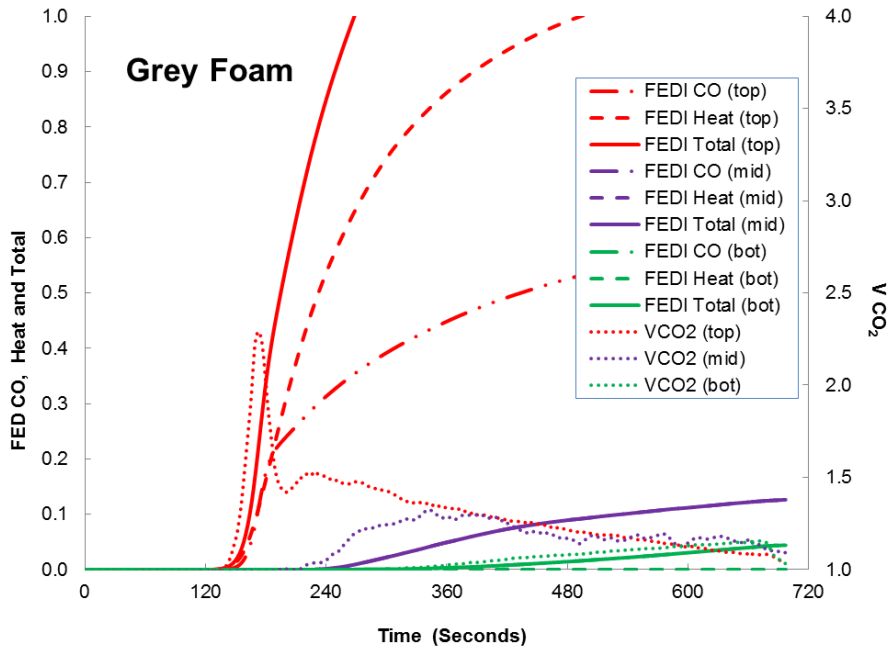


**Figure 37. Gas histories with the 300 mL heptane fire igniting the auto headliner**



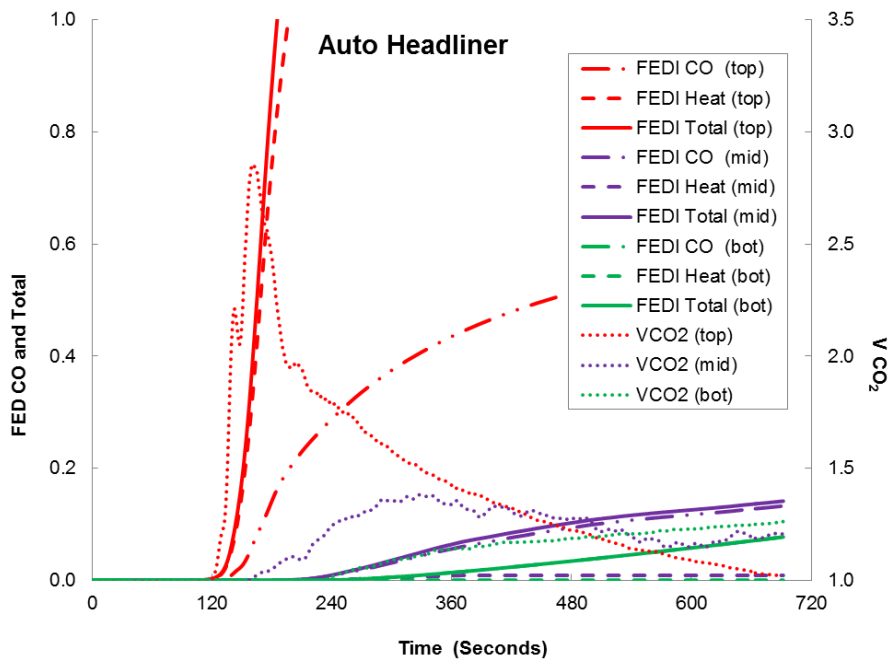
**Figure 38. Gas histories with the 300 mL heptane fire igniting the white material**

Figure 39 shows the corresponding  $FED_{1S}$  computed at the three sample heights for the gray foam. Heat and gases drive the  $FED_I$  at the top position, with the  $FED_{Icrit}$  exceeded in approximately 1 minute. Gases are the only contribution to the  $FED$  at the lower positions. The  $FED_{Icrit}$  of 0.3 is not approached at the mid and bottom positions for the 5-minute duration after ignition.



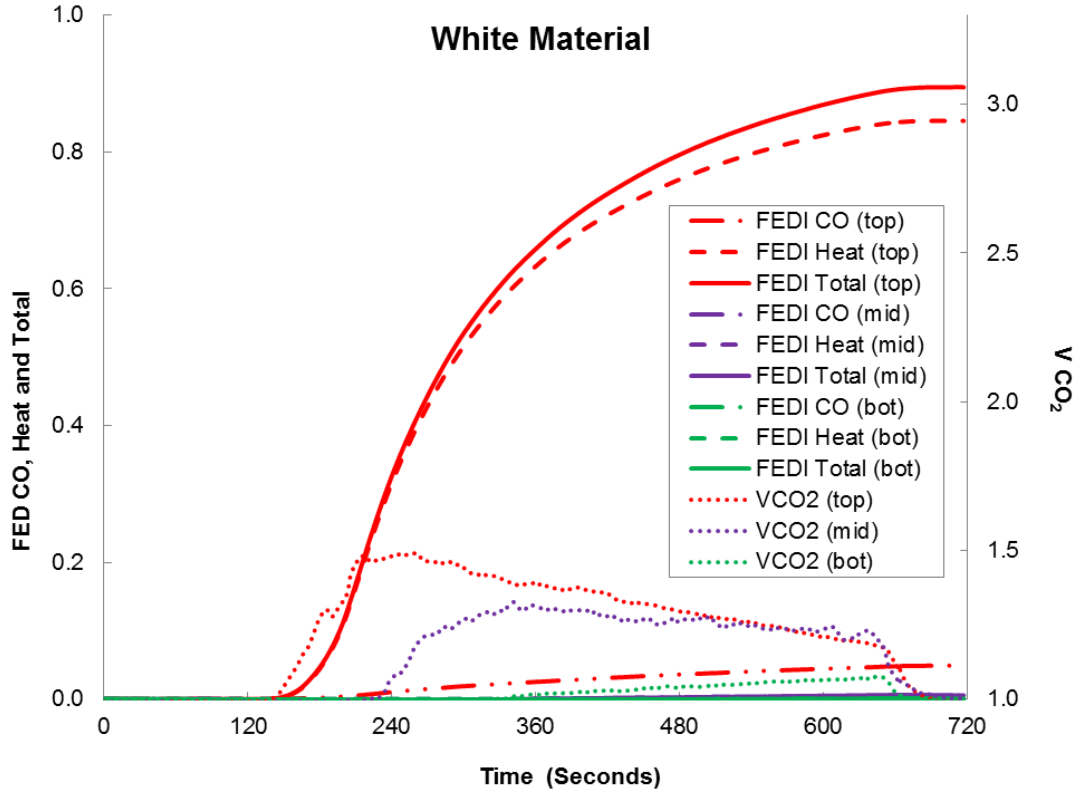
**Figure 39. FED<sub>I</sub>s and V<sub>CO2</sub>s with the 300 mL heptane fire igniting the gray foam**

Figure 40 shows the corresponding FED<sub>I</sub>s computed for the three sample heights for the auto headliner. Heat and gases drive the FED<sub>I</sub> at the top position, with the FED<sub>Icrit</sub> exceeded within a minute. Gases are the primary contribution to the FED at the lower positions. The FED<sub>Icrit</sub> of 0.3 is not approached at the mid and bottom positions for the 5-minute duration after ignition.



**Figure 40. FED<sub>I</sub>s and V<sub>CO2</sub>s with the 300 mL heptane fire igniting the auto headliner**

Figure 41 shows the corresponding  $FED_I$ s computed for the three sample heights for the white material. Heat drives the  $FED_I$  at the top position, with the  $FED_{Icrit}$  exceeded within 2 minutes. Gases are the primary contribution to the  $FED_I$  at the lower positions. The  $FED_{Icrit}$  of 0.3 is not approached at the mid and bottom positions for the 5-minute duration after ignition.



**Figure 41.  $FED_I$ s and  $V_{CO_2}$ s with the 300 mL heptane fire igniting the white material**

The tests all resulted in ignition but did not spread as shown in the aftermath photographs in figure 42. The initial radius of the attack design fire was approximately 20 cm (0.197 m) and, because the sections are approximately 60 cm wide, the damaged area by burning can be seen to be approximately 50 cm in diameter. The damage radius is consistent with the initial computed flame radius.

**Figure 42. After-test photographs of burned materials**

Figures 43–45 show the three materials and the associated damage area from the mock-up tests. The burn damage radius for the gray foam, auto headliner, and white material are 26.7 cm, 20.3 cm, and 24.1 cm, respectively.



**Figure 43. The damage area is shown for the gray foam:  
diameter of damaged area = 21" = 53.3 cm, radius = 26.7 cm**



**Figure 44. The damage area is shown for the DOT headliner:  
diameter of damaged area = 16" = 40.6 cm, radius = 20.3 cm**



**Figure 45. The damage area is shown for the white material:  
diameter of damaged area = 19" = 48.26 cm, radius = 24.1 cm**

These mock-up tests were not performed to validate the performance of the materials relative to the test protocol developed. Such intention would have required much more testing with respect to the number of materials, the accuracy of the developed material properties, and deeper experimental analyses. The mock-up tests were performed to characterize the environment of a typical combat vehicle fire under worst conditions, to corroborate literature correlations on flame heat flux, and to establish that the design attack fire was of no significant harm to occupants.

## 12.2 RESULTS AND PROCESSING OF CONE CALORIMETER TESTS

The testing conducted here should be considered illustrative, exploratory, and insufficient for arriving at accurate material properties. First, the sample size available was sufficient only to test at four cone radiant heat fluxes: 20, 35, 50, and 65 kW/m<sup>2</sup>. More are necessary for sufficient accuracy, and lower values should probe the location of the CHF. Ten data points over incident flux levels 5–65 kW/m<sup>2</sup> are needed for sound results. Also, the CHF should be found by direct experimental means, not by extrapolation. The applicable cone data are examined and processed into properties in table 3, and have been taken directly from the standard test output.

**Table 3. Cone data needed to develop properties**

Material	Heat Flux kW/m <sup>2</sup>	Time to Ignite s	Peak HRR kW/m <sup>2</sup>	AEP MJ/m <sup>2</sup>	$y_{CO}$ g CO/g	$h_c$ kJ/g
Auto Headliner	20	94	317	23	0.0075	20.5
	35	6	405	29.8	0.007	21.4
	50	4	438	29.4	0.0147	20.6
	65	8	377	21	0.041	14.8
White Material	20	40	77	9.1	na	na
	35	23	261	45.7	0	25.2
	50	29	291	65.5	0	23.7
	65	11	179	47.4	0	16
Gray Foam	20	14	176	10.2	0.128	14.5
	35	4	239	18.5	0.131	14.5
	50	4	264	21.9	0.128	15.2
	65	1	232	16.7	0.089	10.6

### 12.2.1 Determining HRP

The HRP is determined from the slope of the peak energy release rate per unit area with the incident radiant heat flux. The establishment of a suitable peak is a procedural issue. For previous work in which this issue was explored [8], an average of the data within 80% of the absolute peak has worked well. Here, the peak value listed on the standard cone processed data is used. Figure 46 shows the results. Four data points are insufficient, especially because they do not conform to the expected increasing burning rate with increasing incident heat flux. The energy release rate must

be monotonic with increasing heat flux. For illustrative purposes, a best linear fit is drawn, favoring conforming points. To demonstrate this data analysis process and to ensure a higher level of accuracy, more data were taken for the gray foam material because that was available. Those additional results will be discussed in section 12.2.6.

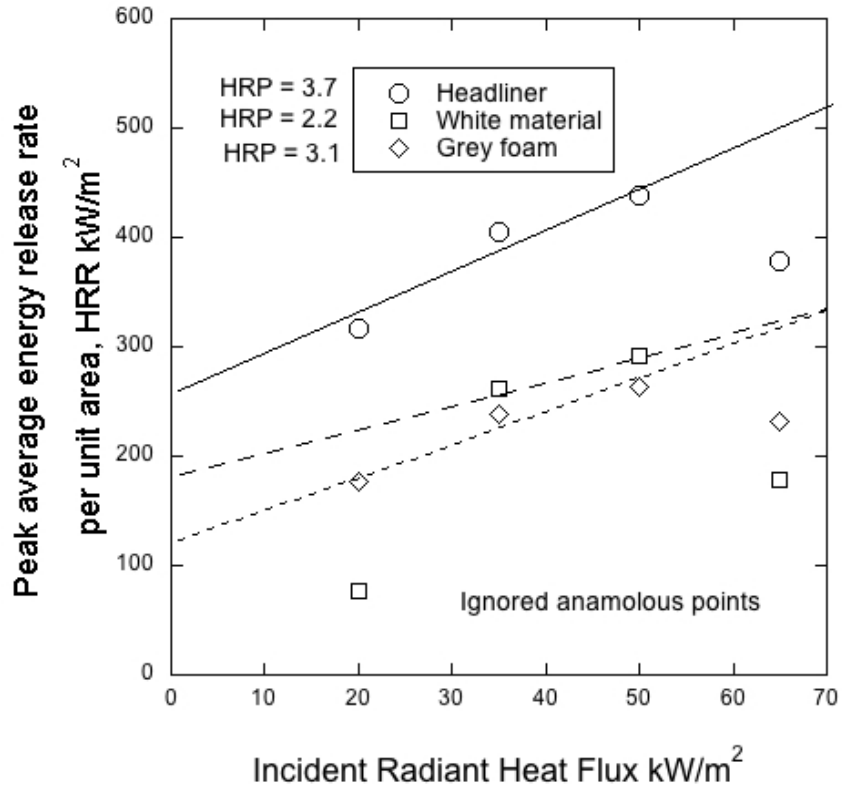
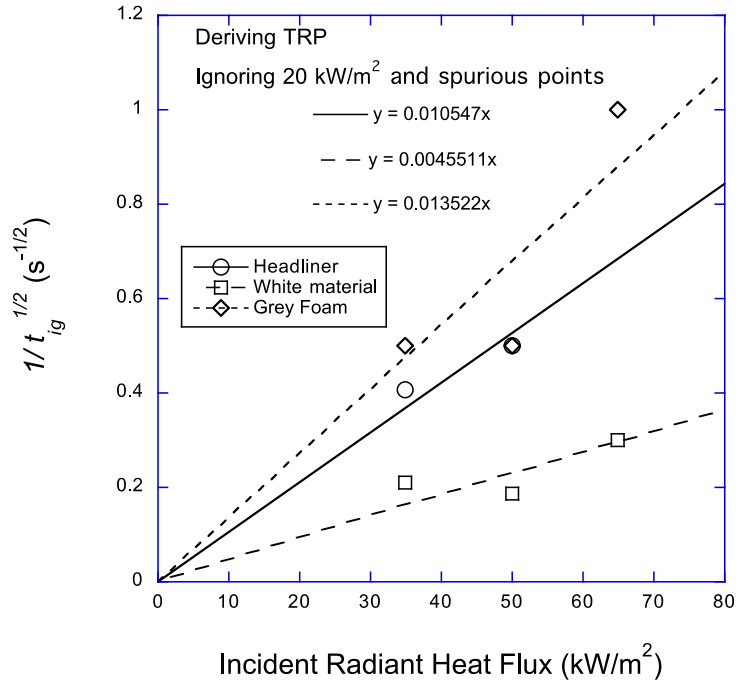


Figure 46. HRP from peak energy release data from cone

### 12.2.2 Determining TRP

TRP is determined from the equation holding at high-incident heat flux  $t_{ig} = \left( \frac{TRP}{\dot{q}_{incident}''} \right)^2$ . Plotting  $t_{ig}^{-1/2}$  with heat flux, emphasizing the high heat flux points, and forcing the linear fit through the origin allows the computation of TRP. Figure 47 shows the results for the three materials.



**Figure 47. TRP from ignition data**

### 12.2.3 Determining CHF

The CHF should properly be found by reducing the heat flux in small increments to find the heat flux at which piloted ignition is not possible. The CHF is between the ignition and no-ignition heat flux. That was not done for these materials; an extrapolation method, although accurate with sufficient data points, was used. The limited data points make the process questionable. The results are shown in figures 48–50.



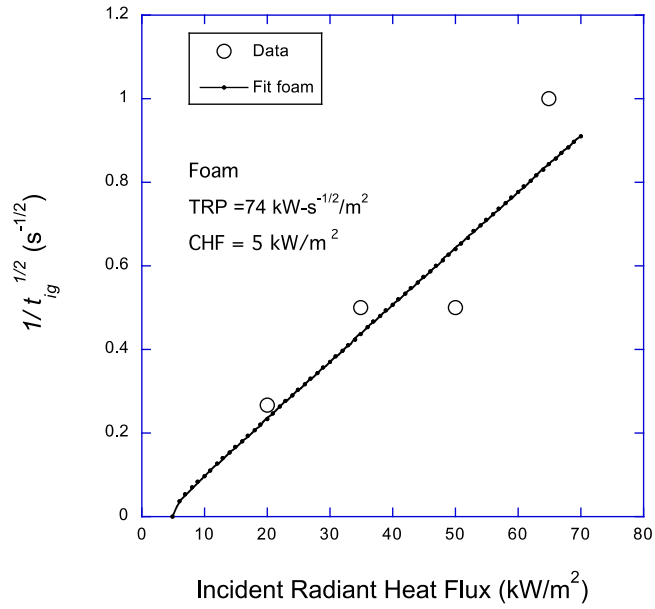


**Figure 48. TRP and CHF for gray foam material**

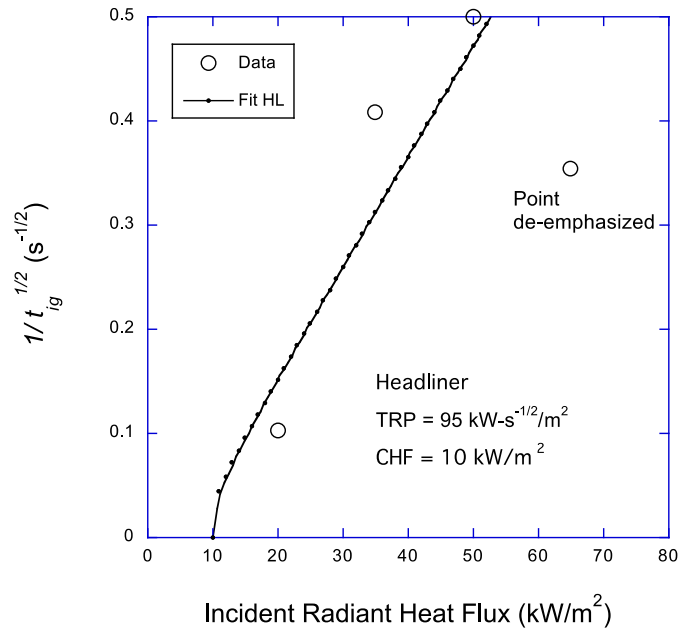


**Figure 49. TRP and CHF for auto headliner**

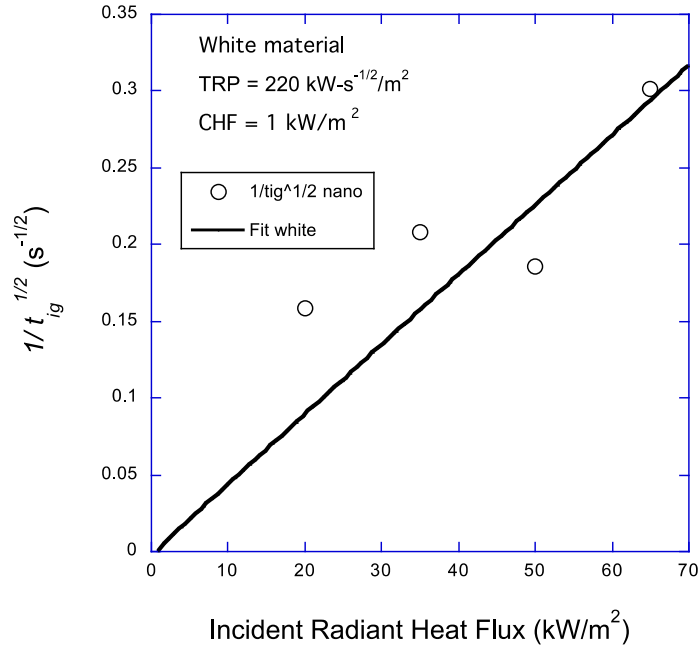


**Figure 50. TRP and CHF for white material**

Figure 51 shows data for high-impact polystyrene taken in the cone calorimeter that shows a more complete and consistent dataset for identifying HRP, TRP, CHF, and other conditions for upward and downward flame spread [24].

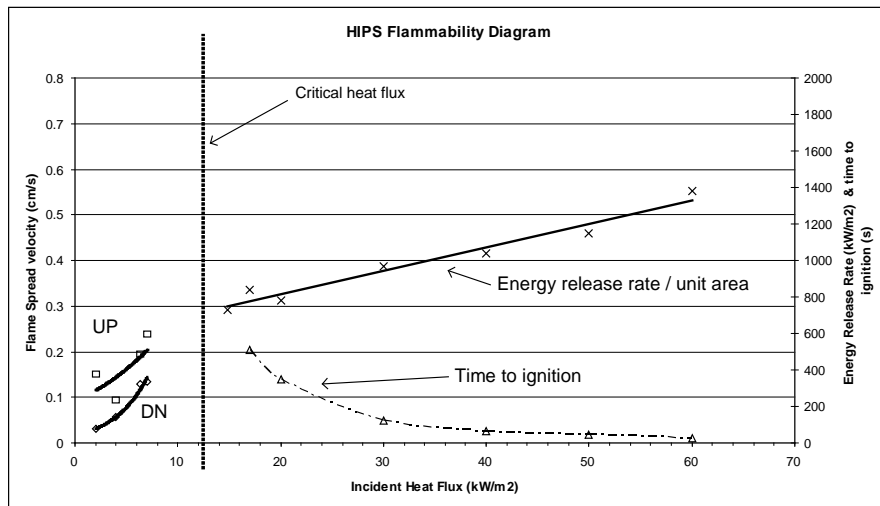


**Figure 51. HIPS flammability diagram [24]**

### 12.2.4 Determining the AEP

The AEP is the total energy available per unit area of material. That is a direct output of the normally processed cone data. It is the time integral of the energy release rate and connotes the amount of available energy to burn. For a fixed thickness, this quantity should be constant for complete burning. However, various factors can affect the AEP. For example, the white material contains silicone and forms an ash at the surface; also, it was seen to melt and drip, losing burnable material. Figure 52 shows the AEP values for the materials measured and their consistency.

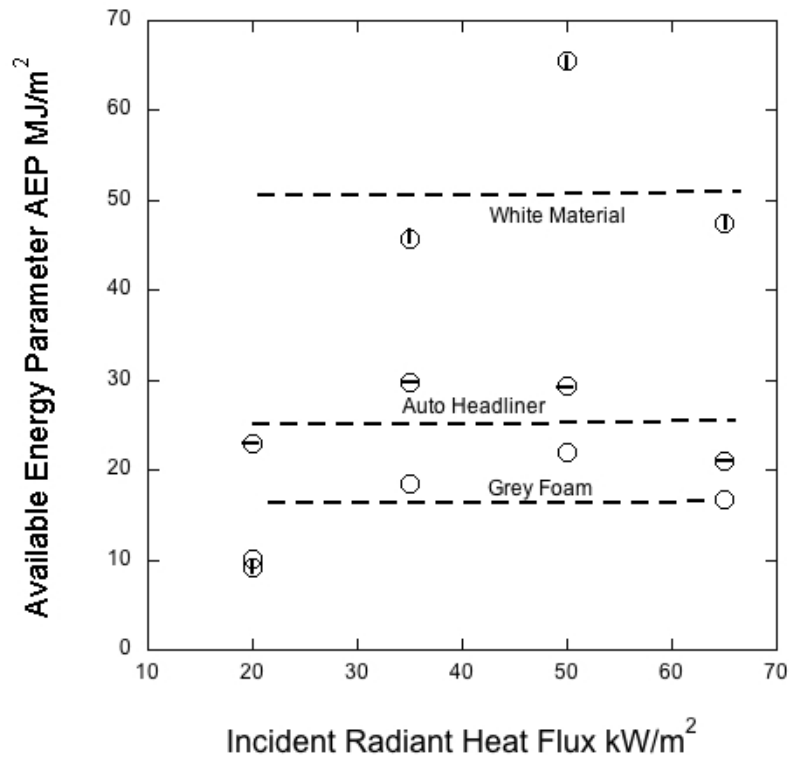


**Figure 52. AEP for tested materials**

### 12.2.5 Compilation

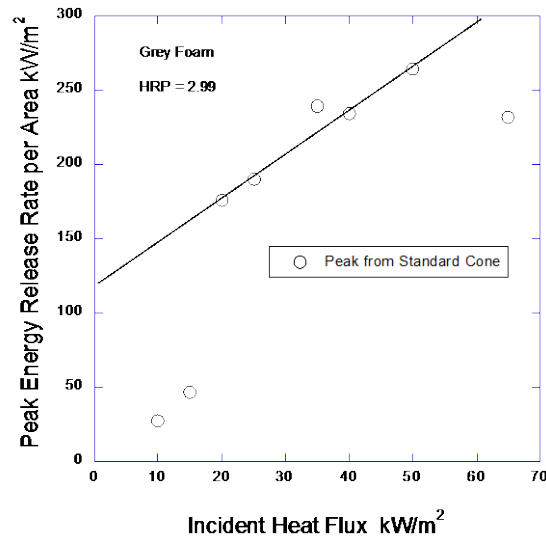
Table 4 shows the derived properties for the three materials.

**Table 4. Material properties**

Property Parameter	units	Auto Headliner	White Material	Gray Foam
HRP	-	3.7	2.2	3.1
TRP	$\text{kW}\cdot\text{s}^{-1/2}/\text{m}^2$	95	220	74
CHF	$\text{kW}/\text{m}^2$	10	1	5
AEP	$\text{MJ}/\text{m}^2$	26	50	17
Yield CO, $y_{CO}$	$\text{g CO}/\text{g fuel}$	~ 0.09	~ 0	0.13
Heat of combustion	$\text{kJ}/\text{g}$	21	24	15

### 12.2.6 Refinement of Results for Gray Foam

Additional data were taken for the gray foam material because there was more in supply. It is needed to fully show an accurate determination of the fire properties. The following graphs (figures 53–56) indicate the new results. Despite the sparse original data, the results do not change much. However, accuracy in determining the properties requires a sufficient set of data and their interpretation.



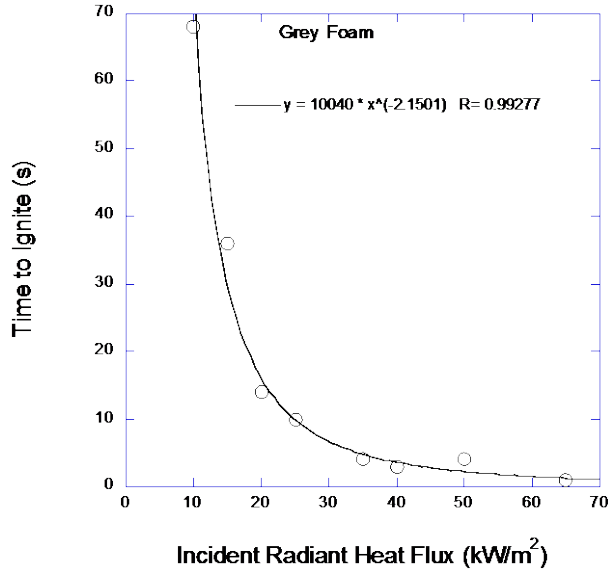
**Figure 53. Refined HRP determination for gray foam**

Figure 53 shows that some points need to be ignored. At the low heat, flux ignition occurred, but burning was not sustained for a long enough time.

The data for ignition in figures 54 and 55 indicate a good set of data; however, the heat flux was not reduced enough to determine the CHF directly. In this case, the CHF was determined by fitting the approximate theory:

$$\sqrt{t_{ig}} = -\frac{TRP}{CHF} \ln\left(1 - \frac{CHF}{\dot{q}''_{incident}}\right) \quad (62)$$

after TRP was determined by the straight line in figure 55.



**Figure 54. Additional ignition data for gray foam**

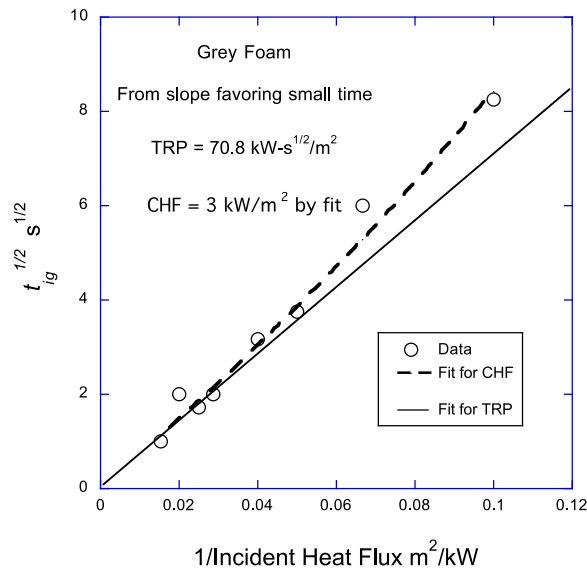


**Figure 55. Refined CHF and TRP for gray foam**

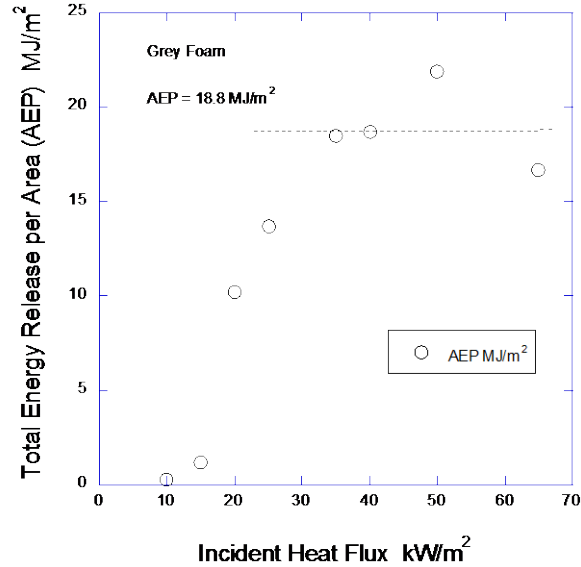


**Figure 56. Refined AEP for gray foam**

The determination of AEP in figure 56 clearly shows that the low heat flux data do not burn completely. The high heat flux data show the true AEP.

### 12.3 CRITICAL CONDITIONS BASED ON SCENARIO HEAT FLUX AND MODELING FIRE GROWTH

As an example, the three materials tested will be evaluated in terms of the pass-fail criteria laid out. The critical conditions are based on the following:

$$CHF_{crit} = 25 \text{ kW/m}^2$$

$$TRP_{crit} = 274 \text{ kW}\cdot\text{s}^{-1/2}/\text{m}^2$$

$$HRP_{crit} = 140/(30 \text{ kW/m}^2 - CHF)$$

$$AEP_{crit} = TRP^2 (30 - CHF) HRP / 900 \text{ kJ/m}^2.$$

The acceptance with respect to toxic hazard depends on the concentration of toxic species in the mock-up sized vehicle. From these concentrations, the FED for incapacitation must be calculated. The acceptance level of the FED between 0 and 1 must be decided based on a selected tolerance limit for the population. The FED value of 1 represents the level at which 50% of an exposed population would be incapacitated.

The concentration in mass fraction terms is computed for each species by:

$$Y_{i,b} = (0.0189 \text{ kJ/g})(30 - CHF) HRP y_i / \Delta h_c \quad (63)$$

The values of the critical parameters and the CO mass fraction were computed for the three materials and are shown in table 5.

**Table 5. Material pass-fail outcome**

Material	CHF kW/m <sup>2</sup>	TRP kW-s <sup>-1/2</sup> /m <sup>2</sup>	Time To Ignite s	HRP --	HRP <sub>crit</sub>	AEP MJ/m <sup>2</sup>	AEP <sub>crit</sub> MJ/m <sup>2</sup>
Auto headliner	10	95	19	3.7	7.0	26	0.74
White material	1	220	100	2.2	4.9	50	3.4
Gray foam	5	74	11	3.1	5.6	17	0.47

The following is concluded from table 5:

1. All materials have CHF < 25 kW/m<sup>2</sup> and, therefore, ignite.
2. All materials ignite in less than 2 minutes.
3. All materials have HRP < HRP<sub>crit</sub>, and, therefore, do not spread.
4. All materials have enough available energy to enable spread.
5. All of these materials, based on the preliminary derived parameters, would pass the test requirements from a thermal fire hazard consideration.
6. The inclusion of safety factors later will alter these preliminary conclusions.

#### 12.4 TOXICITY ASSESSMENT FROM CONE TESTS

The acceptance with respect to toxic hazard depends on the concentration of toxic species in the mock-up sized vehicle. From these concentrations, the FED for incapacitation must be calculated. The acceptance level of the FED between 0 and 1 must be decided on based on a selected tolerance limit for the population. The FED value of 1 represents the level at which 50% of an exposed population would be incapacitated.

##### 12.4.1 Methods of Gas Sampling and Analysis for Cone Tests

The three methods of gas analysis were: non-dispersive infrared gas analyzers for CO and CO<sub>2</sub>; post-test ion chromatographic analysis for fluoride, chloride, bromide, sulfate, and nitrate from gas sample tubes; and post-test Draeger tube analysis of HCN from gas bag samples. Samples for gas analyzer, bag sampling, and ion chromatography (IC) sampling were pulled separately from a cross connected directly to the cone sample ring. A flow of 0.5l pm was set for both the bag and tube sampling. The cone test duration was 5 minutes for the gray foam and auto headliner at 65, 50, and 35kW/m<sup>2</sup>. The test duration for the white material was 785s, 1375s, and 898s at 65, 50, and 35kW/m<sup>2</sup>, respectively.

The bag sample train ran from the cross to a 0.2-micron filter with a filtration area of 600 cm<sup>2</sup>, to a stainless steel bellows pump, to a flow meter, to a Tedlar<sup>®</sup> sample bag. The tube sample was pulled from the cross into a 20-cm length of ¼" perfluoroalkoxy fluoropolymer (PFA) tubing directly to the sample tube, then to a filter, Drierite<sup>™</sup>, flow meter, and vacuum pump.

The PFA gas-collection tube is 26 cm long with an inner diameter of 9 mm. It is filled with 3mm/OD glass beads coated with an NaOH solution. The tube was placed in an ice water bath during sample collection.

After the test, the sample tube and the 20 cm length of PFA tubing is eluted with 30ml of a dilute NaOH solution. The 30 ml sample is diluted for further analysis when any analyte is outside the calibration range of the ion chromatographic method.

The anions were quantified using external standardization with a 7-point calibration curve. The limits of detection for IC analysis are 0.1uM for fluoride and 0.5 uM for the remaining anions.

The samples were filtered through a Pall® IC Acrodisc® 25 mm x 0.45-micron syringe filter and injected neat into the IC, except for samples that needed to be diluted. The samples were analyzed according to the following IC conditions:

IC: Metrohm Prof 850 IC  
Column: Metrohm A Supp 5 - 250  
Eluent: 3.2 mM Na<sub>2</sub>CO<sub>3</sub>/1.0 mM NaHCO<sub>3</sub>  
Flow Rate: 0.7 mL/min  
Injection Volume: 20 uL  
Detection: Suppressed Conductivity  
Run Time: 30 min

An example ion chromatogram is shown in figure 57.

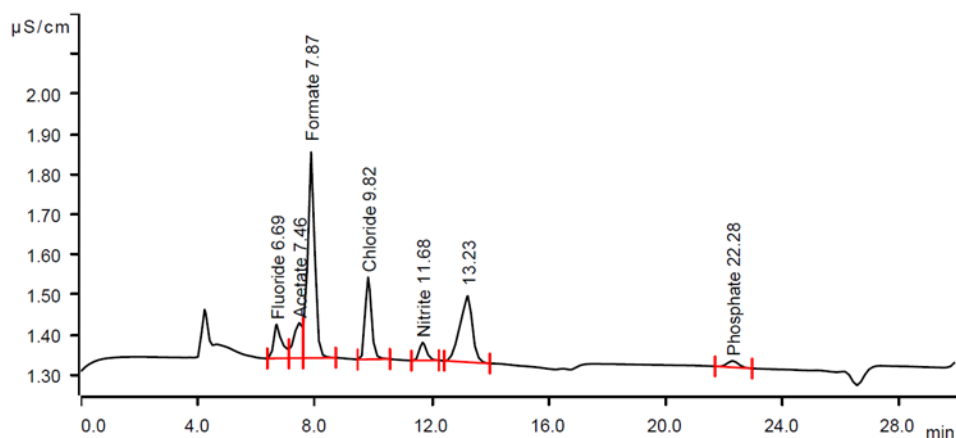


**Figure 57. Ion chromatogram for gray foam sample:  
sample collected from the cone at 65kW/m<sup>2</sup>**

#### 12.4.2 Gas Yields for Cone Tests

The gas yield,  $y_i$  (g-gas/g-fuel), was obtained for the gas corresponding to each anion in solution, given the volume of solution, the volumetric flow rate of gas sampled, the volumetric flow of the cone exhaust gas, the gas sampling time, the molecular weight of that gas, and the molar volume of the analyte gas, assuming a sample temperature of 21.1 °C and 1 atmosphere pressure.

The results of this complete gas analysis for the three-headliner materials are depicted in figures 58–60. The approximate constancy of the species yields supports the yield as a material property.



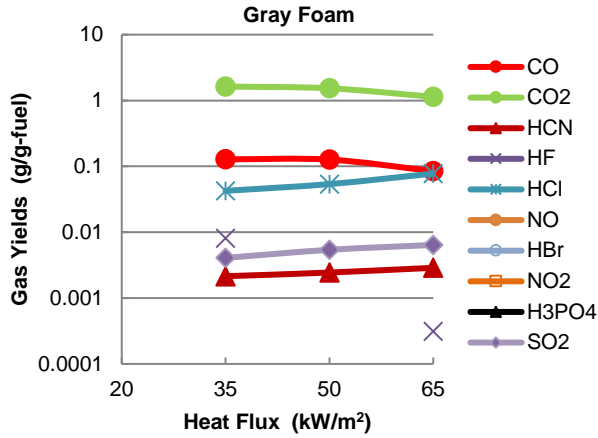


Figure 58. Gas yields for gray foam run on the cone

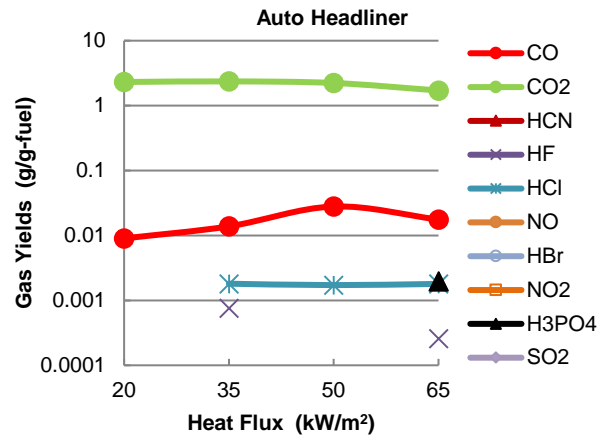


Figure 59. Gas yields for auto headliner run on the cone

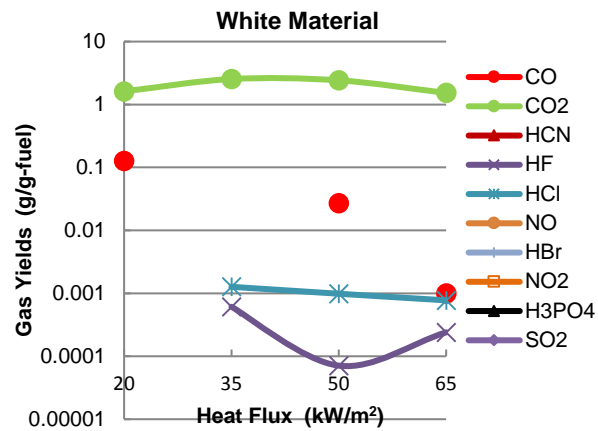
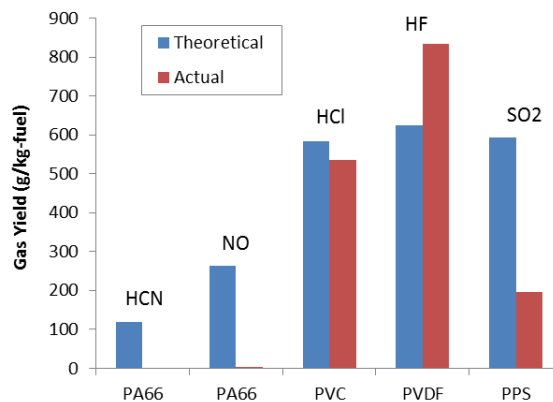


Figure 60. Gas yields for white material run on the cone

The gas yields of pure plastics run on the cone at 50 kW/m<sup>2</sup> are compared with theoretical gas yields in figure 61. The cone tests were run to the time of no mass loss for these plastics. The

reasonable agreement for HCl, HF, and SO<sub>2</sub> is a validation check of the method of collection and analysis for these gases.

The theoretical gas yields were calculated assuming conservation of mass and assuming all atomic N, Cl, F, and S in the sample reacted completely to form HCN or NO, HCl, HF, and SO<sub>2</sub>, respectively. The low SO<sub>2</sub> yield indicates that other S-containing gases may have been produced, such as COS, H<sub>2</sub>S, and CS<sub>2</sub>. The low HCN yields may be due in part to HCN losses in the bag sampling technique performed for HCN. Higher yields of NO were expected. NO<sub>2</sub> was not detected.



**Figure 61. Comparison of cone gas yields for pure plastics: predicted assuming conservation of mass for N, Cl, F, and S versus 5-minute average for 35, 50, and 65kW/m<sup>2</sup>**

#### 12.4.3 Predicted Mock-Up Vehicle Concentrations Obtained from Cone Tests

The gas yields shown in figures 58–60 were converted to gas mass fractions using equations 53 and 61, respectively, then converted to mole fractions using the molecular weight of air and the molecular weight of each gas, and further converted to volumetric concentrations of gas. Equation 53 models the output at the upper vents. Equation 61 models the average concentration in the test chamber. The results are shown in figures 62–64.

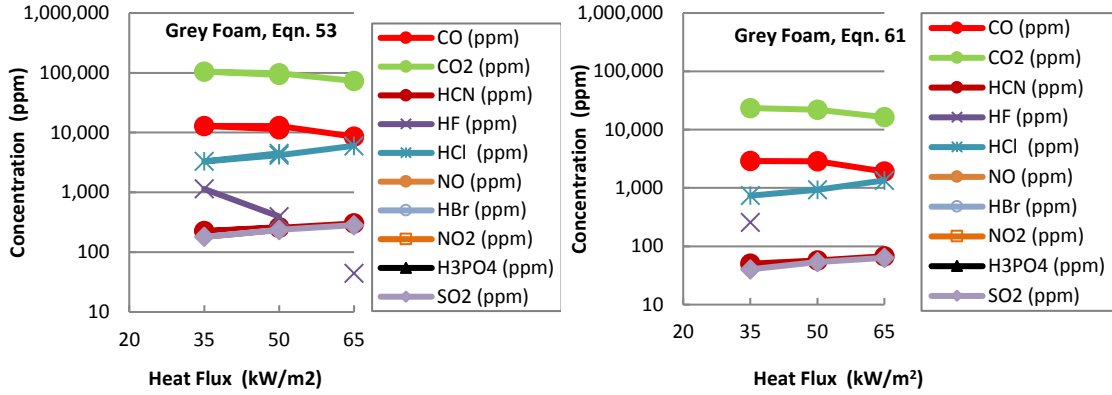


**Figure 62. Predicted mock-up vehicle concentrations for gray foam based on cone yields and equation 53 and 61 mass fractions**

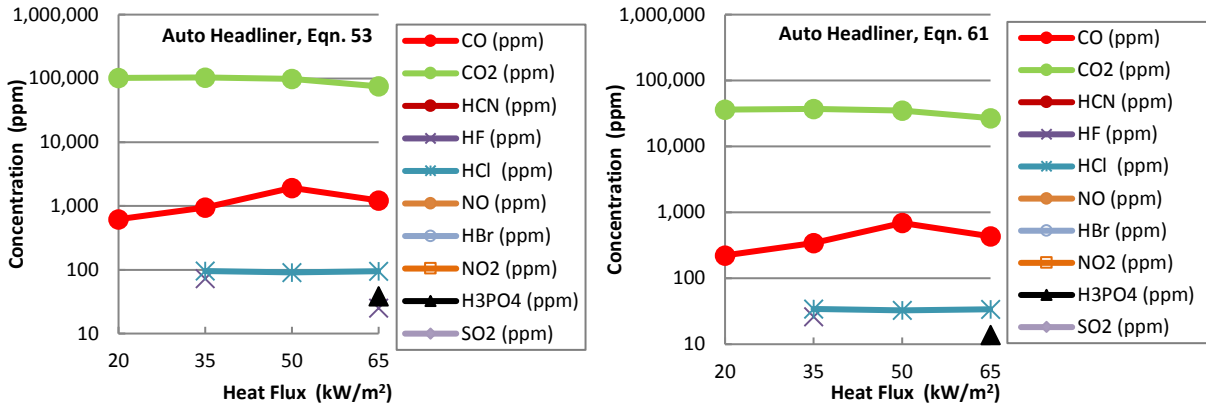


**Figure 63. Predicted mock-up vehicle concentrations for auto headliner based on cone yields and equation 53 and 61 mass fractions**

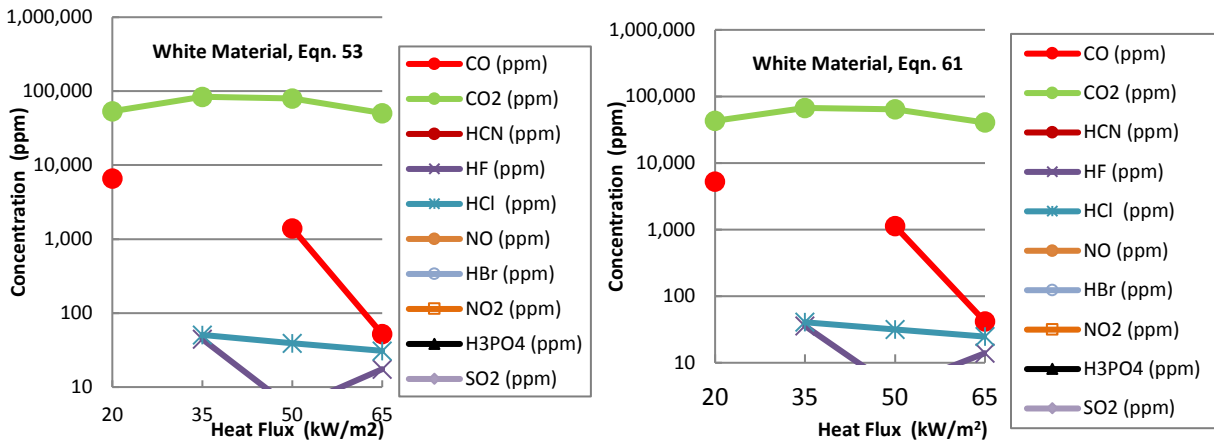


**Figure 64. Predicted mock-up vehicle concentrations for white material based on cone yields and equation 53 and 61 mass fractions**

12.4.4 Comparison of Gas Concentrations Predicted from Cone Tests Using Equation 61 and Concentrations Measured in the Mock-Up Vehicle and Cone Yields Scaled to the Vehicle Volume

Figures 65–67 compare the gas concentrations measured in the test vehicle with the predicted gas concentrations obtained by applying equation 61 to the cone data.

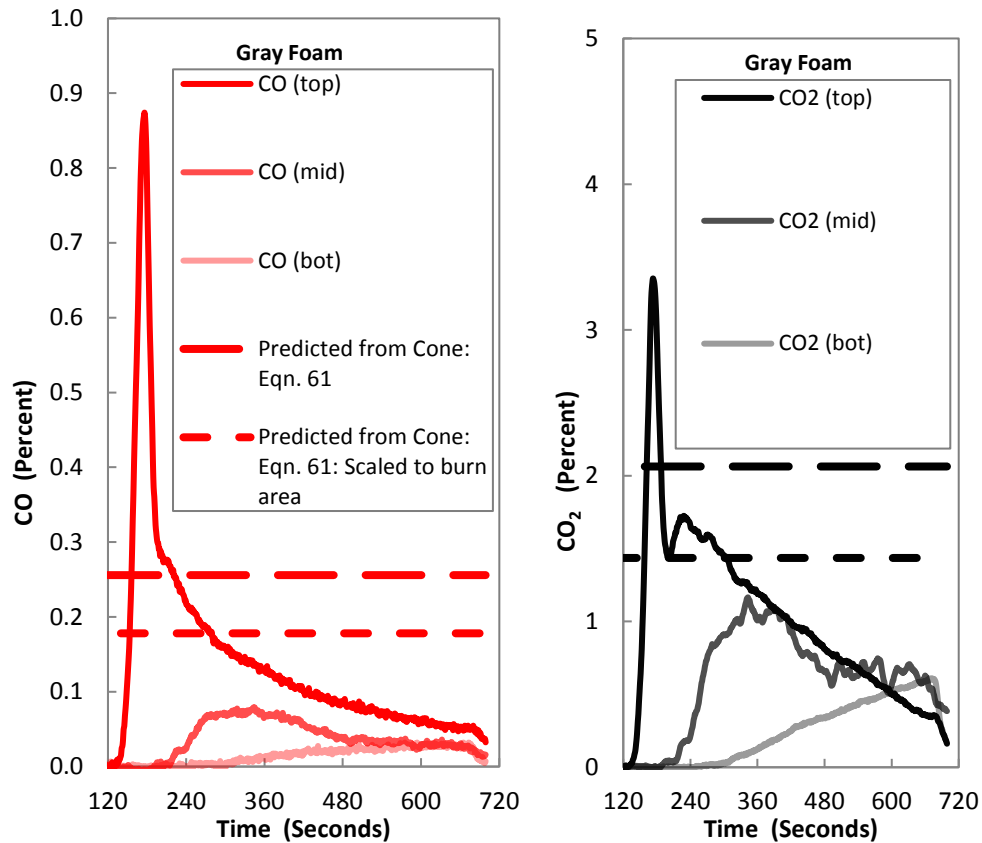


**Figure 65. Gray foam: comparison of CO and CO<sub>2</sub> concentrations in the mock-up vehicle with concentration obtained by applying equation 61 to the cone data at the assumed burn radius of 32 cm and the observed burn radius of 26.7 cm**

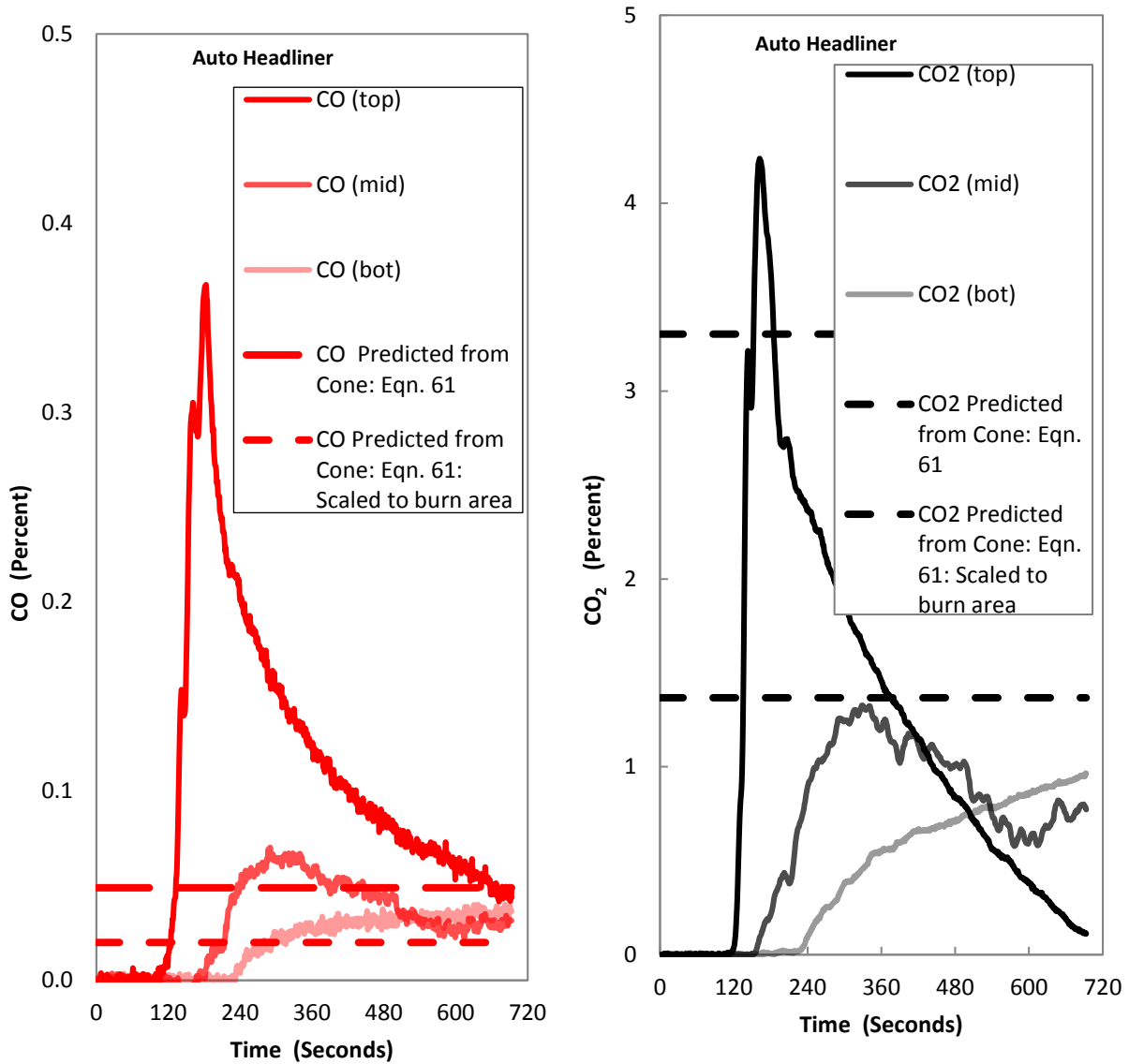


**Figure 66. Auto headliner: comparison of CO and CO<sub>2</sub> concentrations in the mock-up vehicle with concentration obtained by applying equation 61 to the cone data at the assumed burn radius of 32 cm and the observed burn radius of 20.3 cm**

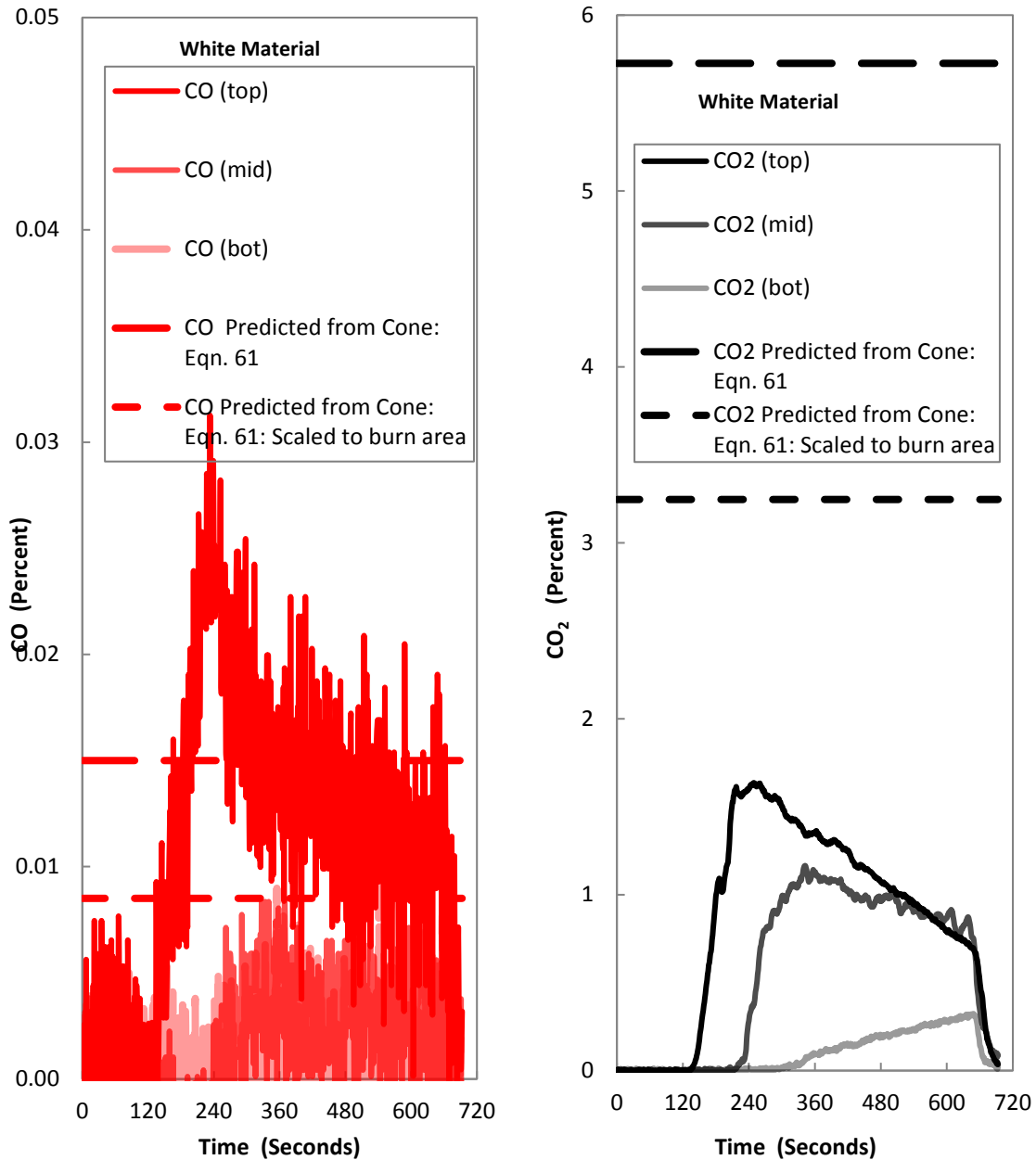


**Figure 67. White material: comparison of CO and CO<sub>2</sub> concentrations in the mock-up vehicle concentration obtained by applying equation 61 to the cone data at the assumed burn radius of 32 cm and the observed burn radius of 24.1 cm**

12.4.5 Toxicity Assessment in Test Vehicle Based on Cone Concentration Data

The FED<sub>I</sub> and FEC were calculated for the three test materials in the test vehicle based on applying equation 53 to the cone yields. Toxicity results are shown in tables 6 and 7 for the protocol toxicity model, as well as other models for comparison.

**Table 6. Comparison of toxicity results for various toxicity models for cone tests averaged for 35, 50, and 65kW/m<sup>2</sup> based on applying equation 61 to asphyxiant gas cone yields**

Material	Single Gas Pass-Fail Models Applied as FED Model		FAA FED Incapacitation Model				ISO13571-2012 FED Tenability Model			
	Boeing-based FED	Airbus-based FED	V <sub>CO<sub>2</sub></sub>	FED <sub>I</sub> CO	FED <sub>I</sub> HCN	FED <sub>I</sub> TOTAL	V <sub>CO<sub>2</sub></sub>	FED CO	FED HCN	FED TOTAL
Gray Foam	1.12	2.95	1.66	0.62	0.30	0.92	1.51	0.55	0.20	0.75
Auto Headliner	0.14	0.49	2.26	0.16	0.00	0.16	1.94	0.14	0.00	0.14
White Material	0.04	0.150	4.14	0.09	0.00	0.09	3.14	0.07	0.00	0.07

**Table 7. Comparison of toxicity results for various toxicity models for cone tests averaged for 35, 50 and 65kW/m<sup>2</sup> based on applying equation 61 to irritant gas cone yields**

Material	Boeing-based FEC	Airbus based FEC	ISO 13571FEC	SPFE (Purser) FEC
Gray foam	2.98	8.13	1.53	7.66
Auto headliner	0.13	0.34	0.06	0.23
White material	0.15	0.39	0.07	0.25

As discussed in the previous section, the concentrations obtained from equation 53 overestimate the actual test article concentrations. The auto headliner and the white material pass the toxicity criteria as both the FED<sub>I</sub> and the FEC < 0.3 for these materials. The gray foam fails both the FED<sub>I</sub> and the FEC criteria because the FED<sub>I</sub> > 0.3 and the FEC > 0.3.

The results from other toxicity models are provided for comparison. These data are plotted in figures 68 and 69.

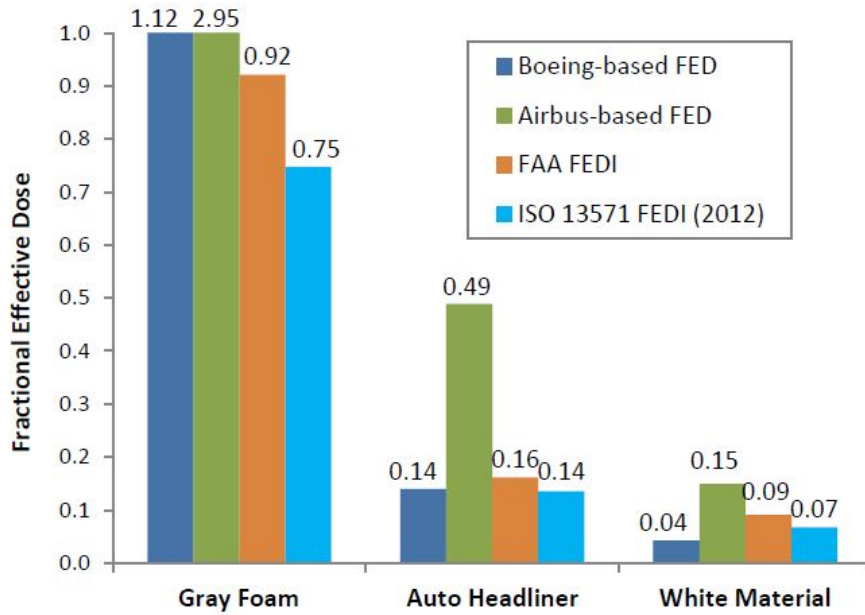


**Figure 68. Comparison of toxicity models for asphyxiant gases using simulated vehicle gas concentrations obtained from 35, 50, and 65 kW/m<sup>2</sup> cone test average yields and equation 61**

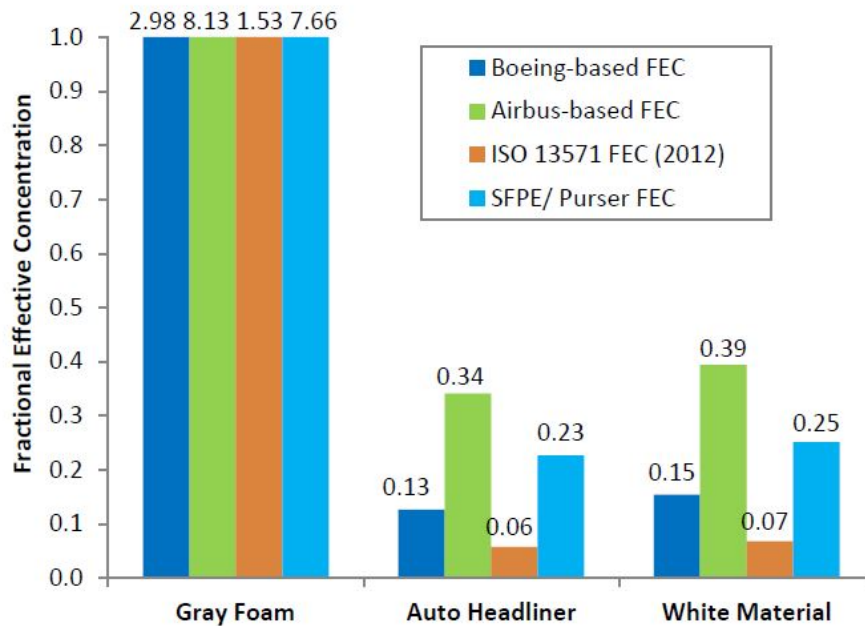


**Figure 69. Comparison of toxicity models for irritant gases using simulated vehicle gas concentrations obtained from 35, 50, and 65 kW/m<sup>2</sup> cone test average yields and equation 61**



## 12.5 PERFORMANCE IN OTHER FLAMMABILITY TESTS

### 12.5.1 FAA/OSU Aircraft Cabin Lining Fire Test

After examining the three materials with respect to the aircraft safety requirements of the FAA/OSU test, it was found that regulation requires that the critical energy release rate per unit area be less than  $65 \text{ kW/m}^2$  and that the AEP for 2 minutes be less than  $65 \text{ kW-min/m}^2$  or  $3.9 \text{ MJ/m}^2$ .

The heat flux in the OSU test is estimated at  $30 \text{ kW/m}^2$  for the flame plus  $35 \text{ kW/m}^2$  from the radiant heater. The energy release rate per unit area under this incident heat flux is found as  $\dot{Q}'' = (30 + 35 - CHF)HRP$ . Table 8 shows the estimated performance of the three materials in the OSU regulation. All these materials would not pass the aircraft-cabin-lining fire regulation.

**Table 8. Estimate of FAA/OSU performance,  $\dot{q}'' = 65 \text{ kW/m}^2$  and  $\dot{Q}'' \leq 65 \text{ kW/m}^2$**

Material	$\dot{Q}'' \text{ kW/m}^2$
Auto headliner	204
White material	141
Gray foam	186

### 12.5.2 ISO 9705 Room Corner Test

Based on figure 24, a material would lead to flashover in the room corner test if the following conditions were met:

$$\frac{(60 \text{ kW/m}^2 - CHF)HRP}{100 \text{ kW/m}^2} \geq 0.5 \text{ or } \dot{Q}'' \leq \dot{Q}''_{crit} = 50 \text{ kW/m}^2$$

*and*

$$\frac{t_b}{t_{ig}} \geq 1, \text{ or } AEP \geq AEP_{crit} = \frac{TRP^2 HRP}{(60 \text{ kW/m}^2 - CHF)} \quad (64)$$

Table 9 gives an estimate of the performance in the room corner test, showing that both the critical values for energy release and AEP are exceeded by the materials; the results indicate that all would lead to flashover.

**Table 9. Estimation of performance in ISO 9705,  $\dot{q}'' = 60 \text{ kW/m}^2$  and  $\dot{Q}''_{crit} = 50 \text{ kW/m}^2$**

Material	$\dot{Q}''$ kW/m <sup>2</sup>	AEP <sub>crit</sub> MJ/m <sup>2</sup>	AEP <sub>crit</sub> MJ/m <sup>2</sup>
Auto Headliner	185	0.67	26
White Material	130	1.8	50
Gray Foam	171	0.31	17

### 12.5.3 Estimation of Performance in the Steiner Tunnel Test, ASTM E 84

The signature flame heat flux for the ASTM E 84 tunnel test is  $35 \text{ kW/m}^2$  [25]. The flame length formula adopted indicated a critical energy of  $100 \text{ kW/m}^2$ . The initial length of the burner flame of 1.37 is taken as the initial length of the material ignited.

An evaluation can be carried out of the materials listed in table 4 for their performance in E 84. Because burnout is not a factor here (the materials have a large AEP), the materials must have a critical energy of less than  $100 \text{ kW/m}^2$  for spread to stop. Because the tunnel is 25 ft (7.6 m) in length, stoppage may theoretically occur after its physical length. According to the solution by Cleary et al [21], the pyrolysis position would stop at:

$$x_{t \rightarrow \infty} = 1.37 \left( \frac{\dot{Q}''_{crit}}{\dot{Q}''_{crit} - \dot{q}''} \right) \text{ m.} \quad (65)$$

Table 10 gives the results, which indicate that flame spread would not be sustained, and the distance predicted for the burning front is likely to lead to a flame length that reaches the end of the tunnel. The tunnel rating for these materials would then be based on the time for the (highly fluctuating) flame to be observed to reach the end.

**Table 10. Estimation of performance in 25 ft (7.6 m) tunnel test**

$$\dot{q}'' = 35 \text{ kW/m}^2 \text{ and } \dot{Q}''_{crit} = 100 \text{ kW/m}^2$$

Material	$\dot{Q}''$ kW/m <sup>2</sup>	$x_{t \rightarrow \infty}$ m
Auto Headliner	95	18
White Material	74	5.3
Gray Foam	93	20

### 12.5.4 Estimation of performance in UL 94

Finally, performance in UL 94 is examined. This is a small flame exposure test of a vertical material. A V-0 rating in the test means that either no ignition occurs or that extinction occurs after flame withdrawal. Work by Downey et al [23] indicates that the ignition flame has a heat flux of approximately  $60 \text{ kW/m}^2$ , and generally materials that have an energy release rate of less than 300

kW/m<sup>2</sup> tend to receive a V-0 rating. The MSDS for the gray foam indicates it received V-0 for the thickness tested. Table 11 confirms that all the materials are computed to have a V-0 rating.

**Table 11. Estimation of performance in UL 94,**  
 $\dot{q}'' = 60 \text{ kW/m}^2$  and  $\dot{Q}''_{crit} = 300 \text{ kW/m}^2$  for V-0

Material	$\dot{Q}''$ kW/m <sup>2</sup>	Rating
Auto headliner	185	V-0
White material	130	V-0
Gray foam	171	V-0

This section shows that CHF, HRP, TRP, and AEP all play roles in flammability tests. The key is to tie the test and its performance to the actual hazard scenario for the end-use of the material. The material results examined here are for illustration only because the material properties may lack accuracy, and models have made the estimations. However, it cannot be denied that these properties underlie the flammability attributes of a material.

### 13. CONCLUSIONS

The fire hazards with respect to thermal or toxic effects on the occupants of a combat vehicle were examined. A 65 kW fire 0.76 m below the ceiling, selected as the design ignition source for the ceiling material, was found to be a worst case. This fire imposed a flame of approximately 32 cm radius on the ceiling and an average heat flux of approximately 25 kW/m<sup>2</sup>. A ceiling fire alone was also examined but proved to be a lesser threat.

For the thermal threat, a criterion of safety was defined as no ignition within 2 minutes or no flame spread over the ceiling. For the toxic threat, the criterion for safety was defined as no crew incapacitation or performance decrements of more than 5 minutes in a small (worst-case) compartment 2.2 x 3.2 x 2 m high with an upper wall vent of 61 x 15.3 cm high in total size. A well-mixed fire model is used to determine the toxic gas concentration in this compartment. Then a fractional effective dose and fractional effective concentration (FEC) are computed to determine whether the toxic hazard exceeds the acceptable safety thresholds (fractional effective dose for incapacitation, critical (FED<sub>Icrit</sub>) and fractional effective concentration, critical (FEC<sub>crit</sub>) for the crew.

The basis of the test protocol is the determination of material properties by ASTM E 1354 (or comparable ASTM E 2058). The properties include:

1. Critical heat flux for ignition (CHF)
2. Thermal response parameter (TRP)
3. Heat release parameter (HRP)
4. Available energy parameter (AEP)
5. Toxic gas yields,  $y_i$ .

The pass-fail criteria developed in the analyses are described as follows:

Meeting the ignitability criterion, OR the flame spread AND the toxicity criteria qualifies the material for use as a headliner in military combat vehicles.

#### IGNITABILITY

1. The material will not ignite if the measured critical heat flux for ignition CHF is greater than the heat flux from the fire threat. If CHF is less than  $CHF_{crit}$ , the material will ignite and the thermal response parameter TRP will determine the ignition delay.
2. If TRP is greater than  $TRP_{crit}$ , the material will take more than 2 minutes to ignite, after which flame spread and toxicity will determine the fire hazard.

IGNITABILITY CRITERION:  $CHF > CHF_{crit}$  or  $TRP > TRP_{crit}$

#### FLAME SPREAD

1. The HRP is the slope of a line fitted to the maximum/peak heat release rate during the test (peak heat release rate,  $kW/m^2$ ) on the ordinate versus the external heat flux ( $q_{ext}$ ,  $kW/m^2$ ) on the abscissa. The material will not spread if  $HRP < HRP_{crit}$ .
2. The material has the potential to spread flames along the ceiling if the fuel load, also called the AEP ( $kJ/m^2$ ), is greater than  $AEP_{crit}$ .

FLAME SPREAD CRITERION:  $AEP < AEP_{crit}$  or  $HRP < HRP_{crit}$

#### TOXIC POTENCY OF SMOKE

The toxic potency of the smoke is computed from the yields of the asphyxiant gases carbon monoxide, carbon dioxide, and hydrogen cyanide, and the irritant gases hydrogen chloride, hydrogen bromide, hydrogen fluoride, nitrogen dioxide, and sulfur dioxide obtained by sampling the gases during flaming combustion of the sample.

1. The fractional effective dose of the combination of the asphyxiant gases is computed from the sum of the product of the concentration and time for each gas divided by its critical dose for incapacitation. The criterion for incapacitation is the fractional effective dose of asphyxiant combustion gases.  $FED_I$  is less than the fractional effective dose for incapacitation  $FED_{I,crit}$  after 5 minutes in the vehicle. The  $V_{CO_2}$  multiplication factor for the enhanced uptake of CO and HCN was factored into the concentration term in the regression equations for those gases.

ASPHYXIAN GAS CRITERION:  $FED_I < FED_{I,crit}$ .

2. The FEC of the irritant gases is computed from the sum of the average concentration of each gas divided by its tenability endpoint  $F_i$ . The criterion for irritant effects is the sum of the FEC of irritant combustion gases. FEC is less than the FEC  $FEC_{crit}$  after 5 minutes in the vehicle.

IRRITANT GAS CRITERION:  $FEC < FEC_{crit}$ .

The pass-fail criteria have been based on analyses, scientific correlations, and judgment. The process has been laid out in a transparent and engineering-design methodology. Some approximations have inclined the results to favor an increase in safety. However, no safety factors have been introduced. A regulator may wish to skew the protocol to a higher degree of safety. A recommendation with a safety factor introduced is explicitly suggested here as:

$$CHF_{crit} = 30 \text{ kW/m}^2 (+ 20 \%)$$

$$TRP > TRP_{crit} = 350 \text{ kW-s}^{1/2}/\text{m}^2 (+20 \%)$$

$$HRP_{crit} = 70/(30 \text{ kW/m}^2 - CHF) (-50 \%) \quad (66)$$

$$AEP_{crit} = TRP^2(30-CHF) HRP/900 \text{ kJ/m}^2 \text{ (no change)}$$

$$FED_{I,crit} = 0.3$$

$$FEC_{crit} = 0.3$$

A summary of the material properties, test methods and performance criteria are provided in table 12.

**Table 12. Recommend Headliner Protocol**

Transportation Sector	Interior Material Component	Material Property	Test Method	Performance Criterion
<div style="border: 1px solid black; padding: 5px; margin-bottom: 5px;"> <b>Military Ground Vehicles</b> </div> <div style="border: 1px solid black; padding: 5px;"> <b>US Army Tank Automotive Research, Development and Engineering Center</b> </div>	Ceiling Head Impact Protective Material	Ignitability (Option 1)	ASTM E 1354-15 Oxygen Consumption Cone Calorimeter	<p><b>Material will not ignite;</b>  <math>CHF &gt; CHF_{crit} = 30 \text{ kW/m}^2 (+ 20 \% - SF^*)</math>  <b>OR</b>  <b>Time to Ignition &gt; 2 minutes;</b>  <math>TRP &gt; TRP_{crit} = 350 \text{ kW-s}^{1/2}/\text{m}^2 (+20 \% - SF^*)</math></p>
		Flame Spread (Option 2)	ASTM E 1354-15 Oxygen Consumption Cone Calorimeter	<p><b>Material will not spread;</b>  <math>HRP &lt; HRP_{crit} = 70/(30 \text{ kW/m}^2 - CHF) (-50 \% - SF^*)</math>  <b>OR</b>  <b>Material with potential to spread;</b>  <math>AEP_{crit} = TRP^2(30-CHF)HRP/900 \text{ kJ/m}^2</math></p>
		Toxicity	ASTM E 1354-15 Oxygen Consumption Cone Calorimeter w/ Gas Collection	<p><b>Asphyxiant Gases (CO<sub>2</sub>, CO, HCN, HCl) Incapacitation;</b>            Exposure &gt; 5 Minutes;  <math>FED_1 &lt; FED_{I,crit} = 0.3</math>  <b>or</b>  <b>Irritant Gases (HCl, HBr, HF, NO<sub>2</sub>, SO<sub>2</sub>) Effect;</b>            Exposure &gt; 5 Minutes;  <math>FEC &lt; FEC_{crit} = 0.3</math></p>

\* Includes Recommended Safety Factor (SF) for increased degree of safety.

A flowchart for the test protocol to determine the fire safety of a candidate head impact material is illustrated in figure 7.

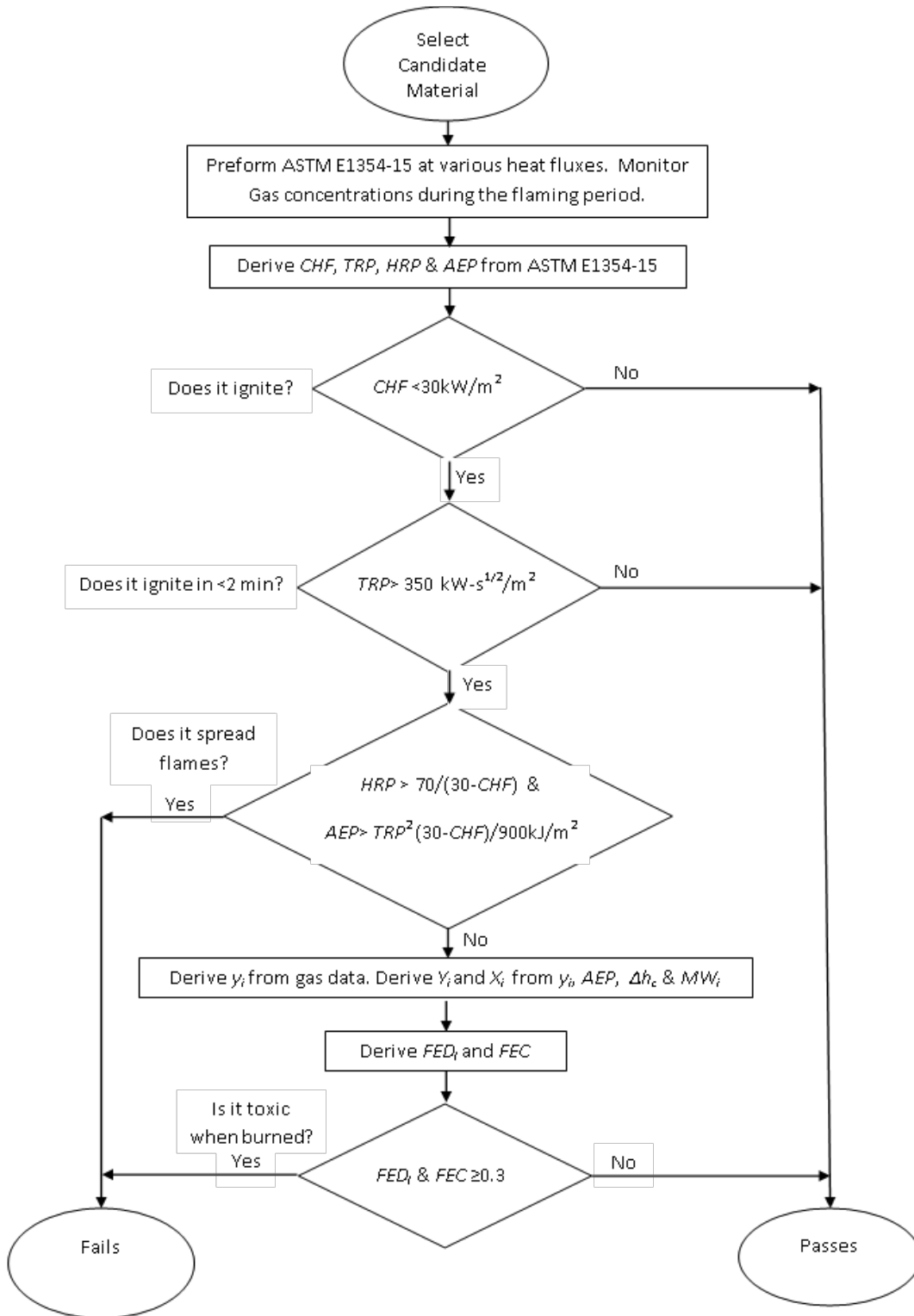


**Figure 70. Flowchart for test protocol to determine fire safety of a candidate head-impact material**

## 14. REFERENCES

1. Tewarson, A. (2008). Generation of heat and gaseous, liquid and solid products in fire. In DiNenno, P. J. (Ed.), *SFPE Handbook of Fire Protection Engineering, 4th ed.* (3–109). Quincy, MA: National Fire Protection Assoc.
2. N. A. (2016). *SFPE Handbook of fire protection engineering, 5th ed.* Hurley, M. J. (Ed.). New York, NY: Springer.
3. Wieczorek, C. J., & Dembsey, N. A., (2016). Effects of thermal radiation on people: Predicting 1st and 2nd degree skin burns. In Hurley, M. J. (Ed.), *SFPE Handbook of fire protection engineering, 5th ed.* (2705–2737). New York, NY: Springer.
4. Hasemi, Y., Yokobayashi, S., Wakamatsu, T., & Ptchelintsev, A. (1995). *Fire safety of building components exposed to a localized fire: Scope and experiments on ceiling/beam system exposed to a localized fire.* Proceedings from Asia Flam 95—1st International Conference, London, England.
5. Quintiere, J. G. (2006). *Fundamentals of fire phenomena.* Hoboken, NJ: John Wiley & Sons.
6. FAA Report. (2007). Flammability Properties of Clay-Nylon Nanocomposites (DOT/FAA/AR-07/29).
7. Dillon, S. E., Quintiere, J. G., & Kim, W. H. (2000). Discussion of a model and correlation for the ISO 9705 Room-Corner Test. In Curtat, M. (Ed.) *Fire Safety Science – Proc. of the Sixth International Symposium (1015-1026).* Marne-La-Vallee, France: Int. Assoc. For Fire Safety Science.
8. NIST Report. (1998). Determination of Properties and the Prediction of the Energy Release Rate of Materials in the ISO 9705 Room-Corner Test. (NIST GCR 98-753).
9. NIST Report. (1998). Determination of Properties and the Prediction of the Energy Release Rate of Materials in the ISO 9705 Room-Corner Test. Interim Report. Appendices. (NIST GCR 98-754).
10. Quintiere, J. G., Lian, D. (2009). Inherent Flammability Parameters—Room Corner Test Application. *Fire and Materials*, 33(8), 377–393.
11. FAA Report. (1995). Toxicity Assessment of Combustion Gases and Development of a Survival Model. (DOT/FAA/AR-95/5).
12. ISO Report. (2012). Life Threatening Components of Fire- Guidelines for the Estimation of Time to Compromised Tenability in Fires (ISO 13571:2012).
13. Purser D. A. (2008). Assessment of hazards to occupants from smoke, toxic gases, and heat. In DiNenno, P. J. (Ed.), *SFPE Handbook of fire protection engineering, 4th ed.* (2–96). Quincy, MA: National Fire Protection Assoc.
14. ASTM Standard E1354-09, “Standard Test Method for Heat and Visible Smoke Release Rates for Materials and Products Using an Oxygen Consumption Calorimeter,” ASTM International, West Conshohocken, PA, 2009, DOI: 10.1520/E1354-09, [www.astm.org](http://www.astm.org).
15. ASTM Standard E2058-13a, “Standard Test Methods for Measurement of Material Flammability Using a Fire Propagation Apparatus (FPA),” ASTM International, West Conshohocken, PA, 2013, DOI: 10.1520/E2058, [www.astm.org](http://www.astm.org).
16. Karlsson, B., & Quintiere, J. G. (1999). *Enclosure fire dynamics.* Boca Raton, FL: CRC Press.
17. McCormick, S., (2015). *Overview of US Military Vehicle Fire Protection.* Proceedings from the ARL/TARDEC Fire Protection Information Exchange Meeting, Aberdeen, MD

18. Hasemi, Y., Yoshida, M., & Takaike, R. (1999). *Flame length and flame heat transfer correlations in ceiling fires*. Proceedings from Fire Safety Science—6th International Symposium, International Association for Fire Safety Science, Poitiers.
19. Safronava, N., Lyon, R. E., Crowley, S., & Stoliarov, S. I. (2014). Effect of moisture on ignition time of polymers. *Fire Technology*, 51(5), 1093–1112.
20. Zarzecki, M., Quintiere, J. G., Lyon, R. E., Rossmann, T., & Diez, F. J. (2013). The effect of pressure and oxygen concentration on the combustion of PMMA. *Combustion and Flame*, 160(8), 1519–1530.
21. Cleary, T., & Quintiere, J. G. (1991). A framework for utilizing fire property tests. In Cox, G., Langford, B. (Eds.), *Fire safety science: Proceedings of the Third International Symposium* (647–656). London: Elsevier Applied Science.
22. Speitel, L. C., (1996). Fractional effective dose model for post-crash aircraft survivability. *Toxicology* 115(1–3). 167-177.
23. FAA Report. (2012). An Investigation of the Vertical Bunsen Burner Test for Flammability of Plastics (DOT/FAA/AR-TN11/19).
24. Panagiotou, J. (2004). A Methodology for Flammability Diagrams, MS Thesis, Department of Fire Protection Engineering, U. of Maryland College Park.
25. Janssens, M., Huczek J., & Saucedo, A. Development of a Model of the ASTM E 84 Steiner Tunnel Test, *Fire safety science: Proceedings Of The Ninth International Symposium*, (279-290).



APPENDIX A—TRANSPORTATION SECTORS FLAMMABILITY, SMOKE, AND TOXICITY PERFORMANCE CRITERION

I-A

Transportation Sector	Interior Material Component	Material Property	Test Method	Regulatory/Standard Performance Criterion
<b>Air</b> <b>Commercial Aviation Aircraft</b>  <b>Federal Aviation Regulation (FAR)</b>  <b>Title 14</b> <b>Code of Federal Regulations (CFR)</b> <b>Parts 23 and 25</b>	<b>Cabin and Cargo Compartment Interior Materials</b>  Seat, Panel, Liner, Ducting, Interior ceiling panels, interior wall panels, partitions, large cabinet walls, structural flooring)	<b>Flame Resistance</b> Interior Panels; under seat, floor coverings; cargo liners, textiles, galley furnishings	<b>FAA Handbook, Chapter 1</b>  Vertical Bunsen Burner Test for Cabin & Cargo Compartment Materials 60- or 12-Second Ignition Tests)	<b>REGULATION: FAR 25.853 (a-b) EFFECTIVE: May 1, 1972</b>  Flame Extinguishing Time: NTE 15.0 sec Drip Extinguishing Time: NTE 3.0 Sec for 60 Sec. NTE 5.0 sec for 12 Sec. Burn Length: NTE 6.0 Inch (150 mm) for 60 Sec NTE 8.0 inch (200 mm) for 12 Sec
		<b>Flame Penetration</b> <b>Flame Propagation</b> <b>Glow Propagation</b> Cargo Liners Class B & E	<b>FAA Handbook, Chapter 2</b>  45-Degree Bunsen Burner Test for Cargo Compartment Liners and Waste Stowage Compartment Materials (30-Second Ignition Test)	<b>REGULATION: FAR 25.855(a); FAR 25.857 EFFECTIVE: May 1, 1972</b>  Materials Flame Penetration : None Flame Extinguishing Time: NTE 15.0 sec After Glow Time: NTE 10.0 sec
		<b>Flame Resistance</b> Cabin, Cargo Compartment, Misc. Materials	<b>FAA Handbook, Chapter 3</b>  Horizontal Bunsen Burner Test for Cabin, Cargo Compartment, and Miscellaneous Materials (15-Second Ignition Test)	<b>REGULATION: FAR 25.853 (b-2;b-3) EFFECTIVE: May 1, 1972</b>  Rate of Flame Spread (Average Burn Rate): - Class b-2: NTE 2.5 in/min - Class b-3: NTE 4.0 in/min
	<b>Large Area Cabin Interior Materials</b>	<b>Rate of Heat Release</b>	<b>FAA Handbook, Chapter 5</b>  Heat Release Rate for Cabin Materials	<b>REGULATION: FAR 25.853 (a-1) EFFECTIVE: August 20, 1986</b>  Peak HRR in 5 min: NTE 65 kW/m <sup>2</sup> Total HRR in 2 min: NTE 65 kW-Min/m <sup>2</sup>
		<b>Max Optical Density</b>	<b>FAA Handbook, Chapter 6</b>  Smoke Test for Cabin Material	<b>REGULATION: FAR 25.853 (a-b) EFFECTIVE: May 1, 1972</b>  Max. Specific Optical Density (4 mins.): <sup>4</sup> D <sub>m</sub> ≤ 200
	<b>Seating Material - Cushions</b>	<b>Burn Resistance</b>  <b>Weight Loss</b>	<b>FAA Handbook, Chapter 7</b>  Oil Burner Test for Seat Cushions	<b>REGULATION: FAR 25.853 (a-b) EFFECTIVE: May 1, 1972</b>  Avg. Burnlength: NTE 17 inches (43.2 cm) Avg. Weight loss: NTE 10 percent
	<b>Cargo Compartment Lining Materials</b>	<b>Flame Resistance</b>  <b>Burnthrough</b>	<b>FAA Handbook, Chapter 8</b>  Oil Burner Test for Cargo Liners	<b>REGULATION: FAR 25.853 (a-b) EFFECTIVE: May 1, 1972</b>  No Burn through within 5 minute flame exposure. Speciman Peak Temperature ≤ 204°C at backside, monitored during flame exposure.

Transportation Sector	Interior Material Component	Material Property	Test Method	Regulatory/Standard Performance Criterion
<b>Surface Passenger Cars, Multipurpose Passenger Vehicles, Trucks and Buses</b> National Highway Traffic Safety Administration (NHTSA) Title 49 CFR Part 571 Subpart B	<b>Interior Materials</b> Panels, Seat Cushions, head restraints, floor covering, headlining, arm rests, curtains, shades, engine compartment covers	<b>Burn Resistance</b>	<b>Federal Motor Vehicle Safety Standard (FMVSS) No. 302 *</b> Flammability of Interior Materials (Horizontal Bunsen Burner)	<b>REGULATION:</b> 49CFR 571.302 <b>EFFECTIVE:</b> September 1, 1972 Rate of Flame Spread: $\leq 4$ inches/min
<b>Railroad Surface Mass Transit Vehicles Passenger Cars and Locomotive Cabs</b> Federal Railroad Administration (FRA) Title 49 Code of Federal Regulations Part 238	<b>Cushions, Mattresses</b>	<b>Flammability</b>	<b>ASTM D 3675-98</b> Surface Flammability of Flexible Cellular Materials Using a Radiant Heat Energy Source	<b>REGULATION:</b> 49 CFR 238, App. B <b>EFFECTIVE:</b> June 25, 2002 Flame Spread Index: $I_s \leq 25$
		<b>Smoke Emission</b>	<b>ASTM E 662-01</b> Specific Optical Density of Smoke Generated by Solid Materials	<b>REGULATION:</b> 49 CFR 238, App. B <b>EFFECTIVE:</b> June 25, 2002 Max. Specific Optical Density: $D_s(1.5) \leq 100$ Max. Specific Optical Density: $D_s(4.0) \leq 175$
	<b>Fabrics Upholstery</b>	<b>Flammability</b>	<b>FAA Handbook, Chapter 1</b> Vertical Bunsen Burner Test for Cabin & Cargo Compartment Materials 60- or 12-Second Ignition Tests	<b>REGULATION:</b> 49 CFR 238, App. B <b>EFFECTIVE:</b> June 25, 2002 Flame Time: NTE 10 Seconds Burn Length: NTE 6 inches (15.2 cm)
		<b>Smoke Emission</b>	<b>ASTM E 662-01</b> Specific Optical Density of Smoke Generated by Solid Materials	<b>REGULATION:</b> 49 CFR 238, App. B <b>EFFECTIVE:</b> June 25, 2002 Max. Specific Optical Density: $D_s(4.0) \leq 250$ Coated Max. Specific Optical Density: $D_s(4.0) \leq 100$ Uncoated
	<b>Panels</b> Wall, ceiling, partition, tables and shelves	<b>Flammability</b>	<b>ASTM E 162-98</b> Surface Flammability of Materials Using a Radiant Heat Energy Source	<b>REGULATION:</b> 49 CFR 238, App. B <b>EFFECTIVE:</b> June 25, 2002 Flame Spread Index: $I_s \leq 35$

\*A December 18, 2015 NHTSA correspondence pertinent to Safety Recommendation H-15-12 states "Revise Federal Motor Vehicle Safety Standard 302 to adopt the more rigorous performance standards for interior flammability and smoke emissions characteristics already in use throughout the U.S. DOT for commercial aviation and rail passenger transportation." [1]

Transportation Sector	Interior Material Component	Material Property	Test Method	Regulatory/Standard Performance Criterion
<b>Railroad</b> <b>Surface Mass Transit Vehicles</b> <b>Passenger Cars and Locomotive Cabs</b>  <b>Federal Railroad Administration (FRA)</b>  <b>Title 49</b> <b>Code of Federal Regulations</b> <b>Part 238</b>	<b>Panels</b> Wall, ceiling, partition, tables and shelves	<b>Smoke Emission</b>	<b>ASTM E 662-01</b> Specific Optical Density of Smoke Generated by Solid	<b>REGULATION:</b> 49 CFR 238, App. B <b>EFFECTIVE:</b> June 25, 2002  Max. Specific Optical Density: $D_s(1.5) \leq 100$  Max. Specific Optical Density: $D_s(4.0) \leq 200$
				<b>REGULATION:</b> 49 CFR 238, App. B <b>EFFECTIVE:</b> June 25, 2002  Flame Spread Index: $I_s \leq 25$
	<b>Thermal and acoustic Insulation</b>	<b>Flammability</b>	<b>ASTM E 162-98</b> Surface Flammability of Materials Using a Radiant Heat Energy Source	<b>REGULATION:</b> 49 CFR 238, App. B <b>EFFECTIVE:</b> June 25, 2002  Max. Specific Optical Density: $D_s(4.0) \leq 100$
				<b>REGULATION:</b> 49 CFR 238, App. B <b>EFFECTIVE:</b> June 25, 2002  Critical Radiant Flux (C.R.F.): $\geq 5\text{ kW/m}^2$
	<b>Flooring Covering</b>	<b>Flammability</b>	<b>ASTM E 648-00</b> Critical Radiant Flux of Floor-Covering Systems Using a Radiant Heat Energy Source.	<b>REGULATION:</b> 49 CFR 238, App. B <b>EFFECTIVE:</b> June 25, 2002  Max. Specific Optical Density: $D_s(1.5) \leq 100$ Max. Specific Optical Density: $D_s(4.0) \leq 200$
				<b>REGULATION:</b> 49 CFR 238, App. B <b>EFFECTIVE:</b> June 25, 2002  Rate of Flame Spread: $\leq 4$ inches/min
<b>Military Ground Vehicles</b> <b>United States Department of Defense</b>  <b>Military Standard MIL-STD</b>	<b>Interior Materials</b> Type I (except trailers), Type II Tactical Tracked and Type III Military Ground Vehicles	<b>Burn Resistance</b>	<b>Federal Motor Vehicle Safety Standard (FMVSS) No. 302</b> Flammability of Interior Materials (Horizontal Bunsen Burner)	<b>REGULATION:</b> MIL-STD-1180B Rqmt. 302.1 <b>EFFECTIVE:</b> September 20, 1986  Rate of Flame Spread: $\leq 4$ inches/min

Transportation Sector	Interior Material Component	Material Property	Test Method	Regulatory/Standard Performance Criterion
<b>U.S. Flag Passenger Marine Vessels</b> United States Dept. of Homeland Security U.S. Coast Guard Title 46 Code of Federal Regulations Subchapter H, Part 70	<b>Interior Finish</b> Coating, Overlay, or Veneer except standard paint applied for decorative or other purpose	<b>Flame Spread</b>	<b>ASTM E 84-98 NFPA No. 255</b> Surface Burning Characteristics of Building Materials	<b>REGULATION:</b> 46 CFR 164.012 <b>EFFECTIVE:</b> September 30, 1997  Flame Spread Index: $\leq 20$ Smoke Developed Index: $\leq 10$
<b>Surface Ships</b> United States Dept. of Navy Military Standard MIL-STD	<b>N-Class Division</b> Insulation on fire resistant divisions constructed from steel, aluminum, and polymer composite structures (post Shock Test)	<b>Fire Resistance</b>	<b>UL-1709</b> Rapid Rise Fire Tests of Protection Materials for Structural Steel	<b>REGULATION:</b> MIL-STD-3020 <b>EFFECTIVE:</b> November 7, 2007  No Flame Passage Overhead heat transmission Unexposed Surface-Avg Temp. Increase: $\leq 139^{\circ}\text{C}$ Point Surface Temp. Increase: $\leq 181^{\circ}\text{C}$ <i>(iaw ABS NVR Part 1, Chapter 2, Section 1)</i>
<b>Submarines</b> United States Dept. of Navy Military Standard MIL-STD	<b>Structural Composites In Hulls, Machinery and structural application</b>	<b>Flammability</b>	<b>ASTM E 162-98</b> Surface Flammability of Materials Using a Radiant Heat Energy Source	<b>REGULATION:</b> MIL-STD-2031 <b>EFFECTIVE:</b> February 26, 1991  Flame Spread Index: $\leq 20$
		<b>Ignitability and Heat Release</b>	<b>ASTM E 1354</b> Oxygen Consumption Cone Calorimeter	<b>REGULATION:</b> MIL-STD-2031 <b>EFFECTIVE:</b> February 26, 1991  <b>Heat Flux 25 kW/m<sup>2</sup>:</b> Peak HRR $\leq 50 \text{ kW/m}^2$ Avg HRR (300s) $\leq 50 \text{ kW/m}^2$ $T_{\text{ign}} \geq 300\text{s}$ :  <b>Heat Flux 50 kW/m<sup>2</sup>:</b> Peak HRR $\leq 65 \text{ kW/m}^2$ Avg HRR (300s) $\leq 50 \text{ kW/m}^2$ $T_{\text{ign}} \geq 150\text{s}$ :  <b>Heat Flux 75 kW/m<sup>2</sup>:</b> Peak HRR $\leq 100 \text{ kW/m}^2$ Avg HRR (300s) $\leq 100 \text{ kW/m}^2$ $T_{\text{ign}} \geq 90\text{s}$ :

Transportation Sector	Interior Material Component	Material Property	Test Method	Regulatory/Standard Performance Criterion
<b>Submarines</b>  United States Dept. of Navy  Military Standard MIL-STD	Structural Composites In Hulls, Machinery and structural application	<b>Ignitability and Heat Release</b>	<b>ASTM E 1354</b>  Oxygen Consumption Cone Calorimeter	<b>REGULATION:</b> MIL-STD-2031 <b>EFFECTIVE:</b> February 26,1991  <b>Heat Flux 100 kW/m<sup>2</sup>:</b> Peak HRR ≤ 150 kW/m <sup>2</sup> Avg HRR (300s) ≤ 120 kW/m <sup>2</sup> T <sub>ign</sub> ≥ 60s:
		<b>Smoke Obscuration</b>	<b>ASTM E 662-01</b>  Specific Optical Density of Smoke Generated by Solid Materials	<b>REGULATION:</b> MIL-STD-2031 <b>EFFECTIVE:</b> February 26,1991  Max. Specific Optical Density(4 mins.): 4D <sub>m</sub> ≤ 200
		<b>Combustion Gas Generation</b>	<b>ASTM E 1354</b>  Oxygen Consumption Cone Calorimeter	<b>REGULATION:</b> MIL-STD-2031 <b>EFFECTIVE:</b> February 26,1991  <b>Heat Flux 25 kW/m<sup>2</sup>:</b> CO 200 ppm CO <sub>2</sub> 4 % by Volume HCN 30 ppm HCL 100 ppm
		<b>Oxygen-Temperature Index</b>	<b>ASTM D2863 - 13</b>  Standard Test for Measuring Minimum Oxygen Concentration to Support Candle-Like Combustion of Plastics	<b>REGULATION:</b> MIL-STD-2031 <b>EFFECTIVE:</b> February 26,1991  Percent Oxygen at 25°C - 35% minimum Percent Oxygen at 75°C - 30% minimum Percent Oxygen at 300°C- 21% minimum
		<b>Burn Through Test</b>	<b>David Taylor Research            Center Burn-Through Fire            Test</b>	<b>REGULATION:</b> MIL-STD-2031 Appendix B <b>EFFECTIVE:</b> February 26,1991  No Burn through in 30 Minutes.
		<b>Quarter Scale Test</b>	<b>Quarter Scale Test            Room Fire Test</b>	<b>REGULATION:</b> MIL-STD-2031 Appendix C <b>EFFECTIVE:</b> February 26,1991  No Flashover in 10 Minutes
		<b>N-Gas Model Smoke            Toxicity Screening Test</b>	<b>NIST Guide for the Care            and Use of Laboratory            Animals</b>	<b>REGULATION:</b> MIL-STD-2031 Appendix F <b>EFFECTIVE:</b> February 26,1991  No Deaths

Transportation Sector	Interior Material Component	Material Property	Test Method	Voluntary Standard Performance Criterion														
<b>Air</b> Boeing Aircraft  <b>Boeing Specification Support Standard** (BSS)</b>	<b>Boeing Aircraft Interior Parts and Material</b>	<b>Toxic Gas Generation Using NBS Smoke Density Chamber</b>	<b>BSS-7238</b> Test Method for Smoke Generation by Materials on Combustion  <b>BSS-7239</b> Test Method for Toxic Gas Generation by Materials on Combustion	<b>ISSUED:</b> March 24, 1978 <b>REVISION:</b> June 26, 1997														
				<b>ISSUED:</b> October 13, 1978 <b>REVISION:</b> January 18, 1988  Limiting values of toxic smoke gas components: - Electrical Wires and Cables (16 Min. Duration) - All Other Materials (4 Min. Duration) <table border="1"> <thead> <tr> <th>Smoke Gas Component</th> <th>Max. (ppm)</th> </tr> </thead> <tbody> <tr> <td>HF</td> <td>200</td> </tr> <tr> <td>HCl</td> <td>500</td> </tr> <tr> <td>HCN</td> <td>150</td> </tr> <tr> <td>SO<sub>2</sub>/H<sub>2</sub>S</td> <td>100</td> </tr> <tr> <td>CO</td> <td>3500</td> </tr> <tr> <td>NO/NO<sub>2</sub></td> <td>100</td> </tr> </tbody> </table>	Smoke Gas Component	Max. (ppm)	HF	200	HCl	500	HCN	150	SO <sub>2</sub> /H <sub>2</sub> S	100	CO	3500	NO/NO <sub>2</sub>	100
Smoke Gas Component	Max. (ppm)																	
HF	200																	
HCl	500																	
HCN	150																	
SO <sub>2</sub> /H <sub>2</sub> S	100																	
CO	3500																	
NO/NO <sub>2</sub>	100																	
<b>Air</b> Airbus Commercial Aircraft  <b>Airbus Fire Safety (AFIS) Requirement</b>  <b>Airbus Company*** Directive (ABD)</b>	<b>Airbus Aircraft Materials and Parts for Existing Aircraft Projects and Designs</b>  Materials/parts inside the pressurized section of the fuselage and at fire safety relevant interfaces to the unpressurized areas	<b>Toxicity</b>	<b>AITM3.00005</b> Determination of Specific Gas Components of Smoke Generated by Component Parts or Sub-Assemblies of Aircraft	<b>AIRBUS DIRECTIVE:</b> ABD0031 Issue G <b>EFFECTIVE:</b> October 1993  Limiting values of toxic smoke gas components: - Electrical Wires and Cables (16 Min. Duration) - All Other Materials (4 Min. Duration) <table border="1"> <thead> <tr> <th>Smoke Gas Component</th> <th>Max. (ppm)</th> </tr> </thead> <tbody> <tr> <td>HF</td> <td>100</td> </tr> <tr> <td>HCl</td> <td>150</td> </tr> <tr> <td>HCN</td> <td>150</td> </tr> <tr> <td>SO<sub>2</sub>/H<sub>2</sub>S</td> <td>100</td> </tr> <tr> <td>CO</td> <td>1000</td> </tr> <tr> <td>NO/NO<sub>2</sub></td> <td>100</td> </tr> </tbody> </table>	Smoke Gas Component	Max. (ppm)	HF	100	HCl	150	HCN	150	SO <sub>2</sub> /H <sub>2</sub> S	100	CO	1000	NO/NO <sub>2</sub>	100
	Smoke Gas Component	Max. (ppm)																
HF	100																	
HCl	150																	
HCN	150																	
SO <sub>2</sub> /H <sub>2</sub> S	100																	
CO	1000																	
NO/NO <sub>2</sub>	100																	
	<b>Aircraft Interior component parts or sub-assemblies</b>  Seat cushions, mattress, part curtains, elastomeric parts, insulation, non-textile floor covering	<b>Optical Smoke Density</b>	<b>AITM2.0007A/B</b> Determination of the Specific Optical Smoke Density of Component Parts or Sub-Assemblies of Aircraft Interior	<b>AIRBUS DIRECTIVE:</b> ABD0031 Issue G <b>EFFECTIVE:</b> October 1993  Max. Specific Optical Density(4 mins.): $D_m \leq 200$ . Flaming Max. Specific Optical Density: $D_m \leq 200$ , Non-Flaming														

\*\* Boeing Standard Test Methods are used to demonstrate compliance with 14 CRF Part 25. [2, 3]

\*\*\* Airbus Fire Safety Requirements (AFIS) are based on the Airworthiness Authorities (AA) of the European Aviation Safety Agency and the Federal Aviation Regulations 14 CFR Part 25. [4]

Transportation Sector	Interior Material Component	Material Property	Test Method	Voluntary Standard Performance Criterion
<b>Air</b> <b>Airbus Commercial Aircraft</b> <b>Airbus Fire Safety (AFIS) Requirement</b> <b>Airbus Company Directive (ABD)</b>	<b>Large Aircraft Interior parts</b> (except thermal/acoustic insulation, electrical wiring and heat shrinkable tubing)	<b>Flammability</b>	<b>AITM2.0002B</b> Resistance of Materials when tested according to the 12 sec or 60 sec Vertical Bunsen Burner Test	<b>AIRBUS DIRECTIVE: ABD0031 Issue G</b> <b>EFFECTIVE: October 1993</b> Average Burn Length ≤ 203 mm Average After Flame Time ≤ 15 Sec. Average After Flame Time of Drips ≤ 5 Sec
<b>Air</b> <b>Aviation Aircraft</b> <b>International Organization for Standardization (ISO)</b>	<b>Fire Environment Aircraft in Flight</b>	<b>Life Threat Components including Fire-Effluent Toxicity, Heat and Visual Obscuration Due to Smoke</b>	<b>ISO 13571, Edition 2</b> Fire Threat to People and the Environment	<b>RULE: ISO/IEC Directives, Part 2</b> <b>EFFECTIVE: January 2005</b> ISO Standard entailing fire hazard or risk analysis procedure in determining toxic-gas concentrations, the gas and wall temperatures and the density of smoke throughout the enclosure as a function of time.[5]

#### A.1. REFERENCES

1. US Department of Transportation. National Highway Traffic Safety Administration Correspondence, December 18, 2015.
2. BSS Report. (1997). Test Method for Smoke Generation by Materials in Combustion (BSS 7238).
3. BSS Report. (1988). Test Method for Toxic Gas Generation by Materials on Combustion (BSS 7239).
4. ABD0032 Issue G: Fireworthiness Requirements for the Pressurized Section of Fuselage, August 19, 2014.

## APPENDIX B—FDS MODELING OF MOCK-UP TESTS BY HAI-QING GUO

### B.1 MODEL SUMMARY

The Fire Dynamics Simulator (FDS) was used to simulate four scenarios: base fire (center), base fire (wall), ceiling fire (center), and ceiling fire (wall). Simulation configurations are identical, except for the fire location. Figure B-1 shows the overview of the base fire (center) scenario. Figure B-2 shows the overview of the ceiling fire (center) scenario.

Wall properties are simplified as “INERT” surface, where its temperature is fixed at ambient temperature. The ceiling insulation has a thickness of 4 cm and thermal conductivity of 0.041 W/m-K. Simulation uses a mesh size of 2 cm for the fire region and a mesh size of 4 cm for the rest area.

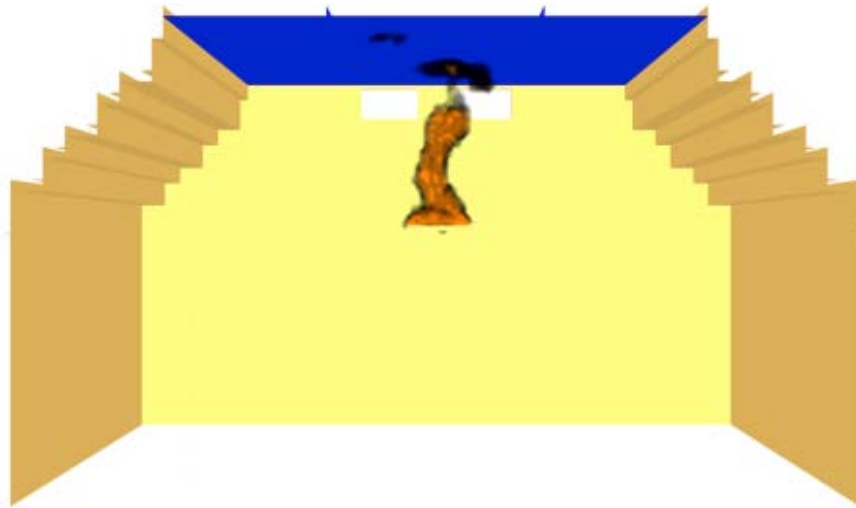


**Figure B-1. FDS model overview of the base fire (center) scenario**

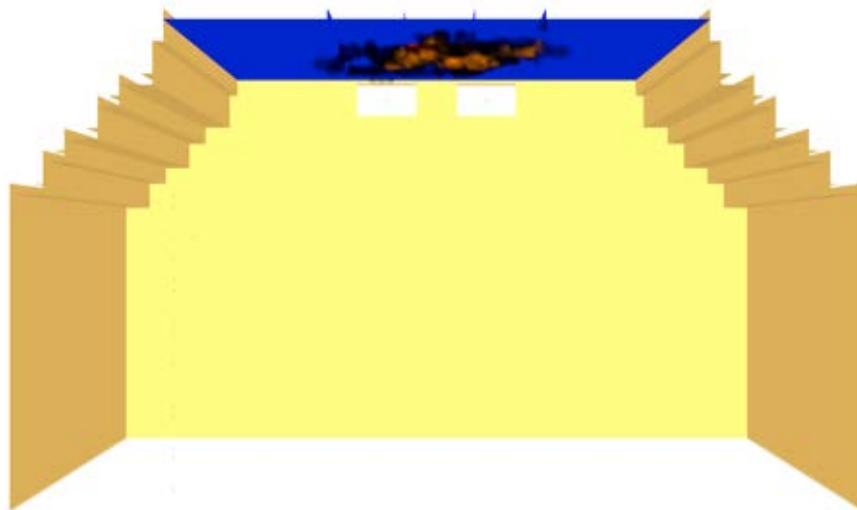


**Figure B-2. FDS model overview of the ceiling fire (center) scenario**



The fire heat release rate (HRR) was calculated from the free-burning test data. The test results are shown in figure. 3. The time derivative of the measured fuel mass was used to calculate the HRR. For the FDS simulation here, six values (the square marker in figure B-3) were chosen, and all the intermediate values are linearly interpolated.

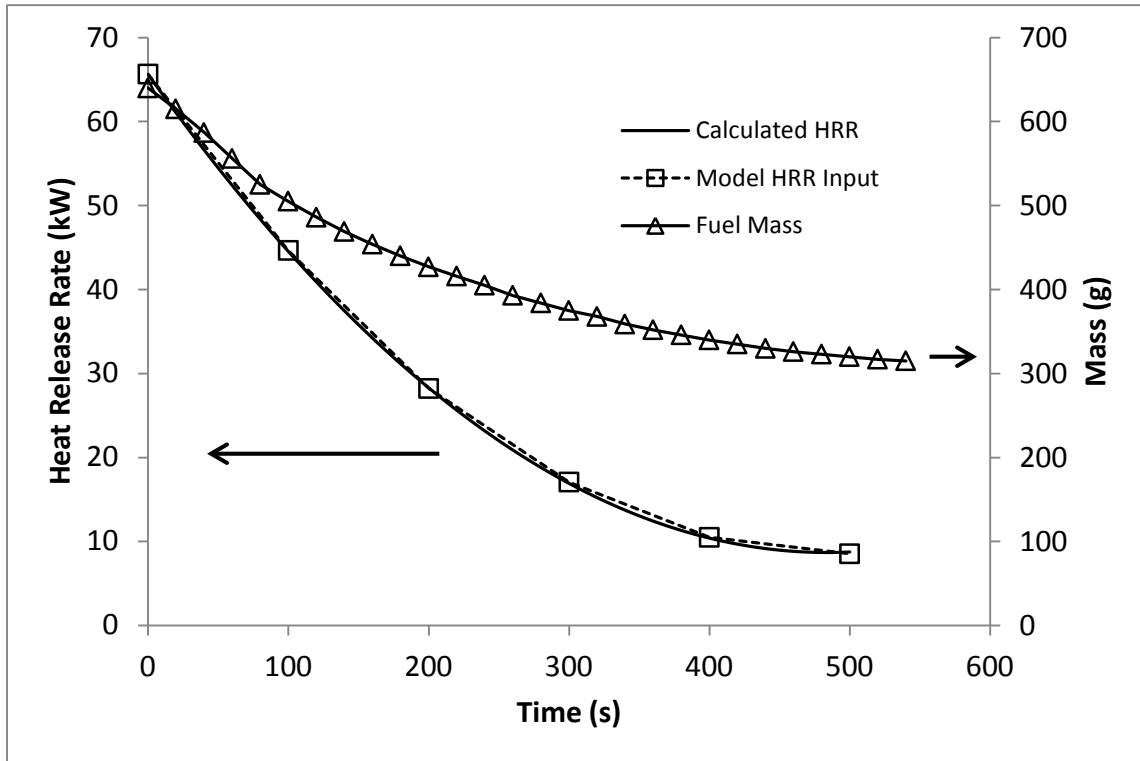


**Figure B-3. Fire heat release rate**

## B.2 RESULTS

### B.2.1. BASE FIRE (CENTER)

#### B.2.1.1. Temperature

The measured and the simulated temperature results for the base fire (center) case at selected time (e.g., 100 s, 200 s, and 300 s) are shown in figures B-4–B-6. At 100 s, the modeled temperatures are systematically higher than the measured temperatures because the fire HRR from the free-burning test were not able to give the fire growth information. The model HRR input peaks at ignition. Therefore, the model tends to over-predict temperature at the early stage.

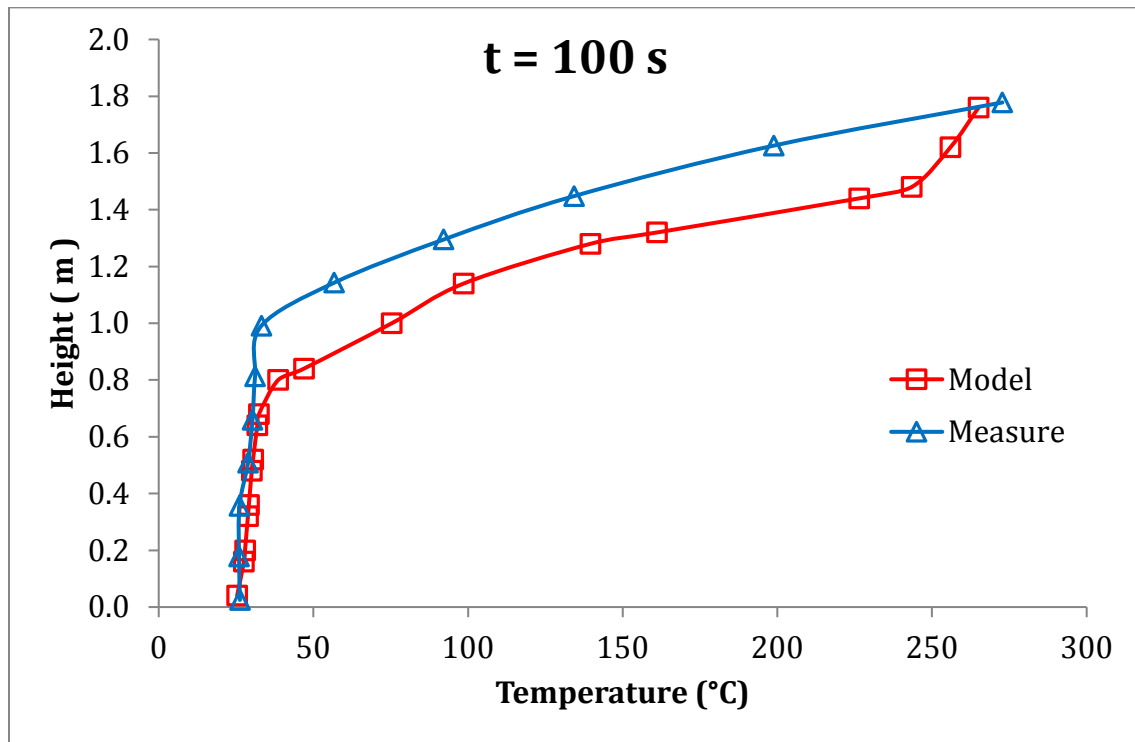


**Figure B-4. Measured and modeled temperature vs. height for the base fire (center) case at 100 s**

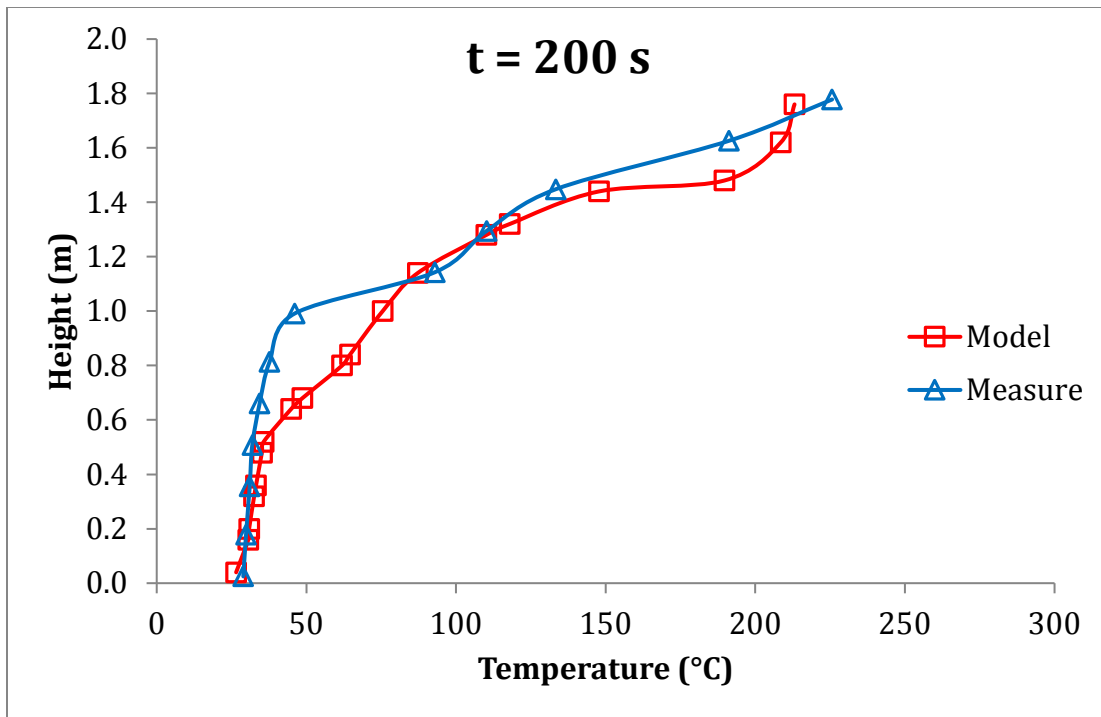


**Figure B-5. Measured and modeled temperature vs. height for the base fire (center) case at 200 s**

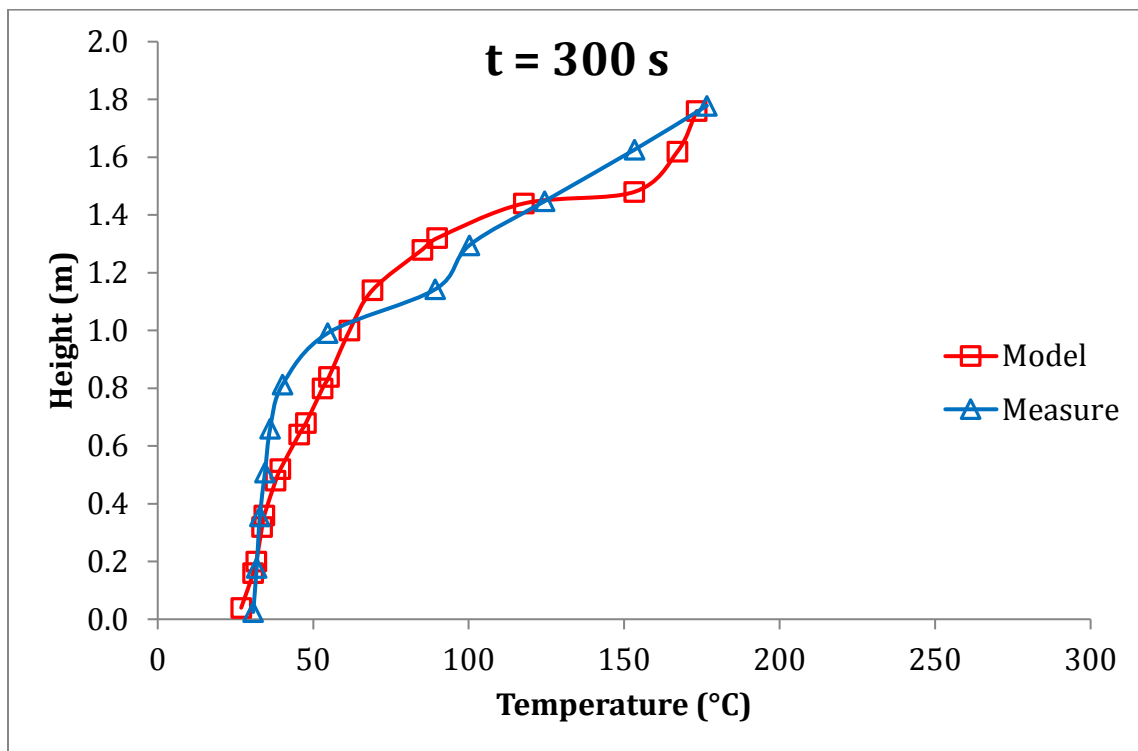


**Figure B-6. Measured and modeled temperature vs. height for the base fire (center) case at 300 s**

### B.2.1.2. Species

The measured and the simulated species results ( $\text{CO}_2$  and  $\text{O}_2$ ) for the base fire (center) case at selected time (e.g., 100 s, 200 s, and 300 s) are shown in figures B-7–B-9.

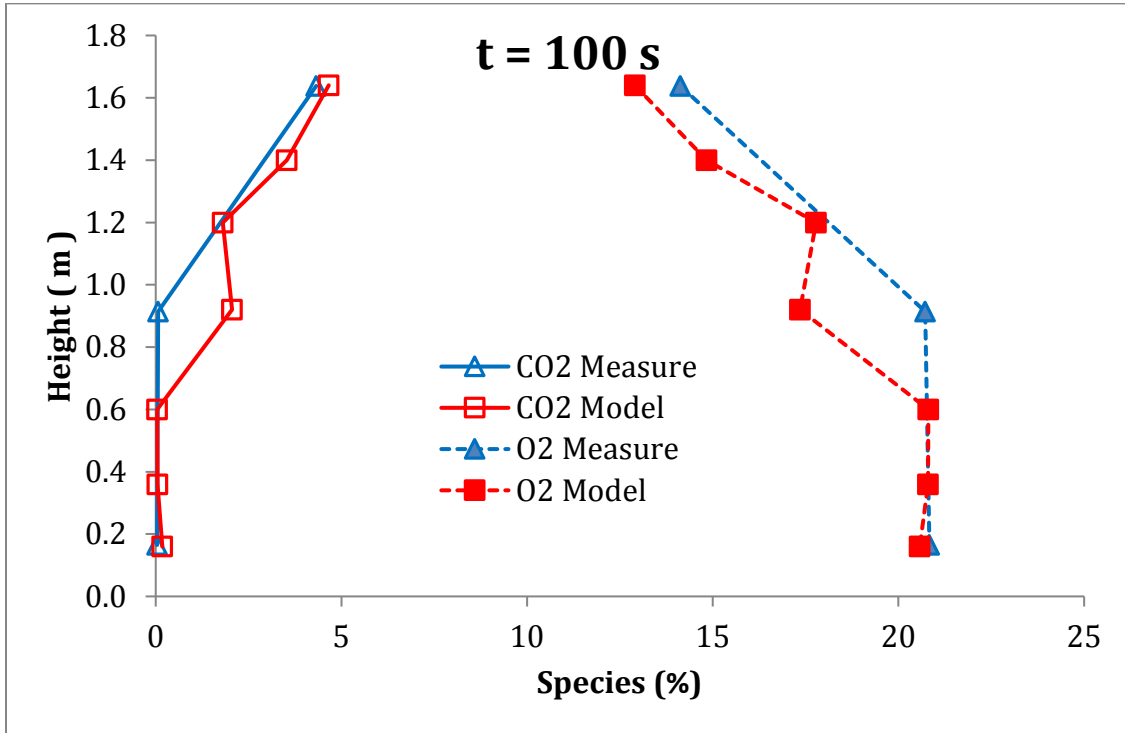


**Figure B-7. Measured and modeled species ( $\text{CO}_2$  and  $\text{O}_2$ ) vs. height for the base fire (center) case at 100 s**

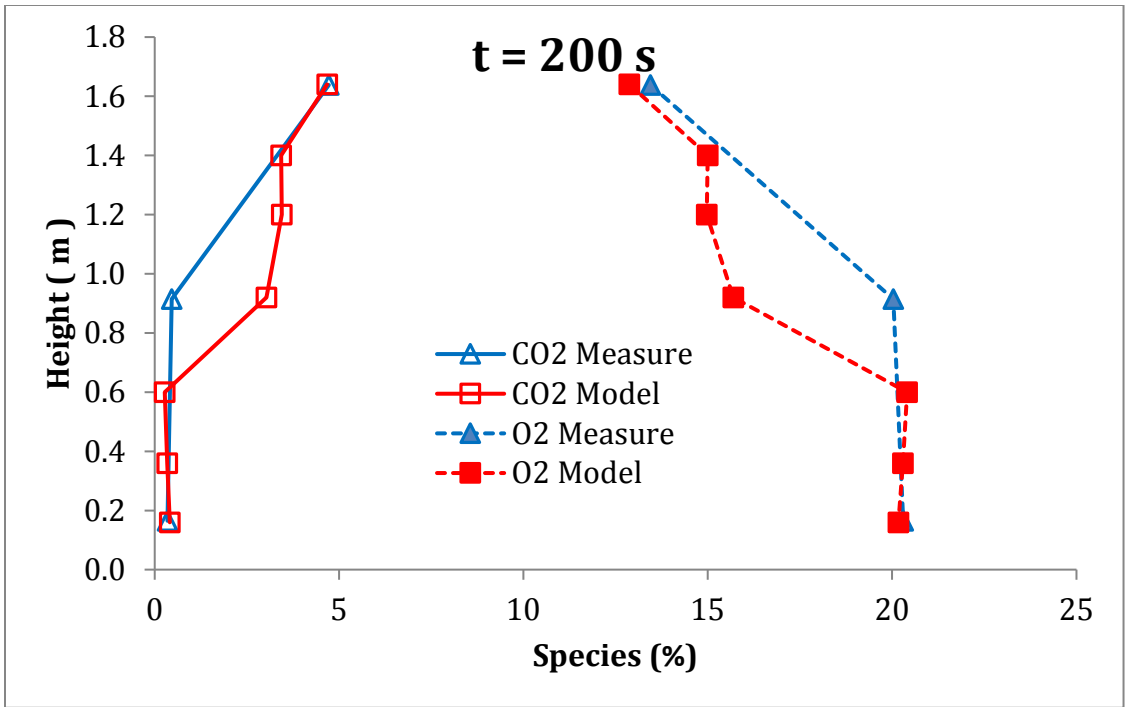


**Figure B-8. Measured and modeled species (CO<sub>2</sub> and O<sub>2</sub>) vs. height for the base fire (center) case at 200 s**

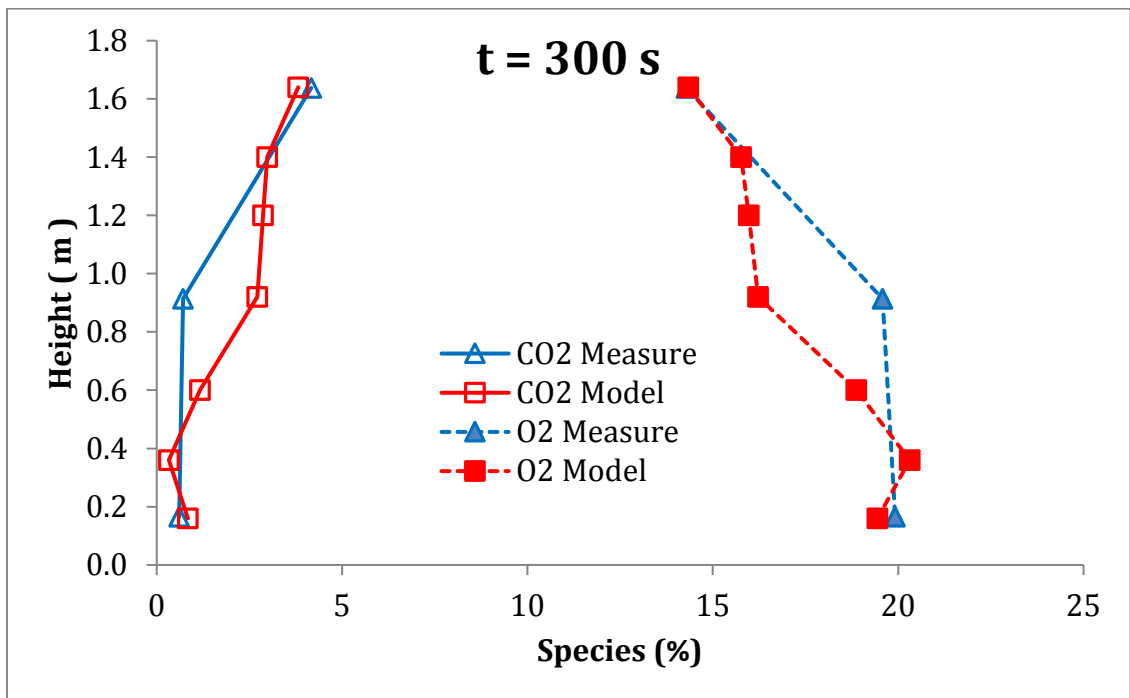


**Figure B-9. Measured and modeled species (CO<sub>2</sub> and O<sub>2</sub>) vs. height for the base fire (center) case at 300 s**

### B.2.1.3. Air Flow Rate

The airflow rate through the openings was not directly measured. Here, the inward airflow rate was estimated from the temperature measurements based on:

$$\dot{m}_a = \frac{2}{3} C_d A \rho_a \sqrt{2gH} \sqrt{\frac{(\rho_a - \rho_g) \rho_a}{[1 + (\rho_a / \rho_g)^{1/3}]^3}} \quad (\text{B-1})$$

where  $C_d$  is the flow coefficient of 0.68,  $A$  is the opening area,  $\rho_a$  is air density at ambient temperature,  $H$  is opening height, and  $\rho_g$  is the gas temperature inside the enclosure. The estimated airflow rate inward was compared with the simulation results in figure B-10.

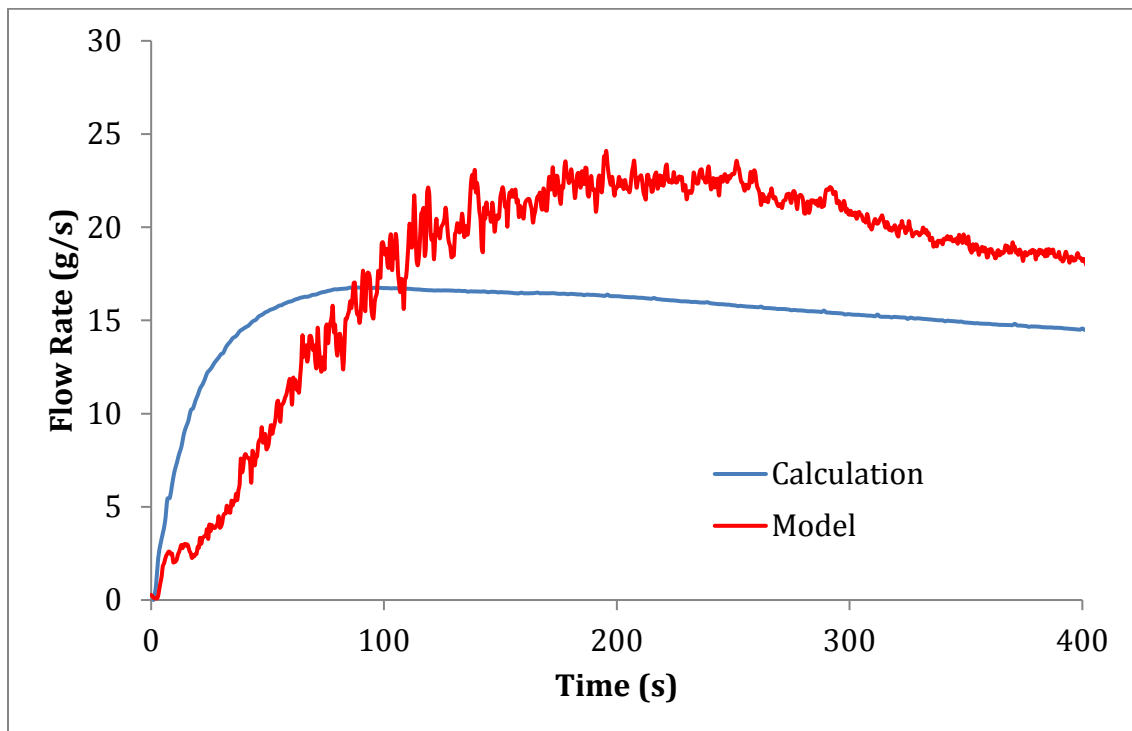


Figure B-10. Calculated and modeled inward airflow rate through the opening for the base fire (center) case

#### B.2.1.4. Heat Flux

The modeled heat flux is also compared with the measured heat flux at center location (directly above the fire), and edge location (25 cm away from center close to opening). Both heat flux gauges are installed at the ceiling. The results are shown in figures B-11 and B-12.

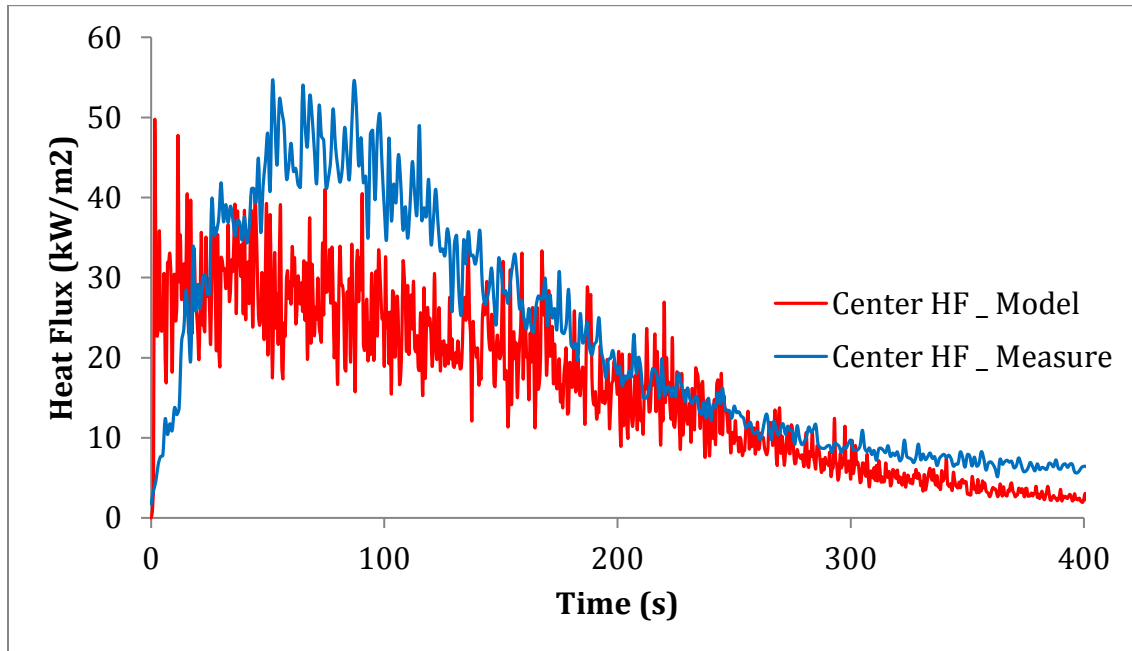


Figure B-11. Measured and modeled heat flux at center for the base fire (center) case

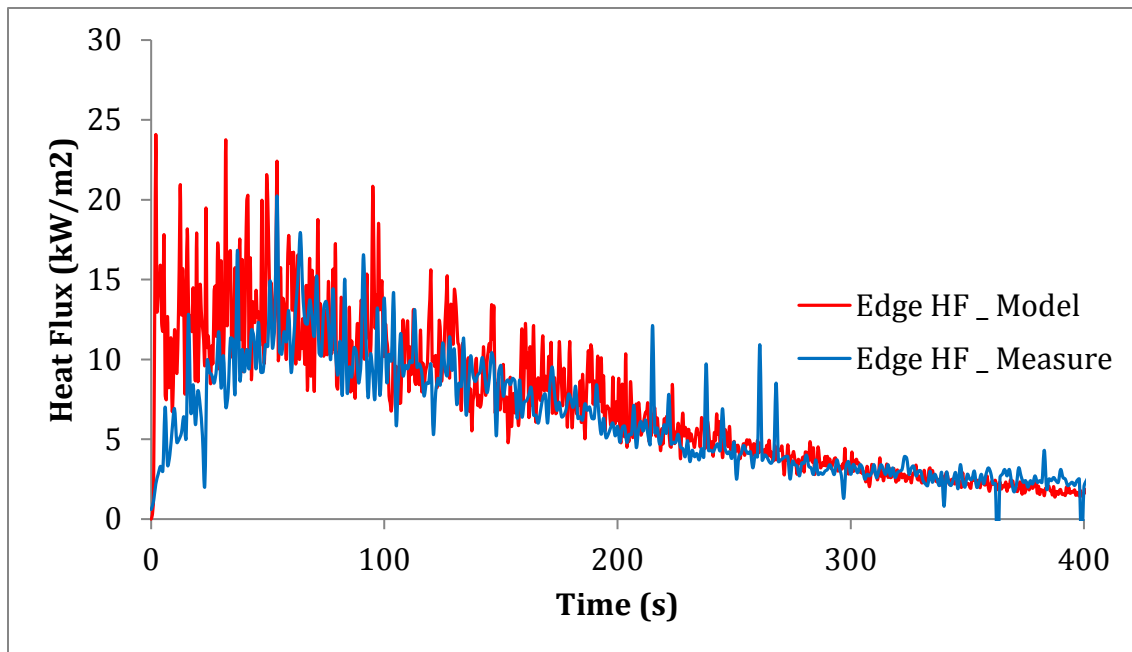


Figure B-12. Measured and modeled heat flux at center for the base fire (center) case

## B.2.2. BASE FIRE (WALL)

### B.2.2.1. Temperature

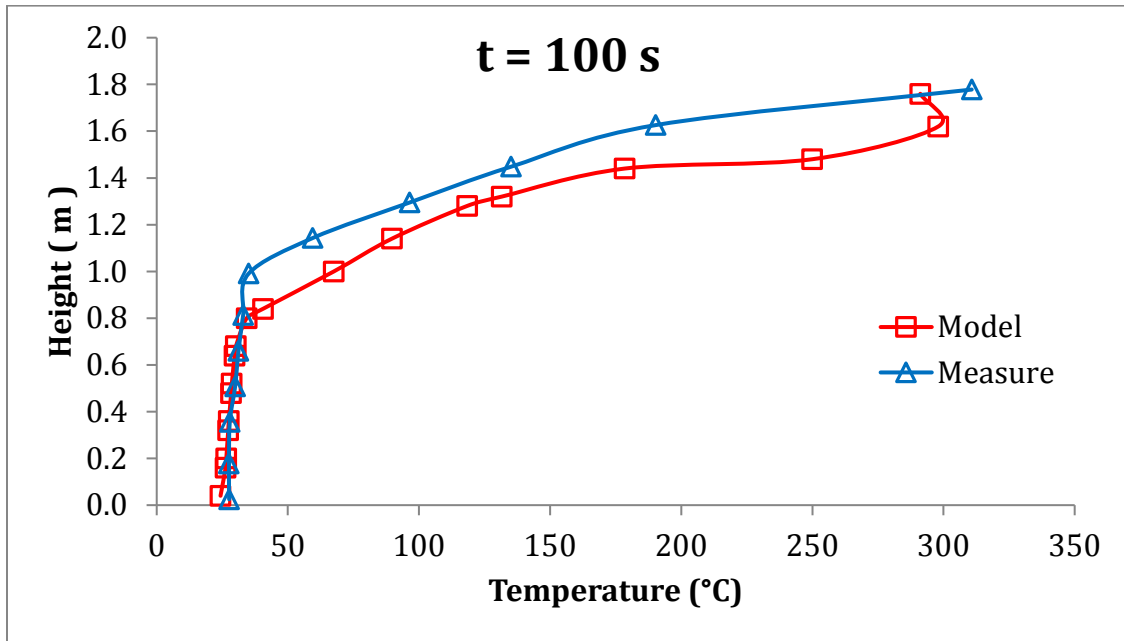


Figure B-13. Measured and modeled temperature vs. height for the base fire (wall) case at 100 s

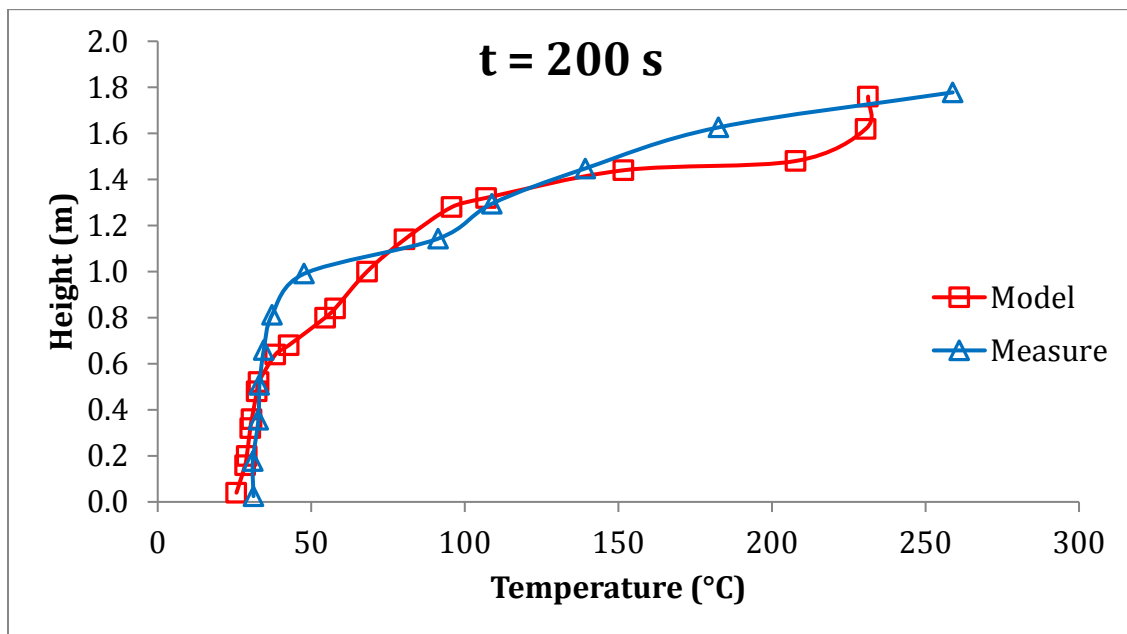


Figure B-14. Measured and modeled temperature vs. height for the base fire (wall) case at 200 s



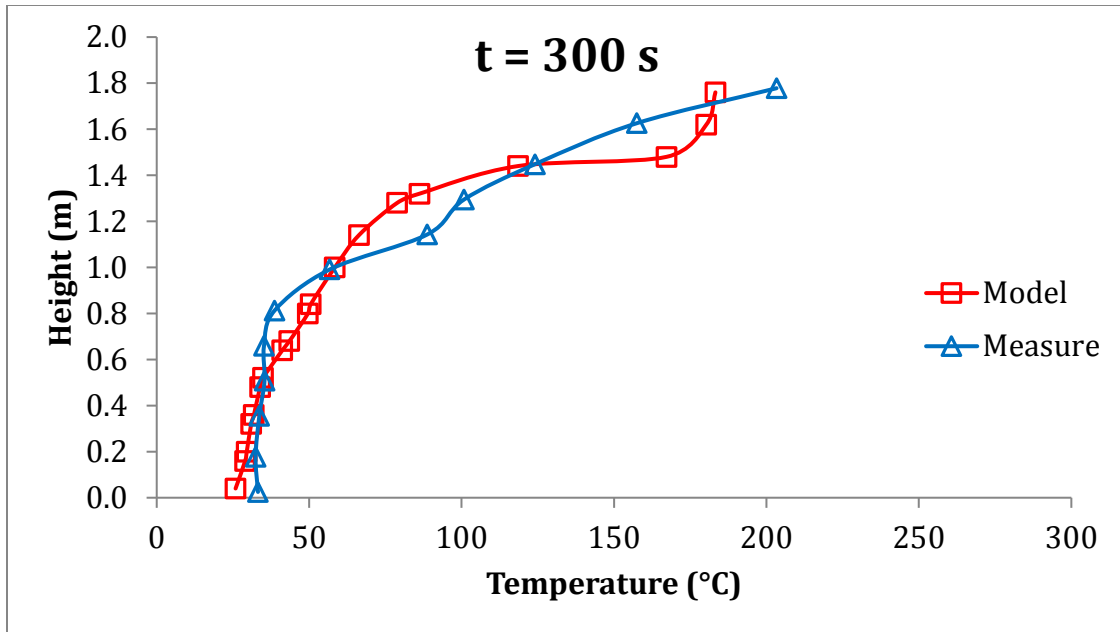


Figure B-15. Measured and modeled temperature vs. height for the base fire (wall) case at 300 s

B.2.2.2. Species

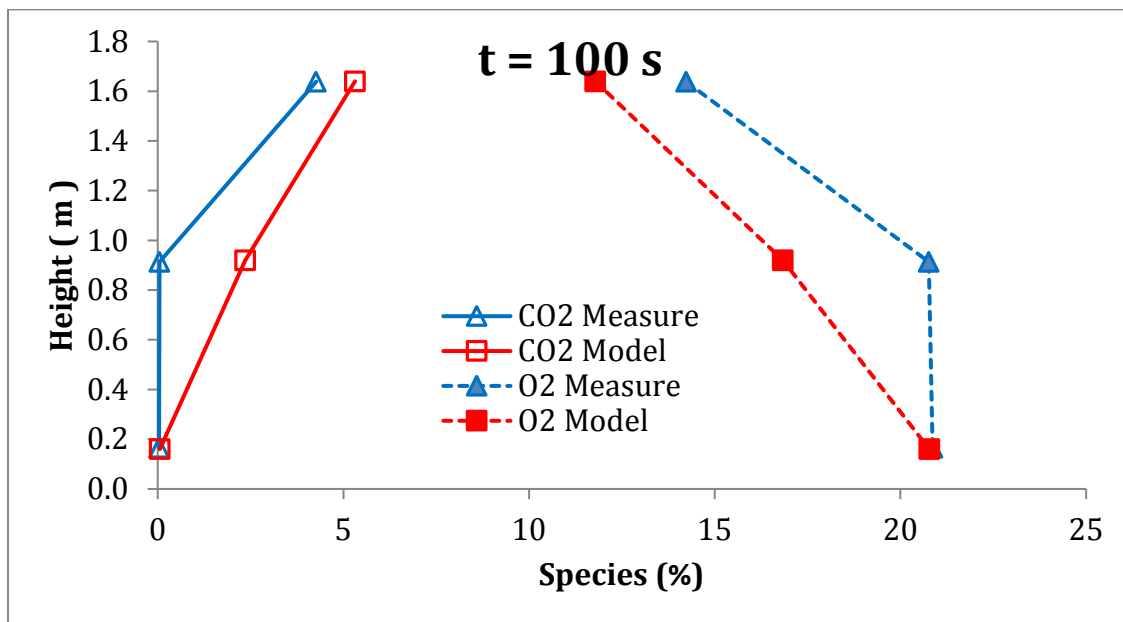
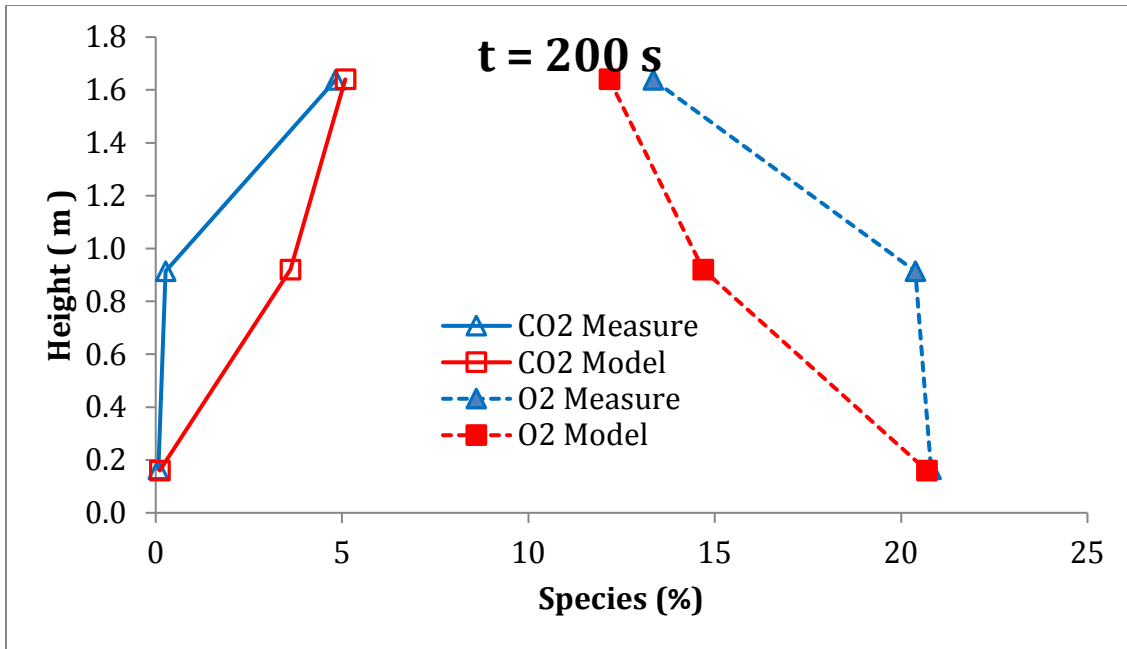
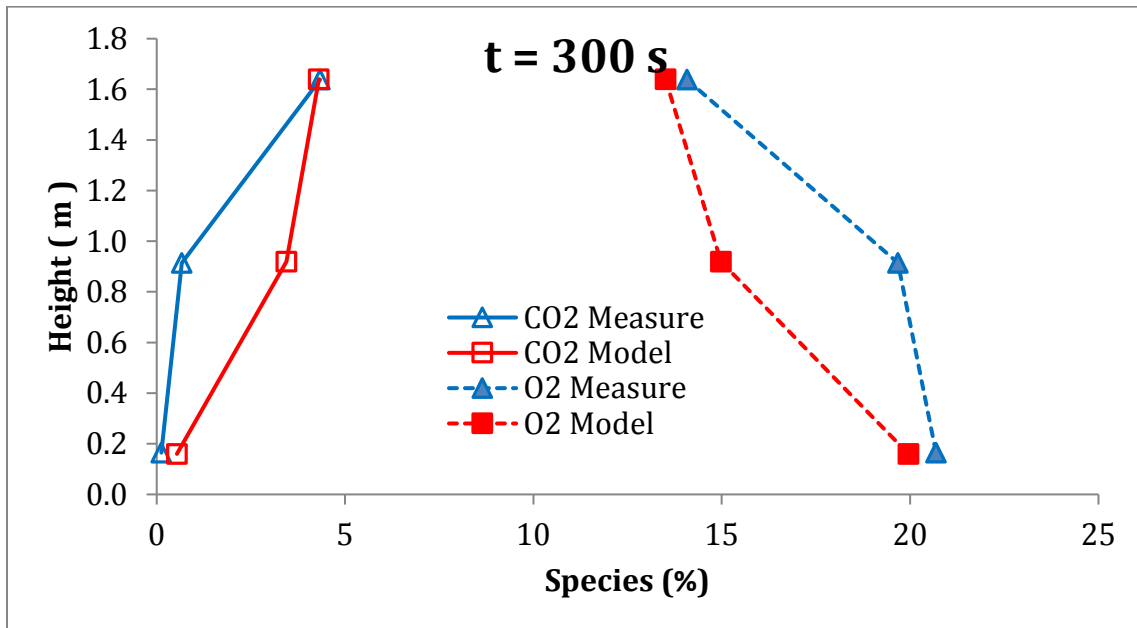


Figure B-16. Measured and modeled species (CO<sub>2</sub> and O<sub>2</sub>) vs. height for the base fire (wall) case at 100 s



**Figure B-17. Measured and modeled species (CO<sub>2</sub> and O<sub>2</sub>) vs. height for the base fire (wall) case at 200 s**



**Figure B-18. Measured and modeled species (CO<sub>2</sub> and O<sub>2</sub>) vs. height for the base fire (wall) case at 300 s**

### B.2.2.3. Air Flow Rate

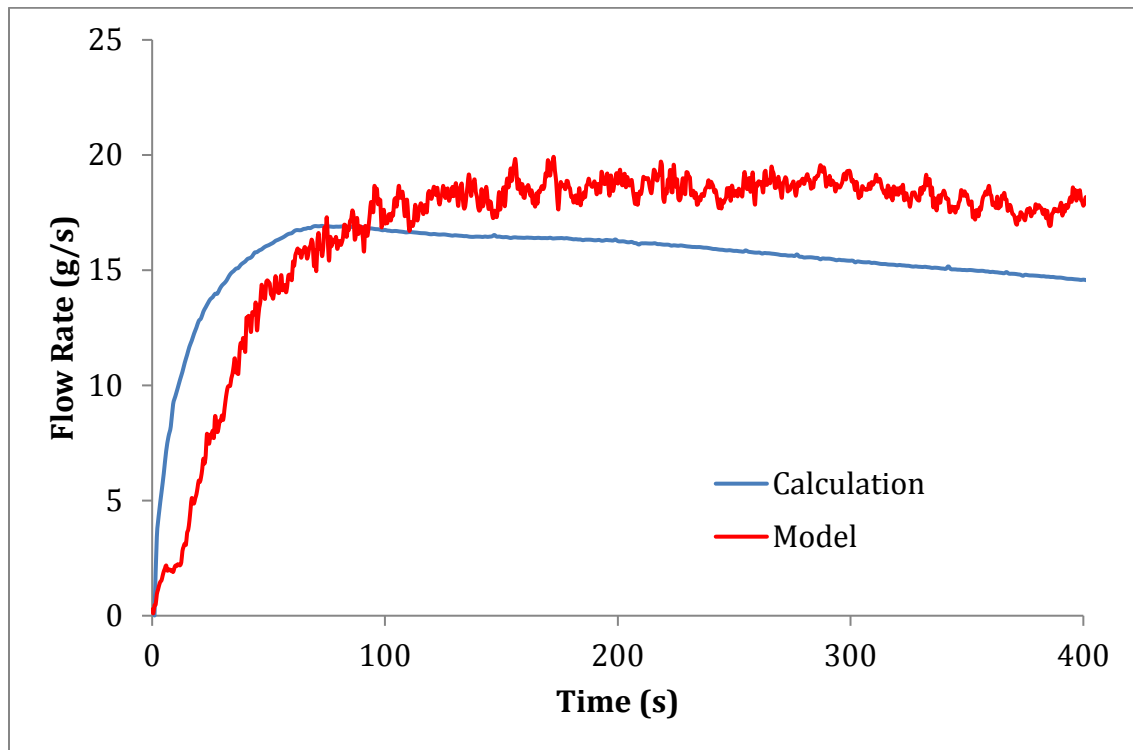


**Figure B-19. Calculated and modeled inward airflow rate through the opening for the base fire (wall) case**

### B.2.3. CEILING FIRE (CENTER)

#### B.2.3.1. Temperature

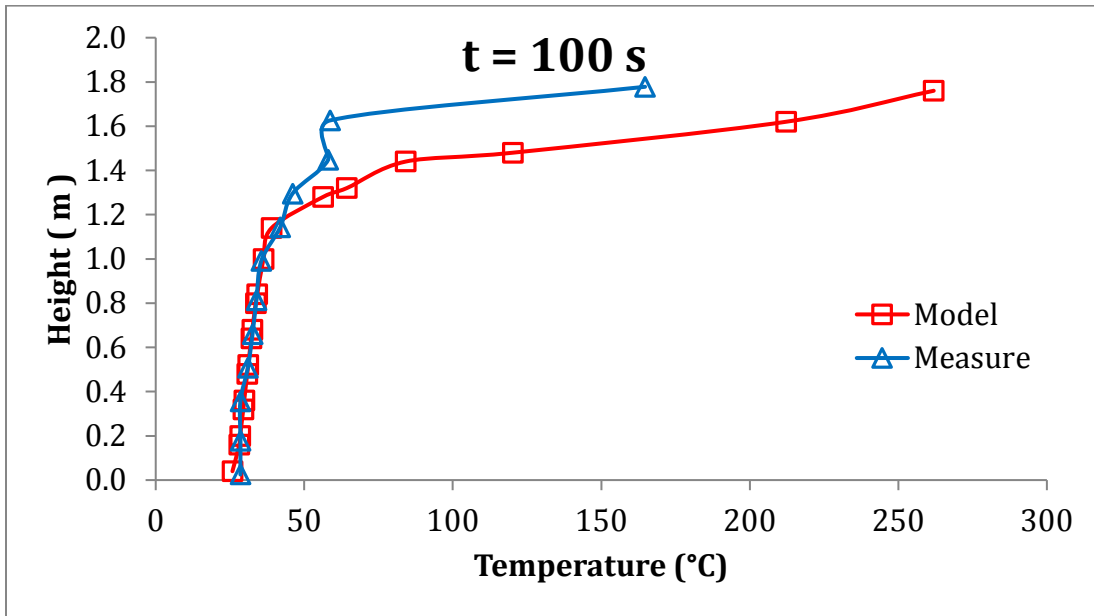


Figure B-20. Measured and modeled temperature vs. height for the ceiling fire (center) case at 100 s

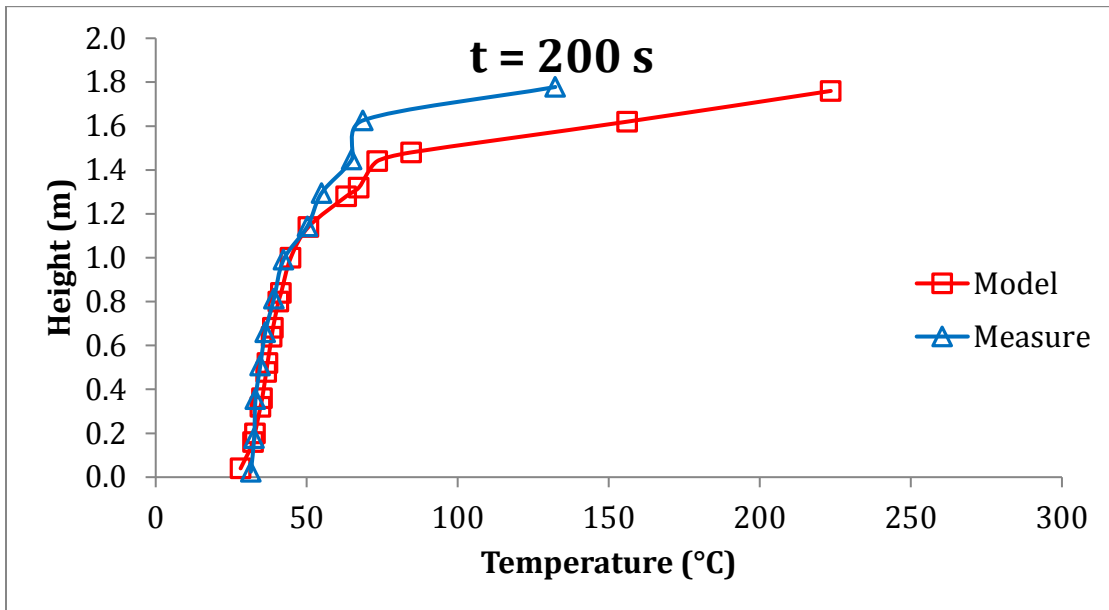


Figure B-21. Measured and modeled temperature vs. height for the ceiling fire (center) case at 200 s

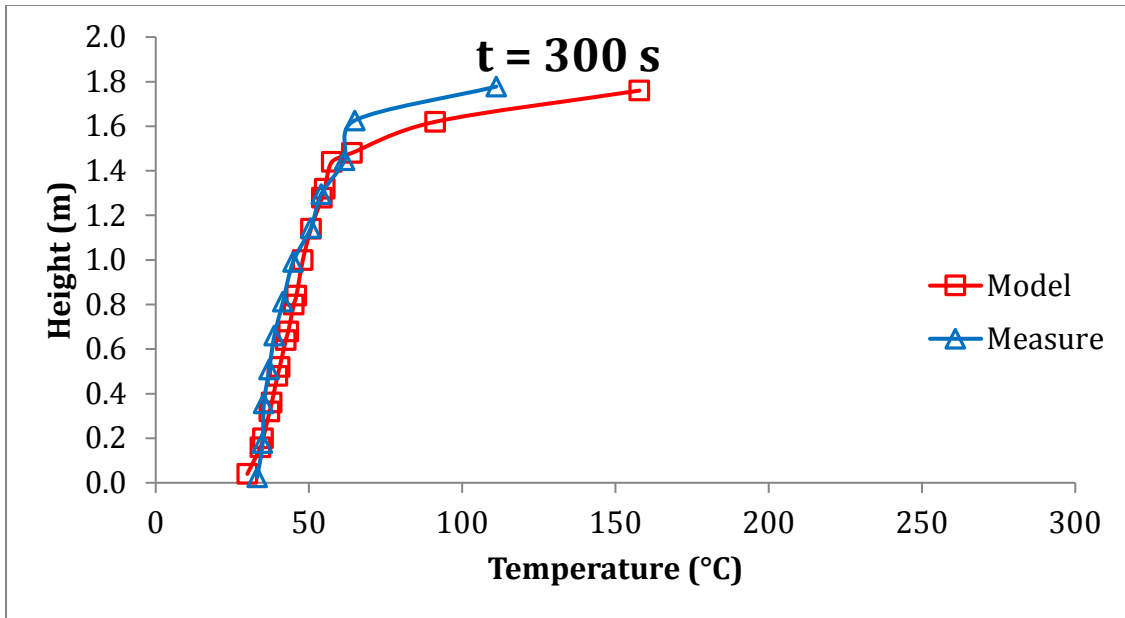


Figure B-22. Measured and modeled temperature vs. height for the ceiling fire (center) case at 300 s

B.2.3.2. Species

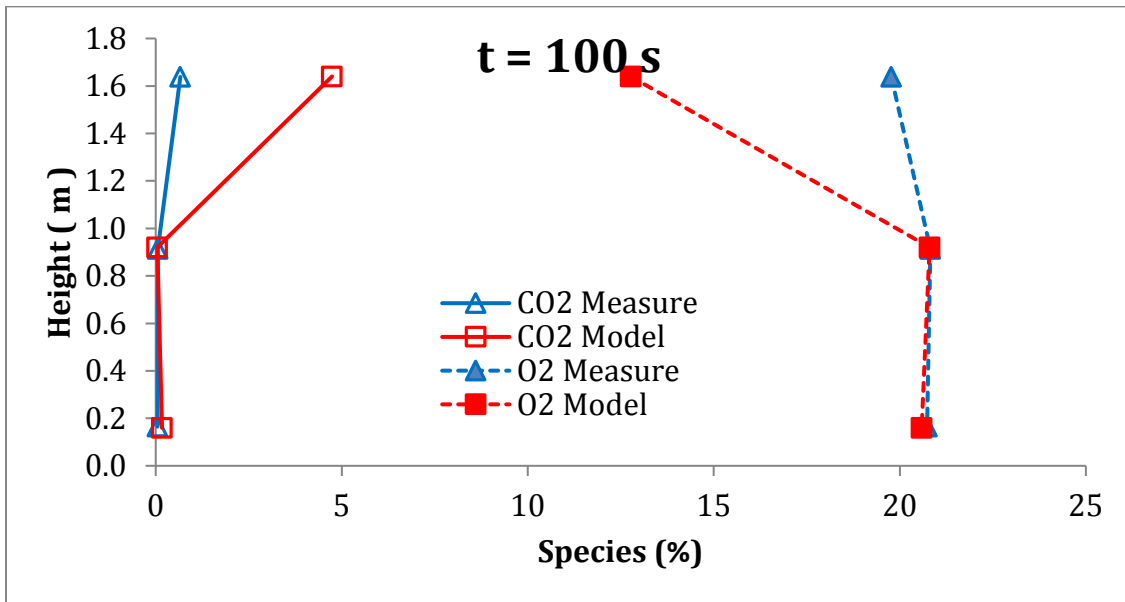


Figure B-23. Measured and modeled species (CO<sub>2</sub> and O<sub>2</sub>) vs. height for the ceiling fire (center) case at 100 s

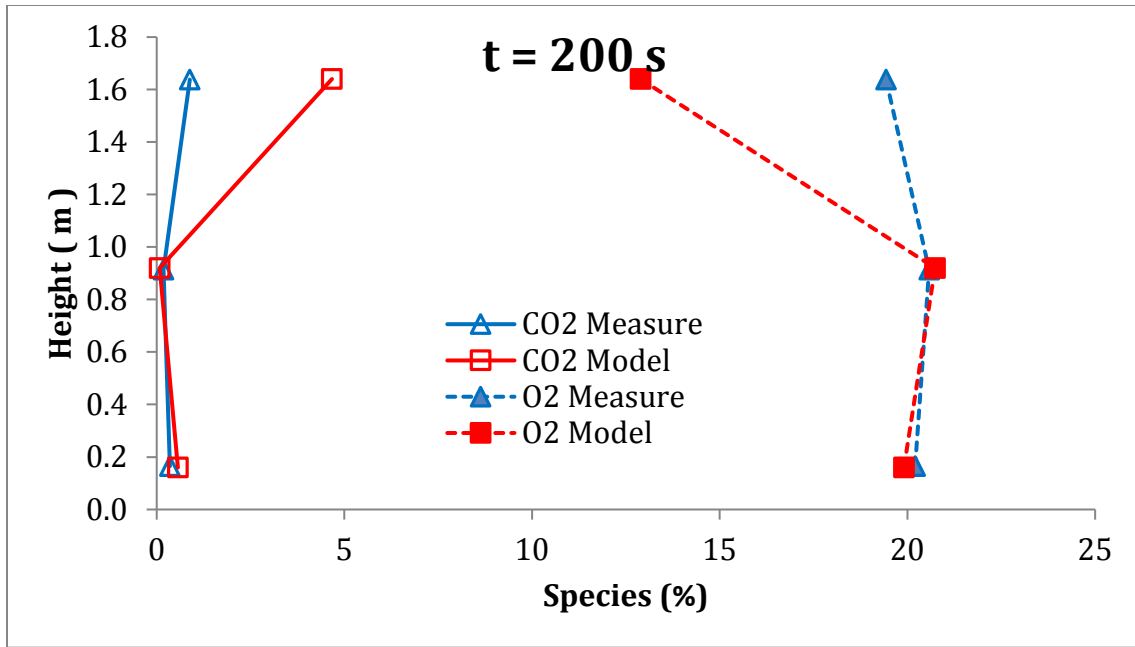


Figure B-24. Measured and modeled species (CO<sub>2</sub> and O<sub>2</sub>) vs. height for the ceiling fire (center) case at 200 s

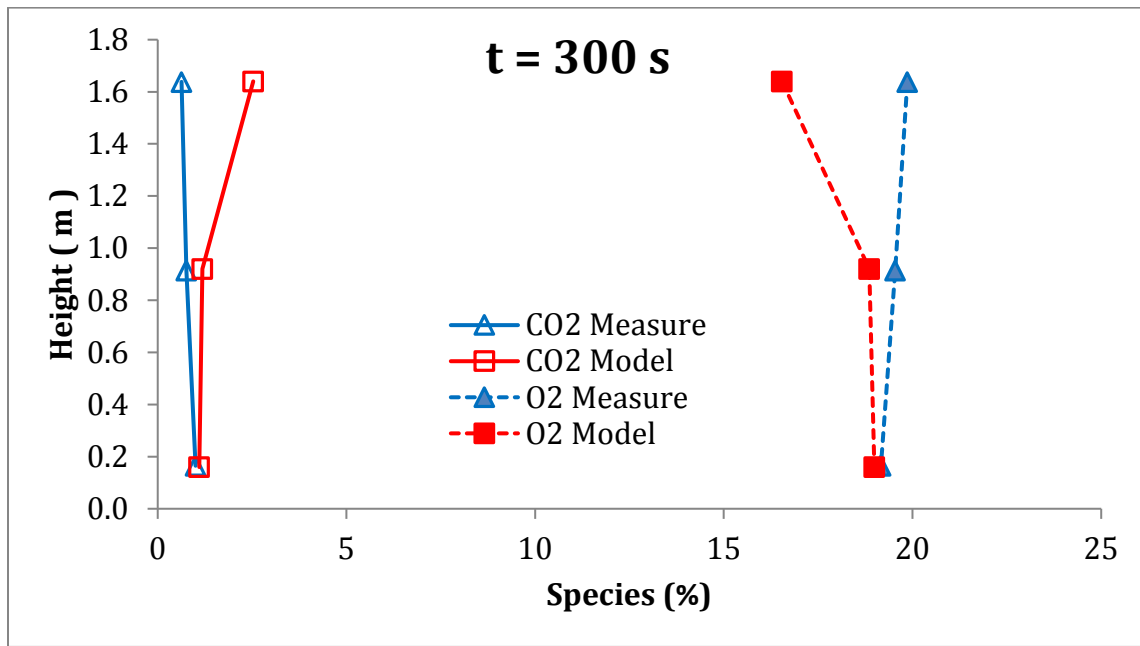
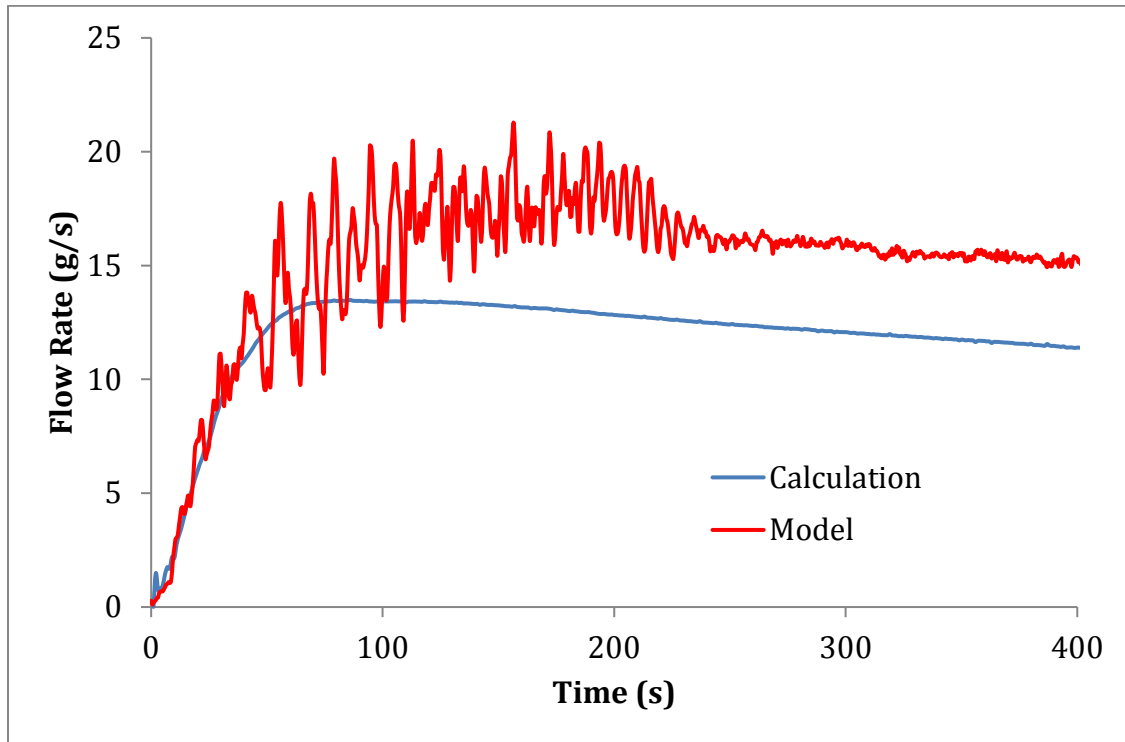


Figure B-25. Measured and modeled species (CO<sub>2</sub> and O<sub>2</sub>) vs. height for the ceiling fire (center) case at 300 s

### B.2.3.3. Air Flow Rate



**Figure B-26. Calculated and modeled inward air flow rate through the opening for the ceiling fire (center) case**

## B.2.4. CEILING FIRE (WALL)

### B.2.4.1. Temperature

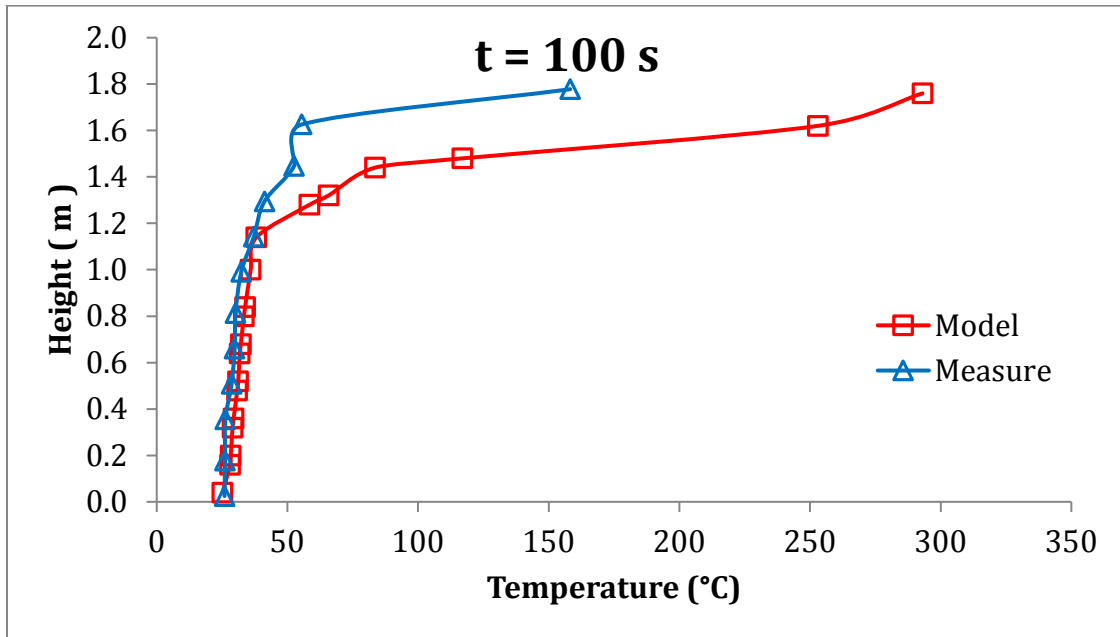


Figure B-27. Measured and modeled temperature vs. height for the ceiling fire (wall) case at 100 s

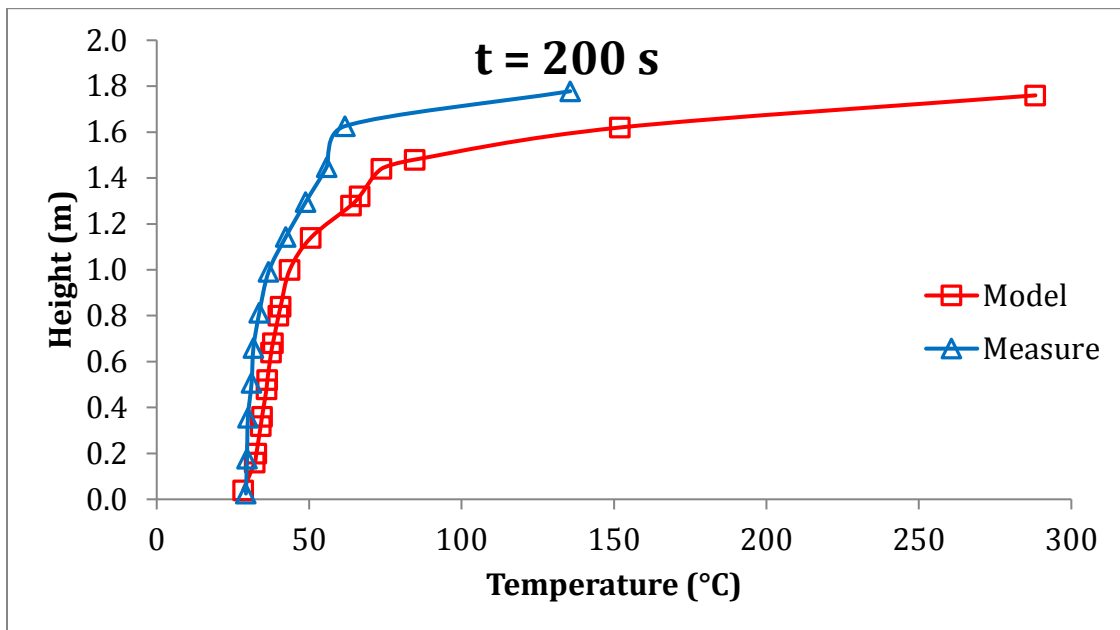


Figure B-28. Measured and modeled temperature vs. height for the ceiling fire (wall) case at 200 s



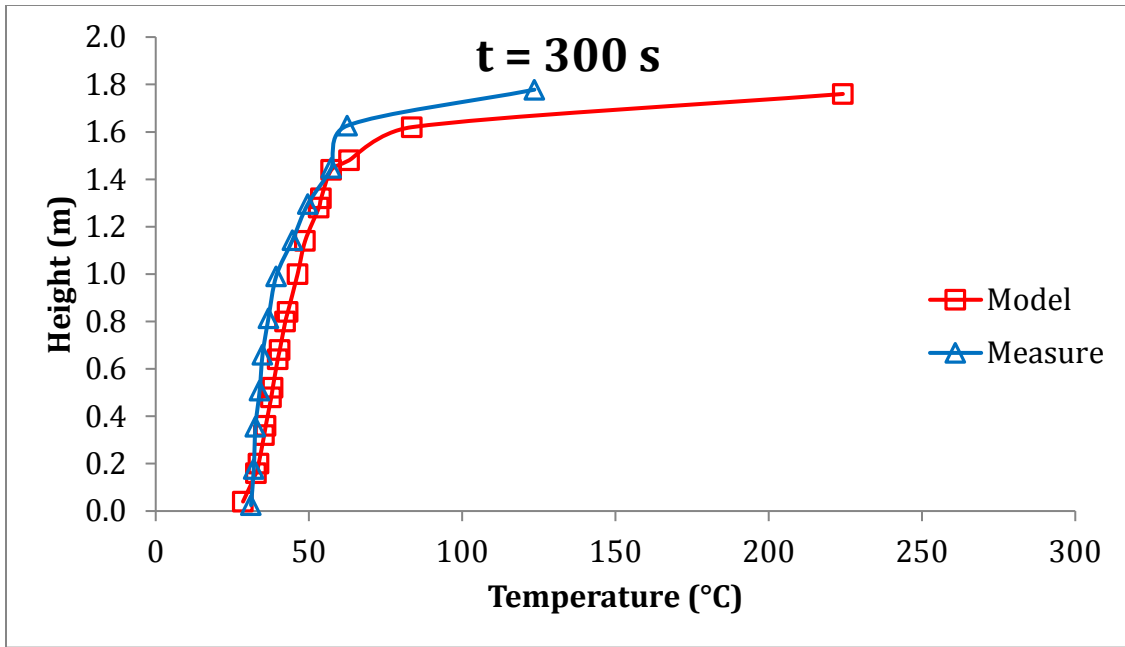


Figure B-29. Measured and modeled temperature vs. height for the ceiling fire (wall) case at 300 s

B.2.4.2. Species

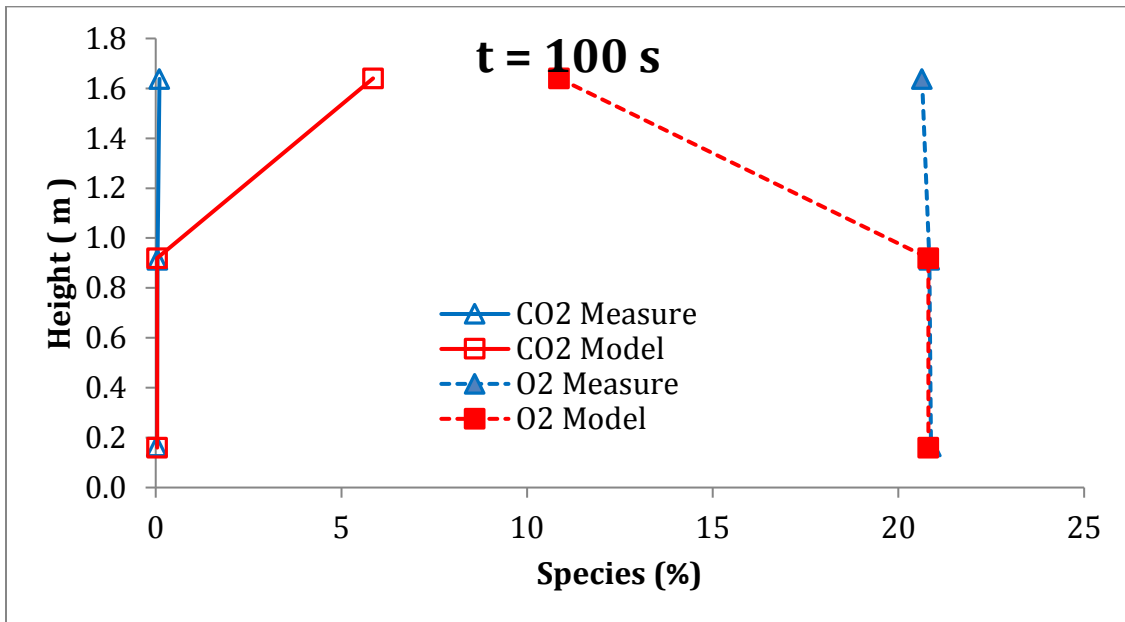
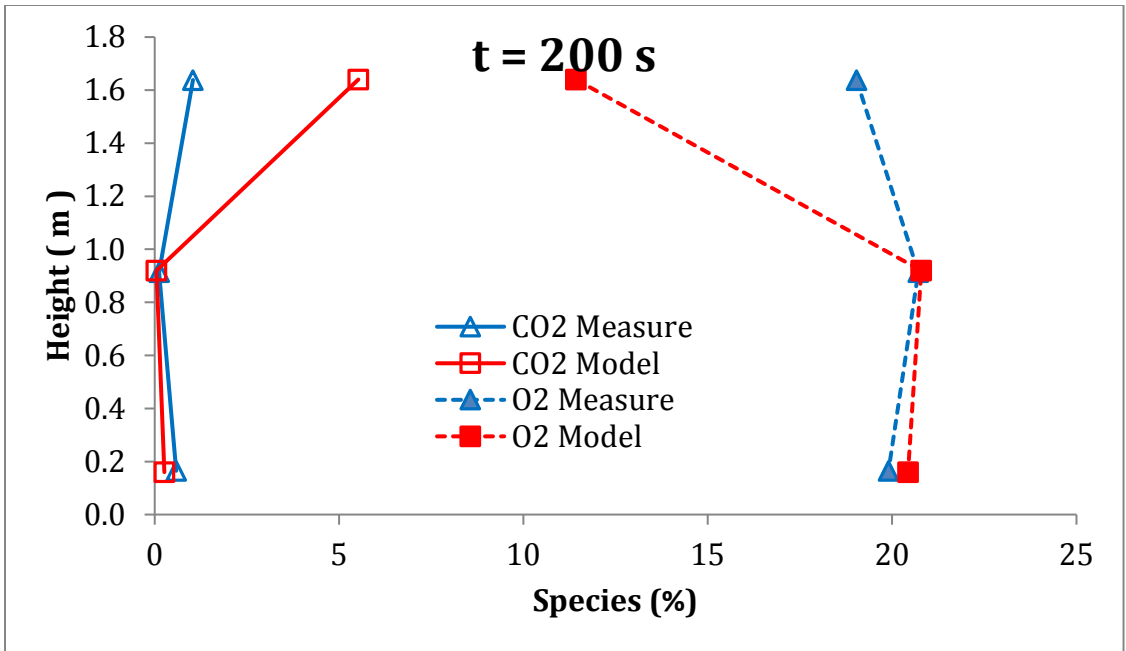
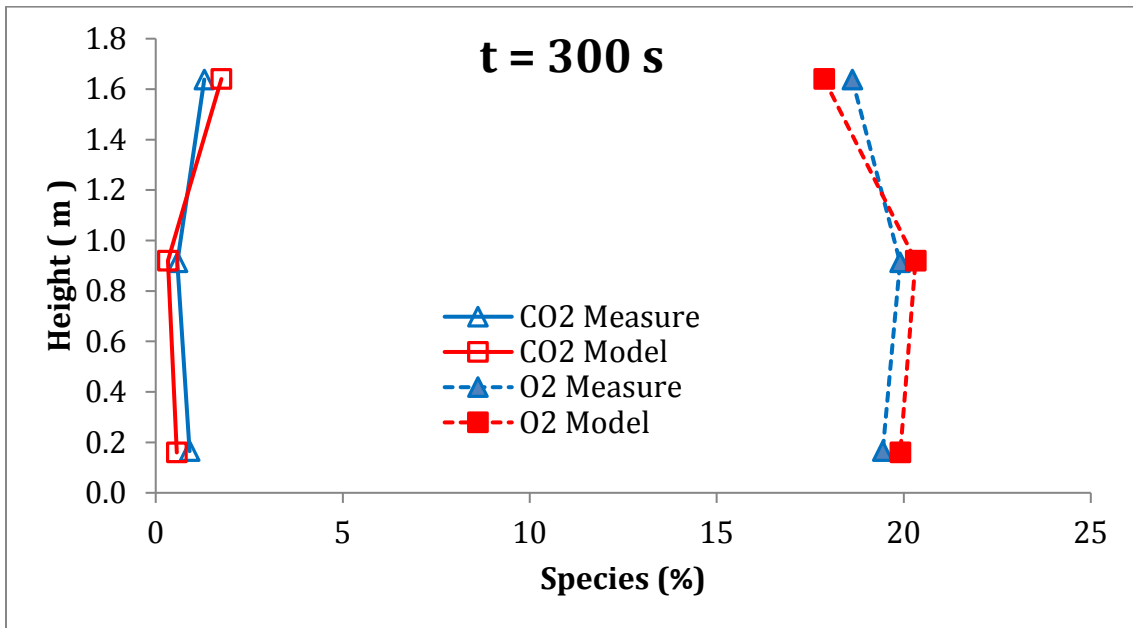


Figure B-30. Measured and modeled species (CO<sub>2</sub> and O<sub>2</sub>) vs. height for the ceiling fire (wall) case at 100 s



**Figure B-31. Measured and modeled species (CO<sub>2</sub> and O<sub>2</sub>) vs. height for the ceiling fire (wall) case at 200 s**



**Figure B-32. Measured and modeled species (CO<sub>2</sub> and O<sub>2</sub>) vs. height for the ceiling fire (wall) case at 300 s**

### B.2.4.3. Flow Rate

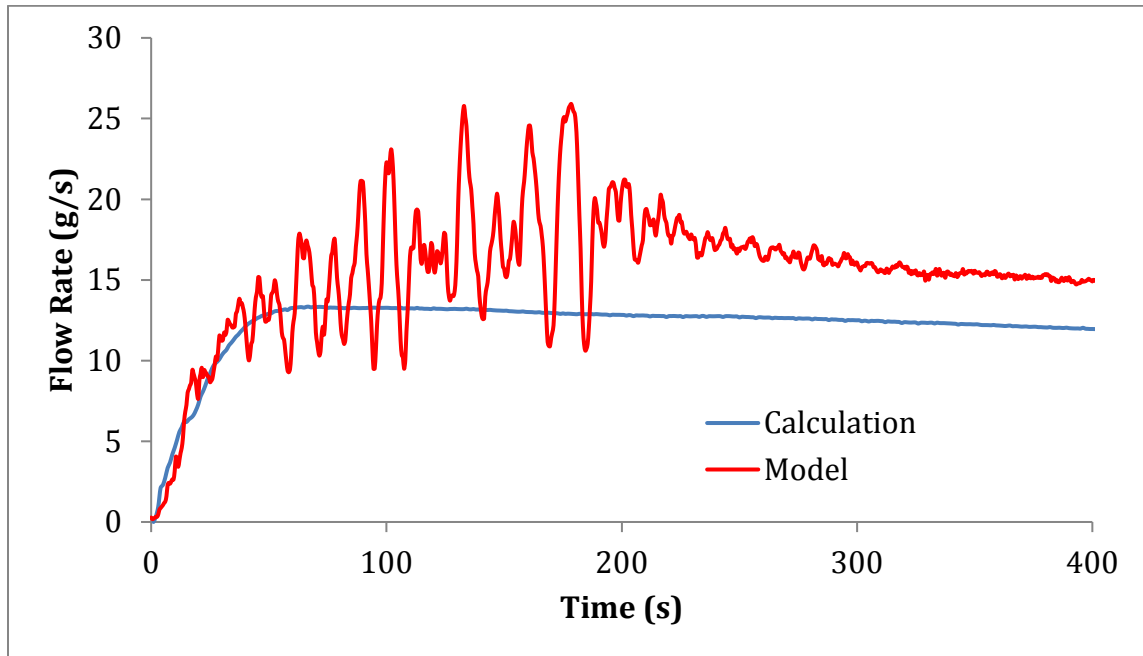


**Figure B-33. Calculated and modeled inward airflow rate through the opening for the ceiling fire (wall) case**